Fakultät für Maschinenwesen

Lehrstuhl für Nukleartechnik

CERN Radiation Protection Group

Development of an In-Situ Radiological Classification Technique for Material from CERN's Accelerator Facilities

Nick Walter

Vollständiger Abdruck der von der Fakultät für Maschinenwesen der Technischen Universität München zur Erlangung des akademischen Grades eines

Doktor‑Ingenieurs (Dr.-Ing.)

genehmigten Dissertation.

Vorsitzender: Univ.-Prof. Phaedon-Stelios Koutsourelakis, Ph.D.

Prüfer der Dissertation:

1. Univ.-Prof. Rafael Macián-Juan, Ph.D.

2. Prof. Gumersindo Verdú Martín, Ph.D.,

(Universitat Politècnica de València, Valencia, Spanien)

Die Dissertation wurde am 09.07.2015 bei der Technischen Universität München eingereicht und durch die Fakultät für Machinenwesen am 17.11.2015 angenommen.

Abstract

CERN, the European Organization for Nuclear Research, operates high energy accelerators for particle physics research. Because of beam losses and subsequent particle interactions, radioactivity can be induced in certain accelerator components. Material and waste taken out of the accelerators facilities as a result of maintenance repair and upgrade actions as well as in case of decommissioning needs to be radiologically classified for future handling. Depending on the level of residual activity, some of these components are candidates for clearance from regulatory control in Switzerland. The Swiss radiation protection ordinance sets as criteria for clearance of material and waste from regulatory control the compliance with radionuclide specific limits for surface contamination and for specific activity as well as an ambient dose equivalent rate criterion. For objects with a mass below $1\,kg$ a radionuclide specific clearance limit for total activity has to be respected. This work is focused on the specific activity criterion, whereby the Swiss clearance limits for specific activity correspond to the exemption limits for specific activity. The clearance from regulatory control performed at the exit of the facility is special, mainly due to the restricted infrastructural conditions and a limited time budget. In most cases the measurement has to be non-destructive, i.e. without measurements of disassembled subcomponents or sampling works for detailed mechanical, chemical or radiochemical analysis. In addition, some information of the complete activation process might not be available, e.g. the irradiation time profile, the chemical material composition or the object location when it has been in the facility.

The present work tackles this challenge by defining enveloping conditions and parameter sets that allow to perform material clearance measurements, even without a detailed knowledge of object characteristics and radiological history. Representative input parameter ranges, e.g. reference material compositions or irradiation conditions, were determined and used for the calculation of the resulting radionuclide inventories. More than 28000 radionuclide inventories were calculated, analysed and visualized. A 600-page report containing these data supplements this work.

It was studied whether the detection limit of a total gamma counter, based on

six large area scintillation detectors (RADOS RTM 661/440 lnc, produced by Mirion Technologies, Germany), is sufficiently low to reliably detect the radioactivity that corresponds to the clearance limits for the calculated radionuclide inventories. The gamma-ray signal per Swiss clearance limit was determined for the calculated radionuclide inventories of all selected reference materials and for all considered irradiation conditions and compared to the detection limit of the RADOS RTM 661/440 lnc. To include the detector response in the calculations, a photon energy dependent efficiency function was determined for the total gamma counter. The dependence of the signal strength on the various parameters was analysed and the most conservative resulting radionuclide inventories, i.e. the ones with the lowest detectable gamma-ray signal per clearance limit, were identified and categorised by material as well as by irradiation condition. These enveloping radionuclide inventories allow performing clearance measurements, even without a detailed knowledge of object characteristics and radiological history. Furthermore, self-absorption effects as a function of the object geometry and material density were quantified by Monte-Carlo simulations and integrated in the clearance method by specifying self-absorption factors.

The gamma-ray signal per Swiss clearance limit of the considered common materials for objects with a mass of 1 kg, the most penalising mass configuration according to the Swiss radiation protection ordinance, is above the detection limit of the RADOS RTM 661/440 lnc, even if the clearance limit is dominated by radionuclides that have no measurable gamma-ray emission. Consequently, by using the developed characterization method, this device can be used for the clearance of material and waste from CERN's accelerator facilities from Swiss regulatory control for the present Swiss clearance limits in force.

Acknowledgements

Table of Contents

List of Figures

List of Tables

List of Acronyms

AD Antiproton Decelerator, CERN facility;

ALICE A Large Ion Collider Experiment, experimental facility at the LHC;

ATLAS A Toroidal LHC Apparatus, experimental facility at the LHC;

BAG/OFSP Federal Office of Public Health, Berne, Switzerland;

CMS Compact Muon Solenoid, experimental facility at the LHC;

DGS-RP CERN Radiation Protection Group;

DIN Deutsches Institut für Normung e.V., Berlin, Germany;

EC European Commission, Brussels, Belgium;

IAEA International Atomic Energy Agency, Vienna, Austria;

ISO International Organization for Standardization, Geneva, Switzerland;

ISOLDE Isotope Separator On Line DEtector, CERN facility;

ISR Intersecting Storage Rings, former CERN facility;

LEIR Low Energy Ion Ring, CERN facility;

LHC Large Hadron Collider, CERN facility;

LHC-b Large Hadron Collider beauty, experimental facility at the LHC;

LINAC Linear Accelerator;

lnc Leading Nuclide Correlation, detection device specification of RADOS;

MDA Minimum Detectable Activity;

NA61, NA62 Experimental facilities in the CERN North Area;

NORM Naturally Occurring Radioactive Materials;

OES Optical Emission Spectroscopy;

PS Proton Synchrotron, CERN facility;

PSB Proton Synchrotron Booster, CERN facility;

RADOS Mirion Technologies (RADOS) GmbH, Hamburg, Germany;

SPS Super Proton Synchrotron, CERN facility;

SUSY Supersymmetry

CHAPTER 1

CERN

1.1 General Description of CERN

CERN, the European Organization for Nuclear Research, is an international particle physics laboratory located in the Geneva area, partially on Swiss as well as partially on French territory. It represents with its accelerator complex one of the largest high-energy physics research facilities. Today CERN counts 21 member states, whereas in 1954 it was established by 12 European countries. Apart from the member states, researchers of more than 100 countries are involved in CERN experiments and research activities. The know-how and knowledge transfer back into the countries as well as the education and training of their citizen is part of the return of investment. CERN fields of research are special scientific fields, like particle accelerator and detector development, cryogenics and high vacuum technologies, as well as common scientific fields, like mechanical, electrical or nuclear engineering. In addition the continuous improvement of data acquisition, handling and storage is one of the major fields of CERN interests.

1.2 CERN Accelerator Complex

The CERN accelerator complex is very large and complex compared to other particle acceleration facilities in the world. From the point of view of this work, two circumstances make the operations at CERN extraordinary and unique. On the one hand, the types of particle beams. Except in some special installations, e.g. the ISOLDE experiment or the antiproton decelerator (AD), in CERN accelerator complex protons and heavy ions are currently the types of particles accelerated. In some experiments, protons are used to create other particles like antiprotons, neutrons or neutrinos. Furthermore the energy of these particles can be sufficiently high to create various heavy secondary particles. This

1

leads to a wide range of secondary particles. On the other hand the accelerator complex consists of several single accelerators with different nominal energies, serially connected as accelerator chain, to reach the worldwide highest nominal energy for particle accelerators. The combination of this particle variety together with the wide and high energy range allows an unique spectrum for particle physic research done at CERN, but also creates very complex conditions for accelerator radiation induced activation in materials (see Sec. 2.3). The particle acceleration process at CERN starts with a linear acceleration for both particle types, for protons in LINAC2 and for heavy ions in LINAC3. After this initial acceleration the accelerator complex consists of a succession of several ring accelerators that work as accelerator and storage rings. After been accelerated up to the nominal power of the actual accelerator, the particle beam can be extracted to either the next higher accelerator in the chain or to adjacent experimental areas. Planing and control of this complex operation is performed by the CERN Control Center (CCC).

LHC Injector Chain

In the following paragraphs the characteristics of the main accelerator complex components are explained. Within the scope of this work the accelerator complex is limited to the LHC injector chain and the transfer tunnels. Adjacent experiments and special beam intersection devices or areas, e.g. collimators or beam dumps, are excluded of the scope of this work. Furthermore the explanation is limited on proton acceleration and excludes heavy ion acceleration due to its minor influence on material activation. Further information and more details about the history, the actual machine status or future programs and experiments of CERN can be found in free accessible publications as well as on the CERN internet presence [1].

A standard **hydrogen gas bottle** serves as proton source for the entire CERN accelerator complex. In an electric field hydrogen atoms are stripped of their electrons. The resulting protons are transferred to the LINAC2.

Since 1978 the first acceleration step for protons takes place in the **LINAC2**. In the 30 m long machine protons are accelerated to a kinetic energy of 50 MeV and thereafter injected in the PSB.

The **Proton Synchrotron Booster (PSB)** is the first ring accelerator of the CERN accelerator chain. This accelerator has a diameter of 50 m and consists of four super-imposed rings which accelerate protons coming from the LINAC2 to a kinetic energy of 1.4 GeV. The PSB was added 1972 to "boost" proton bunches before either delivering them to the Radioactive Ion Beam facility (ISOLDE) or injecting them into the next

accelerator, the PS.

Beginning with the **Proton Synchrotron (PS)** the following accelerators of the CERN accelerator complex can accelerate both, protons and heavy ions. The PS ring consists of 277 warm magnets and has a circumference of 628 meters. In the PS protons can be accelerated to a nominal kinetic energy of 25 GeV. Protons are delivered from the PSB whereby heavy ions come from the Low Energy Ion Ring (LEIR). The PS operates since 1959 and either sends the beam the next higher accelerator, the SPS, or transfers particles to experimental areas like the East Area, the neutron time-of-flight facility (n-Tof) or via the Antiproton Decelerator (AD) target area to the AD.

Since 1976 the **Super Proton Synchotron (SPS)**, that consists of 1317 magnets and has a circumference of 6912 m, accelerates protons to 450 GeV. Adjacent experiments, that can receive beam by the SPS, are for example the North Area experiments like Na61 or Na62. In the past the SPS beam was also extracted to experiments in the West Area or to the CERN Neutrinos to Grand Sasso (CNGS) project which are out of operation today. The SPS has two extraction points to extract the beam into the LHC, one to fill the LHC clockwise beam line and the other to fill the counter clockwise one.

Table 1.1 sums the features of the CERN LHC injector chain and gives together with the data of all transfer lines and of the LHC itself, an idea of the amount of material present in the radiation fields adjacent to the approx. 50 km of beam line. Furthermore the possible variation in the irradiation conditions (beam energy and irradiation time) in the whole CERN accelerator complex has to be considered.

Table 1.1: In this table the nominal kinetic energies of the accelerators of the CERN LHC injector chain are listed for proton operations. Furthermore the accelerator length, the number of magnets as well as the construction date are given. Data taken from [1].

Accelerator	Energy	Length	Magnets	Commissioning
LINAC 2	50 MeV	30 m	-	1978
PSB	1.4 GeV	157 m	~80	1972
PS	25 GeV	628 m	277	1959
SPS	450 GeV	7 km	1317	1976
LHC	7 TeV	27 km	~9600	2008

LHC and LHC Experiments

CERN's accelerator flagship is the **Large Hadron Collider (LHC)** [2]. The LHC consists of two circular beam lines in which the beams travel in opposite direction. The beam lines are surrounded by around 9600 magnets. The superconducting magnets are liquid helium cooled and the temperature is constantly maintained at $2\,K$. In operation since 2008, the LHC is designed to collide proton beams with a centre-of-mass energy of $14\,TeV$. In the $26659\,m$ long ring tunnel system four beam intersection points are present. Huge and very complex detector devices have been installed $100\,m$ under the surface in enormous caverns around the four collision points. These four detectors are built in different ways and/or for different purposes.

The **ATLAS** detector is situated in LHC point 1. This detector traces proton-proton collision events and has a total weight of $7000\,tons$. The ATLAS detector has a length of $45\,m$, a diameter of $22\,m$ and consists of the inner detector, the electromagnetic calorimeter, the hadronic calorimeter and the muon detector. In the ATLAS detector two magnetic fields are generated, one in the inner detector by a huge solenoid and the second one by the barrel toroid that consists of eight superconducting coils and generates a $2\,T$ magnetic field for the muon detection. The physics field of interests of this general-purpose detector is very large with a focus on supersymmetry (SUSY) and on the detection and description of the Higgs particle. Together with the CMS collaboration the discovery of the Higgs boson was officially announced in summer 2012. Detailed information about the ATLAS detector complex can be found in [3].

In LHC point 2 the **ALICE** detector is installed. ALICE is a heavy ion collision detector that consists of a barrel detector unit and a single arm forward muon detector. The ALICE detector has a diameter of $16\,m$, is $26\,m$ long and has a total weight of $10000\,tons$. The study of quark-gluon plasma properties can be considered as main physics goal of the ALICE collaboration. Further information about the ALICE experiment can be found in [4].

At LHC point 5 **CMS**, the Compact Muon Solenoid detector, is located. With its $12500\,tons$ it is the heaviest under the four LHC experiments. Like ATLAS it is also a barrel detector construction with end cap detectors. The CMS barrel has a diameter of $15\,m$ and a length of $22\,m$. Inside CMS a huge superconducting solenoid generates a magnetic field of $4\,T$. CMS has the same major research fields as the ATLAS collaboration but with a different approach of detector design and technique. For detailed CMS information see [5].

The **LHC-b** detector can be found in LHC point 8. It consists of a forward spec-

trometer with planar detectors with a length of 21 m, a height of 10 m, and a width of 13 m. The total weight is about 5600 tons. The main field of LHCb research is the study of CP-violations, i.e. asymmetries between matter and antimatter. See [6] for further information concerning the LHCb detector.

Physics Concepts

The following chapter describes the physics concepts used for this work. The main focus lies on radioactivity, the radioactive decay with the corresponding decay modes as well as the resulting radiation and emitted particle types. To be able to discuss radiation detection methods as well as radiation attenuation effects, the interaction processes of radiation with matter are explained more in detail. Furthermore induced activation phenomena, that play a major role in this work, are outlined.

2.1 Radioactivity

Radioactivity is the spontaneous transformation of unstable and energetically excited radionuclides by emitting various particle and radiation types to relieve the excitation energy. In the following paragraphs radioactivity, the radioactive decay itself and its decay modes as well as the principle of induced radioactivity at high energy proton accelerators are described. The explanations are as detailed as needed for this work and as general as possible, but by no means exhaustive. As main sources for this chapter, references [7], [8], [9], [10], [11], [12], [13] and [14] were used. Quantity definitions and dimensions are taken from [15] and [16].

Radioactive Decay

The radioactive or nuclear decay is a stochastic process where an unstable atomic nucleus decays according to a certain decay mode with a certain decay probability per time into certain decay products. This nuclear decay can formally be described by the *decay law*

$$N(t) = N_0 \, e^{-\lambda t} \tag{2.1.1}$$

where

$$N_0 = \text{Initial number of nuclei}$$
$$\lambda = \text{Decay constant } [\text{s}^{-1}]$$
$$N(t) = \text{Number of not-decayed nuclei after the time } t.$$

In this context also the quantities *mean life-time* τ, the average time for an unstable nucleus before decaying, and *half-life* $t_{1/2}$, the period of time in which half of the initial nuclei $\left(N(t) = \frac{N_0}{2}\right)$ are decayed, are substantial. These quantities depend on the so called *decay constant* λ within the following formal relation

$$\lambda = \frac{1}{\tau} = \frac{\ln 2}{t_{1/2}}. \qquad (2.1.2)$$

Activity A is used as common quantity for radioactivity and is given in [Bq]. The SI unit *Becquerel* is defined as Bq $= \frac{\text{radioactive decay}}{\text{second}}$ $[\text{s}^{-1}]$. For infinitesimal time intervals, and with $A = -\frac{dN}{dt}$, *activity* can be written as

$$A = -\frac{dN}{dt} = \lambda N \qquad (2.1.3)$$

with Eq. 2.1.1

$$A(t) = A_0 \, e^{-\lambda t}. \qquad (2.1.4)$$

Decay Modes and Emitted Radiation Types and Particles

Depending on the radionuclide and their branching ratios, different radioactive transformation, also called decay modes, occur and result in the emission of different radiation and/or particle types. The most common types of decay modes are α-particle emission, β^+/ β^- emission and electron capture. These decay modes are often followed by characteristic X-ray, electron or γ-ray emission. Table 2.1 shows the main decay modes for the present work. Illustrations of decay schemes and emission spectra for common radionuclides are shown in Appendix A.6.ii for γ-ray emitting radionuclides, denoted *key radionuclides*[1], and in Appendix A.6.iii for radionuclides without significant γ-ray emission, denoted *difficult-to-measure radionuclides*[1].

---

[1]Classification into *key radionuclides* and *difficult-to-measure radionuclides* after ISO 21238 [17]:
"difficult-to-measure nuclide: nuclide whose radioactivity is difficult to measure directly from the outside of the waste packages by non-destructive assay means";
"key nuclide: gamma emitting nuclide whose radioactivity is correlated with that of difficult-to-measure nuclides and can be readily measured directly by non-destructive assay means".

Table 2.1: Most common radioactive decay modes. This table is taken from [18].

Mode	Description	Reaction	Example
Alpha Decay (α)	Emission of an alpha particle (^{4}He). The alpha decay is the most efficient way for heavier nuclei to reduce both mass and charge.	$^A_Z P \rightarrow \,^{A-4}_{Z-2} D + \,^4_2 He$	$^{238}_{92} U \rightarrow \,^{234}_{90} Th + \alpha$
Beta-minus Decay (β^-)	High energy electron (β^-) and anti-neutrino ($\overline{\nu}$) emission from a nucleus with excess number of neutrons (nuclide below the line of stability in the Chart of Nuclides).	$n \rightarrow p + \beta^- + \overline{\nu}$	$^{60}_{27} Co \rightarrow \,^{60}_{28} Ni + \beta^- + \overline{\nu}$
Beta-plus Decay (β^+)	Positron (β^+) and neutrino (ν) emission from a nucleus with an excess of protons (i.e. above the line of stability in the Chart of Nuclides). Two 0.511 MeV annihilation photons, emitted in opposite directions to conserve momentum, accompanies always the positron annihilation.	$p \rightarrow n + \beta^+ + \nu$	$^{22}_{11} Na \rightarrow \,^{22}_{10} Ne + \beta^+ + \nu$
Electron Capture (EC)	Capture of an electron from the inner K or L shells✠ in order to reduce the number of protons. When the beta-plus decay is energetically possible, as happens† with ^{22}Na but not with ^{55}Fe, both processes are competing mechanism. The vacancies left from the capture events are filled by electrons from outer shells resulting in X-rays and Auger electrons‡ emission.	$p + e^- \rightarrow n + \nu$	$^{55}_{26} Fe + e^- \rightarrow \,^{55}_{25} Mn + \nu$
Isomeric Transition (IT)	After a radioactive decay, the transforming nucleus is frequently in an excited state. Most of them are short-lived excited states ($< 10^{-9}\, s$) and returns to the ground state through gamma emission $\left(^A_Z P^* \rightarrow \,^A_Z P + \gamma\right)$. For long-lived states (metastable (or isomeric) states: lifetime $> 10^{-9}\, s$) the gamma emission is thought as a separate event and known as an isomeric transition (IT).	$^{Am}_Z P \rightarrow \,^A_Z P + \gamma$	$^{137m}_{56} Ba \rightarrow \,^{137}_{56} Ba + \gamma$
Internal Conversion	Ejection of an orbital electron by a short or long-lived excited nucleus. The excitation energy is directly transferred to an inner shell electron, ejecting it from the atom. Therefore, Internal conversion and gamma emission compete§ to relieve excitation energy held by transformed nuclei. To fill the electron shell vacancy, the internal conversion is followed by X-rays and Auger electrons emission.	$^A_Z P^* \rightarrow \,^A_Z P^+ + e^-$	$^{137m}_{56} Ba \rightarrow \,^{137}_{56} Ba^+ + e^-$

✠ Most capture events involve electrons from K-shell (of the order of 90%), but also from L-shell ($\sim$10%) and, with a much lower probability, from M-shell ($\sim$1%).

† ^{22}Na branching ratio: $\sim$90.5% of the transitions occur through β^+ while $\sim$9.5% through EC.

‡ The Auger effect can be seen as an "inner photoelectric effect": the X-ray produced with the filling of a inner vacancy can interact with an outer shell electron, ejecting it from the atom (Auger electron).

§ ^{137m}Ba branching ratio: $\sim$89.9% of the energy is released through isomeric transition with a $\gamma = 661.7$ keV while $\sim$11.1% occurs by internal conversion.

2.2 Radiation Interaction and Energy Loss of Particles in Matter for the Detection of Radioactivity

For both radiation detection methods and radiation attenuation effects of radiation produced by radioactive decays, it is essential to understand the interaction as well as the energy deposition processes of radiation in matter. This chapter describes the main interaction mechanisms of most commonly emitted particles with matter. Due to the different characteristic properties of the initial particles the description is divided in two parts:

- Direct ionization by charged particles;

- Indirect ionization by neutral particles.

Direct Ionization by Charged Particles

The following types of charged particles are considered for this work:

- electrons;

- positrons;

- α-particles.

While traversing the absorber material, charged particles loose the energy continuously. Depending on the particle type and kinetic energy, the specific energy loss varies (see Fig. 2.1a). Also the type of the absorber material has an influence on the specific energy loss (see Fig. 2.1b). The energy loss increases with the decrease of particle velocity towards low velocity until the particle is entirely stopped. Generally the change of kinetic energy, also called *linear stopping power* S, can be described with

$$S = -\frac{dE}{dx}. \tag{2.2.1}$$

Taking the dependence on the particle velocity in account, the Bethe formula [10] can be used to describe the specific energy loss as

$$-\frac{dE}{dx} = \frac{4\pi e^4 z^2}{m_0 v^2} N B \tag{2.2.2}$$

where

$$B \equiv Z \left[\ln \frac{2m_0 v^2}{I} - \ln \left(1 - \frac{v^2}{c^2} \right) - \frac{v^2}{c^2} \right] \tag{2.2.3}$$

with

v = velocity of the primary particle

e = Electron charge

ze = Charge of the primary particle

m_0 = Electron rest mass, 511 [keV c^{-2}]

N = Number density of the absorber material [atoms cm^{-3}]

Z = Atomic number of the absorber material

I = Average excitation and ionization potential parameter of the absorber material.
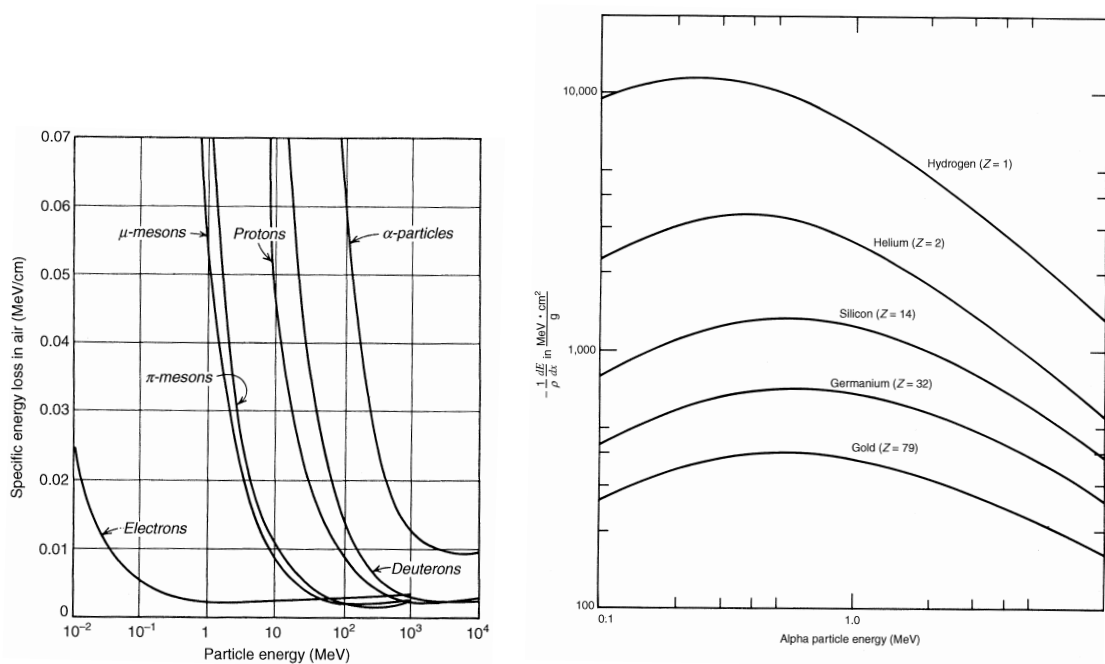
(a) Primary Particle Dependency [19]   (b) Absorber Material Dependency [14]

Figure 2.1: These two figures illustrate the dependency of the specific energy loss on the energy of the primary particle as well as on the particle type itself in (a) and on the absorber material type in (b).

Indirect Ionization by Neutral Particles

Neutral particles have no electric charge. Thus they are not influenced by the coulomb force. The interaction probabilities are much lower and the particles are not stopped in a certain depth but their kinetic energy decreases with the distance travelled in the absorber material. So the penetration depth of neutral particles is generally higher compared to charged particles and strongly depended on the kinetic energy of the particle and the

material type of the absorber. Neutron emission was not considered, due to the fact that radionuclides undergoing spontaneous fission are out of scope of this work. Thus only photons are taken into account as neutral particles.

Photon interaction processes

X-rays and γ-rays are terms to describe photons depending on the production process. The following explanations concentrate on the main photon interactions with matter. When a photon traverses matter, it can interact with a certain probability (cross section) in several ways. Figure 2.2 illustrates the three main photon interactions, that are:

- **Photoelectric absorption**, whereby the photon interacts with an atomic electron, that is then ejected from the atom (see Fig. 2.2a). The energy of the ejected electron is then equal to the kinetic energy of the photon minus the binding energy of the electron;

$$E_e = E_\gamma - E_b \qquad (2.2.4)$$

- **Compton scattering**, whereby the primary photon interacts directly with an electron (see Fig. 2.2b). This reaction results in a recoiled electron and a scattered photon. The kinetic energy of the recoiled electron consists of the energy of the primary photon minus the energy of the scattered photon;

$$E_e = E_\gamma - E_\gamma' \qquad (2.2.5)$$

- **Pair production**, whereby the photon undergoes a transformation into an electron-positron pair. The positron travels only shortly until it meets an electron and the two will annihilate. Thereby two 511 keV annihilation photons are produced (see Fig. 2.2c). In the center of mass system the kinetic energy of the emitted electron as well as of the emitted positron can be described as the kinetic energy of the initial photon minus the rest mass of the electron-positron pair divided by two;

$$E_{e^-} = E_{e^+} = \frac{1}{2}\left(E_\gamma - 2\,m_0 c^2\right). \qquad (2.2.6)$$

Other interaction processes, like for example Rayleigh or Thomson scattering, are not considered further in detail. Beside the information sources mentioned above, [12] served as a good source of information for this subject.
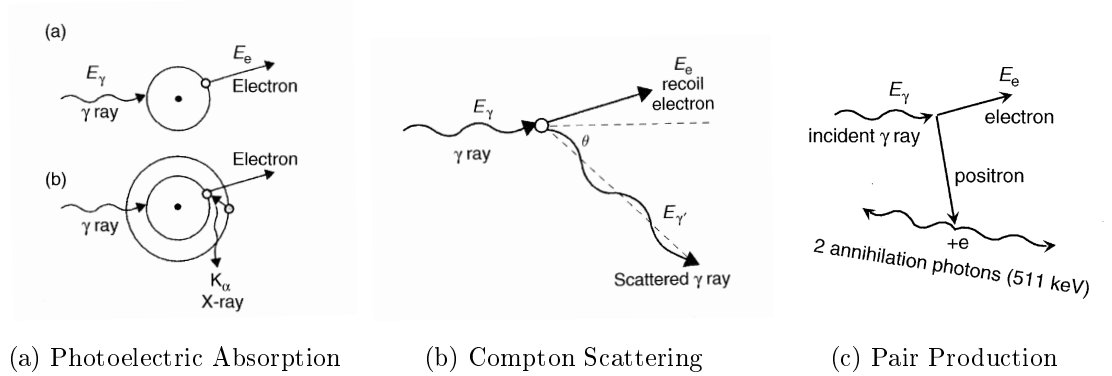
(a) Photoelectric Absorption   (b) Compton Scattering   (c) Pair Production

Figure 2.2: The three figures show the major photon interaction types with matter, whereby the energy of the primary photon is partially transferred to an electron, to a positrons or to a scattered photon. Figures are taken from [12].
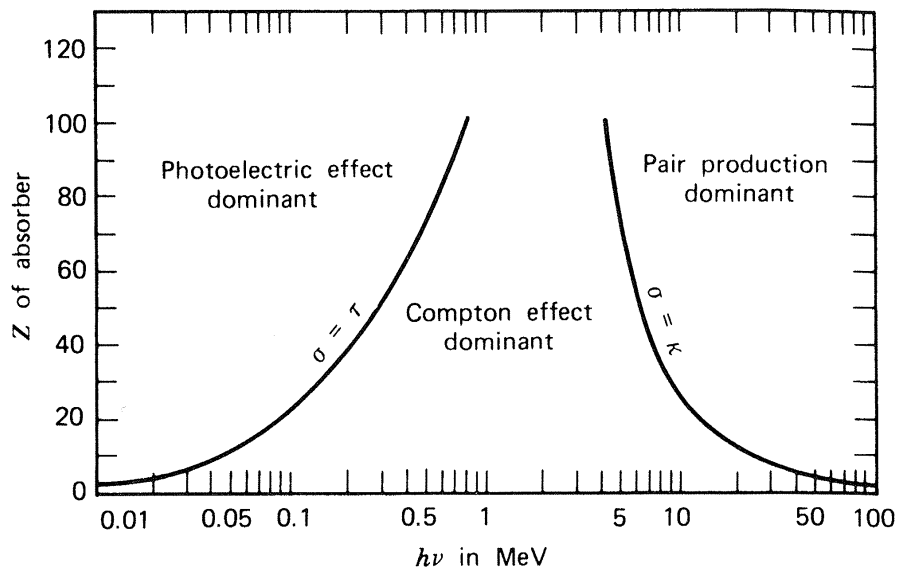
Figure 2.3: The predominance of the three main photon interactions depending on the Z of the absorber material and the photon energy E is illustrated. [20]

The intensity of the photon flux decreases with the penetration depth, due to photon interactions. The decrease can be described with the intensity attenuation formula

$$I = I_0 \, e^{-\mu \, t} \tag{2.2.7}$$

where μ is the *total linear attenuation coefficient* that is given by the sum of the individual attenuation coefficients for the various interactions

$$\mu = \tau + \sigma + \kappa \tag{2.2.8}$$

with

$$I = \text{Intensity after penetrating depth } t$$
$$I_0 = \text{Initial photon intensity before the absorber material}$$
$$t = \text{Penetration depth [m]}$$
$$\mu = \text{Total linear attenuation coefficient [m}^{-1}]$$
$$\tau = \text{Photon attenuation coefficient [m}^{-1}]$$
$$\sigma = \text{Compton scattering attenuation coefficient [m}^{-1}]$$
$$\kappa = \text{Pair production attenuation coefficient [m}^{-1}].$$

The occurrence of the different interaction types is strongly depending on the photon energy as well as on the absorber material. Figure 2.3 shows the predominance of the different interaction types depending on photon energy and atomic number of the absorber material.

The linear attenuation coefficient μ [m^{-1}] is divided by the density of the absorber material ρ [kg m^{-3}] to remove the dependency on the material density and results in the

$$\text{mass attenuation coefficient} = \frac{\mu}{\rho} \ [\text{m}^2 \, \text{kg}^{-1}]. \tag{2.2.9}$$

Figure 2.4 shows the contribution of the different interaction coefficients to the total mass attenuation coefficient of lead, depending on the photon energy. Furthermore it is possible to express the mass attenuation coefficient in terms of the *total cross section* σ

$$\frac{\mu}{\rho} = \sigma \, \frac{N_\text{A}}{M} \tag{2.2.10}$$

where

$$\sigma = \text{Total cross section [m}^2]$$
$$N_\text{A} = \text{Avogadro constant [mol}^{-1}]$$
$$M = \text{Molar mass of the absorber material [kg mol}^{-1}]$$

As displayed in Fig. 2.5 the attenuation coefficient varies with the photon energy and is generally higher for absorber materials with higher atomic mass Z.
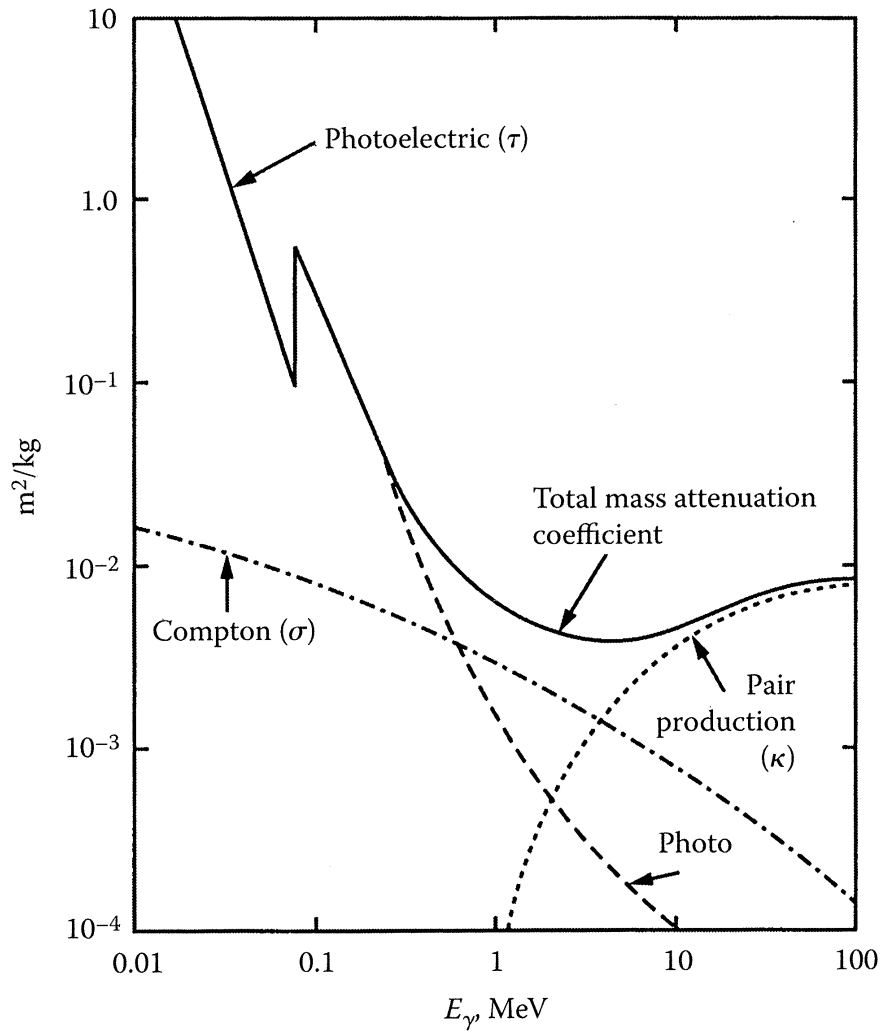
Figure 2.4: The variation of the mass attenuation coefficient $\frac{\mu}{\rho}$ [m^2 kg^{-1}] of lead depending on the photon energy E is illustrated, whereby the fractions of the different photon interactions are displayed as well. [11]
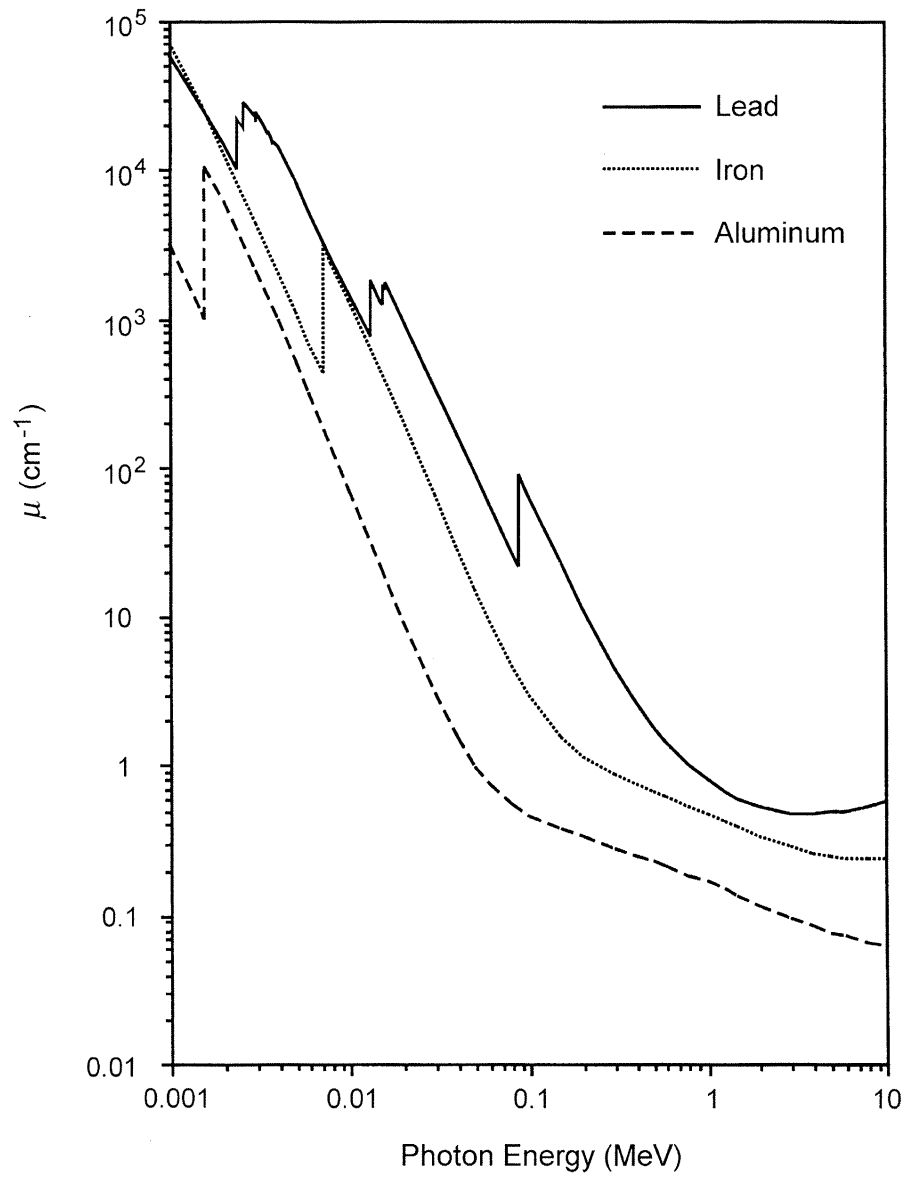
Figure 2.5: Linear attenuation coefficients depending on the photon energy for lead, iron and aluminium [14].

For discussions on photon attenuation and detection, the build-up factor has to be considered as well. Due to the different photon interactions discussed above, photons can be scattered in matter. These scattering effects can lead to a change in direction that could let a photon end up in the detector, even if the the detector would not have been on the initial photon trajectory. Also photons from an annihilation process can scatter into the detector. This increases the photon flux measured in the detector. A rough illustration of this effect can be found in Fig. 2.6. A formal description of the build-up effect can be obtained by adding a *build-up factor B* in Eq. 2.2.7. This build-up factor consists of the ratio of total photons to not scattered photons at a certain point of interest.

$$I = I_0 \, e^{-\mu t} B \qquad (2.2.11)$$

As further explained in [21], for mono-energetic photons the build-up factor can be expressed as

$$B(r) = 1 + \frac{1}{\Phi_0(r)} \int_0^{E_0} dE \, \frac{R(E)}{R(E_0)} \, \Phi_S(r, E), \qquad (2.2.12)$$

where

$$\Phi_0(r, E) = \text{Unscattered photon fluence at position r;}$$

$$\Phi_S(r, E) = \text{Scattered photon fluence at position r;}$$

$$E = \text{Photon energy;}$$

$$E_0 = \text{Initial photon energy;}$$

$$R(E) = \text{Photon energy depending response function.}$$
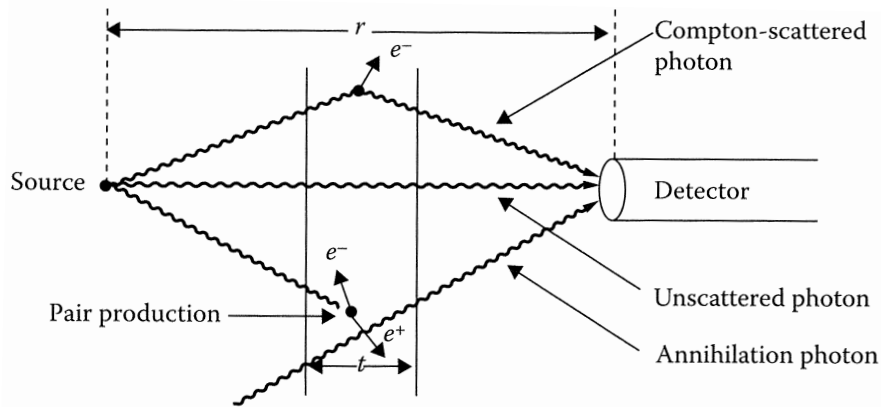
Figure 2.6: Photon build-up illustration for the detection of photons of an isotropic source placed behind a shield, where t is the thickness of the shield and r the total distance between source and detector [11].

2.3   Accelerator Radiation Induced Radioactivity at High Energy Proton Accelerators

When a high energy proton interacts with matter, many secondary particles are emitted which could themselves have a high enough energy to produce further secondaries when they interact, thus creating a nuclear particle cascade [22]. At high energy proton accelerators these nuclear particle cascades, also called hadronic showers, occur due to proton losses in the acceleration process. The hadronic showers consist mainly of neutrons, protons, π^+, π^- and photons. These secondary particles react with the matter on their trajectory. If the particle energy is sufficiently high, activation reactions can take place. During these activation reactions, stable isotopes are transformed into unstable radioisotopes. The resulting radioactivity is called induced radioactivity. Depending on the particle type, on its kinetic energy as well as on the interacting material several different reaction types are possible. The probability for a certain reaction is represented by the reaction cross section. The unit for cross sections is barn $[1\,\text{b} = 10^{-28}\,\text{m}]$. In Appendix A.1 two examples for activation reaction cross sections are illustrated. The major share in activation reactions of high energy proton accelerators results from reactions of neutrons, protons and charged pions. Activation by high energy photons (photo-nuclear reactions) as well as by heavy ions are excluded from this work because their fraction of the total activity is considered to be small. Frequent activation reactions in high energy accelerators like the CERN accelerators [23] are:

At lower energies: Radiative Neutron Capture Reactions,

- (n,γ), e.g. ^{54}Fe(n,γ)^{55}Fe, ^{59}Co(n,γ)^{60}Co

At medium energies: Further Neutron and Compound Nucleus Reactions,

- (n,p), e.g. ^{54}Fe(n,p)^{54}Mn, ^{58}Ni(n,p)^{58}Co, ^{63}Cu(n,p)^{63}Ni
- (n,2n), e.g. ^{23}Na(n,2n)^{22}Na
- (n,α), e.g. ^{27}Al(n,α)^{24}Na
- (p,n), e.g. ^{51}V(p,n)^{51}Cr
- (p,pn), e.g. ^{65}Cu(p,pn)^{64}Cu

At higher energies: Spallation Reactions.

- (n,xn), (n,xp), (p,xn), (p,xp), e.g. ^{27}Al(n,xp)^{22}Na, ^{54}Fe(n,xp)^{44}Ti

CHAPTER 3

Radiation Detection

For radiation detection purposes various different detector techniques and detector types are available. To prove clearance criteria (see Sec. 4.3) different devices are used in the field of nuclear engineering. This work concentrates on the use of a total gamma counter to determine the mass specific activity and on one hand held dose rate meter to determine the ambient dose equivalent rate of the object to be measured.

The work aimed at testing a total gamma detector at the exit of the accelerators, given the existence of the RADOS RTM 661/440 lnc in the Radioactive Waste Section of the CERN Radiation Protection Group, this was taken as candidate. Thus one of the goals of this work was the identification if this device can be used, beside for clearance of waste, also for clearance of objects at the exit of accelerators.

The choice of the AUTOMESS 6150AD6/H together with the scintillation probe AUTOMESS 6150AD-b/H as hand held dose rate meter was taken due to the good experience with this device in the radiation protection group and in agreement with the Swiss authorities.

The basis of counting statistics needed for radiation measurements in the frame of this work as well a short overview of the characteristic limits defined in the norm ISO 11929:2010 are presented in Sec. 3.1 and 3.2. Section 3.3 explains the basics of radiation detection by scintillation light detection. This is the principle of the two measurement devices used, which are described in the two following sections, Sec. 3.4 and Sec. 3.5.

3.1   Statistics

In this section the basic principles of counting statistics are explained. This includes counting statistics for nuclear measurements, statistics for data analysis as well as statistics for device accuracy. Explanations are limited on the needs of this work. Further information, especially about statistics in nuclear engineering can be found in [10] and [11], or more general statistics in [24].

Counting Statistics, Uncertainties and Uncertainty Propagation

The radioactive decay can be considered as a random statistical process. The distribution of the number of radioactive decays for a given time interval follows a Poisson distribution that is defined by a single parameter λ. Considering the expected activity range of this work the corresponding mean values of the counting events are high enough[2] to assume that the discrete Poisson distribution of radioactive decays approaches a continuous Gaussian distribution with $\mu = \lambda$ and $\sigma^2 = \lambda$. Figure 3.1 shows that a Poisson distribution with a mean of 25 already corresponds roughly to a Gaussian distribution with a sigma of 5, whereas a Poisson distribution with a mean of 5 is obviously asymmetric.

Probability Density Function (pdf)

The probability density function $f(x)$ describes the probability distribution for a statistical event of interest. The pdf fulfils the following properties for continuous variables

$$\int_{-\infty}^{\infty} f(x)dx = 1 \tag{3.1.1}$$

or for discrete variables

$$\sum_{i=1}^{N} f(x_i) = 1. \tag{3.1.2}$$

Cumulative Distribution Function (cdf)

The cumulative distribution function $F(x)$ describes the summation of the probabilities of the event of interest for a given pdf between its lower limit and the value x. This results in the cumulative probability that a event takes place within the given limits. This dependence can be mathematically expressed for continuous variables

$$F(x) = \int_{-\infty}^{x} f(x')dx' \tag{3.1.3}$$

---

[2]The expected count rate for the determination of mass specific activity with the RA-DOS RTM 661 (see Sec. 3.4) is in the order of some $10^3 \, \mathrm{counts \, s^{-1}}$ and for dose rate measurements within the clearance process between 50 to $100 \, \mathrm{counts \, s^{-1}}$.
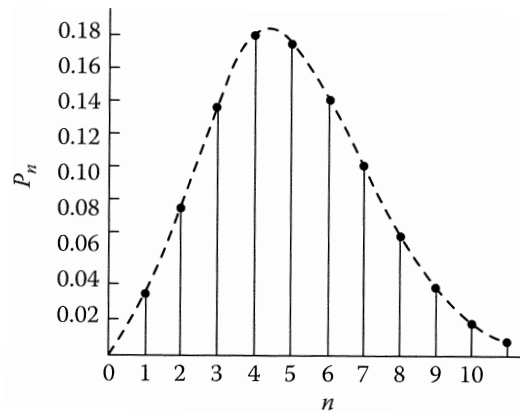
(a) Poisson distribution with $\lambda = \overline{x} = 5$ [11]
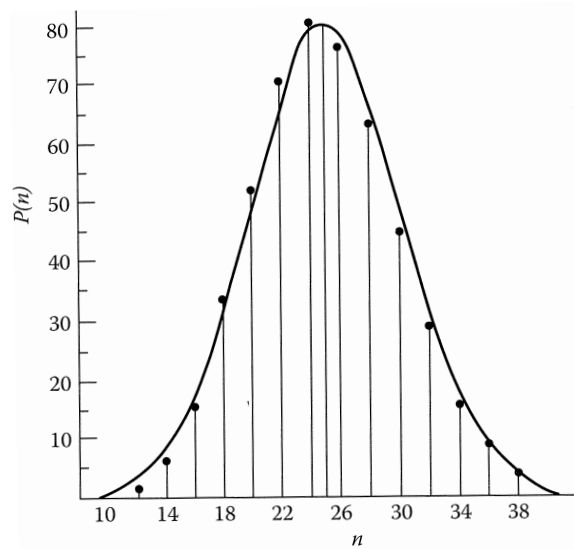
(b) Poisson distribution (points) with $\lambda = \overline{x} = 25$
and Gaussian distribution (line) with $\sigma = \sqrt{\overline{x}} = 5$
and $\mu = 25$ [11]

Figure 3.1: Figure (a) shows a Poisson distribution with $\lambda = \overline{x} = 5$. The shape of the function is asymmetric and cannot be described well by a Gaussian distribution. In (b) a Poisson distribution with $\overline{x} = 25$ is overlaid with a Gaussian distribution with $\mu = 25$ and $\sigma = \sqrt{\overline{x}} = 5$. The points of the Poission distribution are following well the line of the Gaussian distribution.

or for discrete variables

$$F(x_j) = \sum_{i=1}^{j} f(x_i).$$

(3.1.4)

Mean Value

The mean, also called average value, represents the expected value of x for a given distribution function. For a continuous distribution, the mean value $\overline{x}$ is defined as

$$\overline{x} = m = \int_{-\infty}^{\infty} x \, f(x) dx.$$

(3.1.5)

For a discrete distribution, the mean value $\overline{x}$ is defined as

$$\overline{x} = m = \sum_{i=1}^{N} x_i \, f(x_i).$$

(3.1.6)

Variance and Standard Deviation

The two most common quantities that describe the dispersion of a distribution are the variance V and the standard deviation $\sigma = \sqrt{V}$. For a continuous distribution variance and standard deviation are defined as

$$V = \sigma^2 = \int_{-\infty}^{\infty} (x - \overline{x})^2 \, f(x) dx \,,$$

(3.1.7)

with $\overline{x}$ defined by Eq. 3.1.5. For a discrete distribution variance and standard deviation are defined as

$$V = \sigma^2 = \sum_{i=1}^{N} (x_i - \overline{x})^2 \, f(x_i) \,,$$

(3.1.8)

with $\overline{x}$ defined by Eq. 3.1.6. For a Poisson distribution, the standard deviation can be expressed as

$$\sigma = \sqrt{\overline{x}} \,.$$

(3.1.9)

Measurement Uncertainty

A scientific measurement result M is displayed with its *uncertainty* estimate, i.e. an interval in which the real value should be contained with a certain probability, denoted as *confidence level*. Formally, the interval is expressed as the value minus the uncertainty estimate as lower limit and the value plus the uncertainty estimate as upper limit. There are two common ways of denoting an uncertainty estimate. On the one hand the absolute uncertainty E whose dimension is identical to the one of the value,

$$\text{measurement result} = M \pm E \,,$$

(3.1.10)

and on the other hand the relative uncertainty e which is dimensionless and often expressed as a percentage of the value,

$$\text{measurement result} = M \pm e \,, \tag{3.1.11}$$

where

$$e = \frac{E}{M} \, 100 \, [\%] \,. \tag{3.1.12}$$

If the measured value is c_M [counts s^{-1}] the value with its uncertainty estimate can be formalized as the measured value plus and minus (a multiple of) the standard deviation, which is the square root of the measured value

$$\overline{x} \pm \sigma = c_M \pm \sqrt{c_M} \, [\text{counts s}^{-1}] \tag{3.1.13}$$

with Eq. 3.1.9 and $c_M = \overline{x}$ for a confidence level of 68.2 % (see Tab. 3.2).

Uncertainty Propagation

Very often, a measurement result is a function of more than one random variable. The uncertainties of the input variables of the function have to be propagated to obtain the uncertainty of the measurement result. A simple case is sum of two input variables a and b. The corresponding standard deviation can be mathematically expressed as

$$\sigma_{a+b} = \sqrt{\sigma_a^2 + \sigma_b^2} \,. \tag{3.1.14}$$

Further uncertainty propagation rules, e.g. for multiplications or divisions, can be found in [10] or in [11]. The total standard deviation for a combined measurement, consisting of a single measurement of background counts C_B [counts] and a measurement of the counts caused by the radioactive object C_M [counts] is calculated to illustrate the application of Eq. 3.1.14. The measurement time for the background is t_B [s] and for the radioactive object t_M [s]. The total standard deviation can be calculated by

$$\sigma_{total} = \sqrt{\sigma_B^2 + \sigma_M^2} \,. \tag{3.1.15}$$

Substituting

$$\sigma_B = \frac{\sqrt{C_B}}{t_B} \;\; \text{and} \;\; \sigma_M = \frac{\sqrt{C_M}}{t_M} \,, \tag{3.1.16}$$

the total standard deviation results in

$$\sigma_{total} = \sqrt{\frac{C_B}{t_B^2} + \frac{C_M}{t_M^2}} \, [\text{counts s}^{-1}] \,. \tag{3.1.17}$$

Confidence intervals and their limits

The confidence interval is defined by an upper and lower confidence limit and gives a reliable prediction, that a value x of a statistical distribution can be found within this interval, with a certain probability. The limits of the confidence interval x_{lim} are calculated by use of the mean, the quantile k_{1-p} and the standard deviation by

$$x_{lim} = \overline{x} \pm k_{1-p}\,\sigma\,. \tag{3.1.18}$$

The corresponding error probability p is the probability that x does not fulfil the expected criteria, i.e. for a two-side interval x does not lie within the limits x_a and x_b, with

$$x_{a/b} = \overline{x} \pm k_{1-\frac{p}{2}}\,\sigma\,, \tag{3.1.19}$$

and for a single-side interval x exceeds the limit x_a, with

$$x_a = \overline{x} - k_{1-p}\,\sigma \quad \text{or} \quad x_a = \overline{x} + k_{1-p}\,\sigma\,. \tag{3.1.20}$$

For common confidence levels the corresponding error probability as well as the quantile can be found in Tab. 3.1 for single-side intervals and in Tab. 3.2 for two-side intervals. The values are calculated with the error function

$$\text{erf}\frac{x}{\sqrt{2}} = \sqrt{\frac{2}{\pi}} \int_0^x e^{-\frac{t^2}{2}}\,dt \tag{3.1.21}$$

that is related to the cumulative standard normal distribution $E(x)$ [11] by

$$E(x) = \frac{1}{2}\left(1 + \text{erf}\frac{x}{\sqrt{2}}\right)\,. \tag{3.1.22}$$

Table 3.1: Confidence levels together with the corresponding error probability p and quantile k_{1-p} for single-side confidence intervals, $x < x_a$, with $x_a = \overline{x} + k_{1-p}\,\sigma$.

Confidence level [%]	Error probability	Quantile
84.1	0.159	1.00
90.0	0.100	1.28
95.0	0.050	1.64
97.5	0.025	1.96
97.7	0.023	2.00
99.0	0.010	2.33
99.5	0.005	2.58
99.87	0.0013	3.00
99.90	0.0010	3.10
99.95	0.0005	3.30

Table 3.2: Confidence levels together with the corresponding error probability p and quantile $k_{1-\frac{p}{2}}$ for two-side confidence intervals with equal tail area probabilities, $x_a < x < x_b$, with $x_{a/b} = \overline{x} \pm k_{1-\frac{p}{2}}\,\sigma$.

Confidence level [%]	Error probability	Quantile
68.2	0.318	1.00
80.0	0.200	1.28
90.0	0.100	1.64
95.0	0.050	1.96
95.4	0.046	2.00
98.0	0.020	2.33
99.0	0.010	2.58
99.7	0.003	3.00
99.8	0.002	3.10
99.9	0.001	3.30

3.2   Characteristic Limits According to ISO 11929

The International Standard 'ISO 11929:2010' [25], published by the International Organi-
zation for Standardisation (ISO), focuses on three characteristic limits for measurements
of ionizing radiation. These three characteristic limits are:

- The decision threshold;

- The detection limit;

- The limits of the confidence interval.

The decision threshold

The decision threshold, defined as

$$y^* = k_{1-\alpha}\,\tilde{\sigma}(0)\,,\tag{3.2.1}$$

where

$\tilde{\sigma}(0)$ = standard uncertainty of the background effect ;

$k_{1-\alpha}$ = quantile of the standardized normal distribution to avoid the 1st kind error,

gives an indication if radioactivity is present. If a measurement result exceeds the decision
threshold, the measured object is potentially radioactive. The error that this threshold
is exceeded but no radioactivity is present is called *error of the first kind* or *false positive
error*. Its probability is $p_{(1^{st}\text{ kind error})} = \alpha$. For a common confidence interval of 95%,
the resulting quantile for a single-side interval is $k_{1-\alpha} = 1.64$ (see Tab. 3.1).

The detection limit

The detection limit is defined as

$$y^{\#} = y^* + k_{1-\beta}\,\tilde{\sigma}(y^{\#})\,,\tag{3.2.2}$$

where

$\tilde{\sigma}(y^{\#})$ = standard uncertainty of the measurand as a function of the detection limit ;

$k_{1-\beta}$ = quantile of the standardized normal distribution to avoid the 2nd kind error.

The detection limit is the lowest activity that can be quantified with a certain accuracy.
If this threshold is not exceeded but radioactivity is present the error committed is

called *error of the second kind* or *false negative error*. Its probability is $p_{(\text{2nd kind error})}$ $= \beta$. For a common confidence interval of 95% the resulting quantile for a single-side interval is $k_{1-\beta} = 1.64$ (see Tab. 3.1). Figure 3.3 illustrates the detection limit, denoted Minimum Detectable Activity (MDA), as a function of the measurement time for a certain measurement configuration for the RADOS RTM 661. These MDA values were calculated with the Eq. 3.2.2.

The limits of the confidence interval

The confidence interval describes an interval that contains the true value of the measur- and with the specified probability of $p = 1 - \gamma$. The lower limit $y^{\triangleleft}$ and the upper limit $y^{\triangleright}$ can be calculated by

$$y^{\triangleleft} = \ y - k_p\, \sigma(y) \qquad\qquad (3.2.3)$$

$$y^{\triangleright} = \ y + k_q\, \sigma(y) \qquad\qquad (3.2.4)$$

where

$$p = q = 1 - \frac{\gamma}{2} \qquad\qquad (3.2.5)$$

for

$$y \geqslant 4\,\sigma(y) \ \text{ and } \ 0 < y^{\triangleleft} < y^{\triangleright} \qquad\qquad (3.2.6)$$

For a common confidence interval of 95% the resulting quantile for a two-side interval is $k_{1-\frac{\gamma}{2}} = 1.96$ (see Tab. 3.2).

3.3   Scintillation Light Detection

The scintillation process is one of the most common processes for radiation detection. Thereby certain materials produce light by absorbing radiation, i.e. that primary electrons produced by gamma interactions excite the material that then de-excites by emitting photons in detectable wavelengths. The emitted scintillation light is detected by photo-multiplier tubes or photo-diodes and converted into electrical pulses. These pulses are then used as input signal for either counting electronics or radiation spectroscopy analysers. Different organic and inorganic scintillation material types are commercially available. The physical material conditions of the scintillator can vary from solid scintillation crystals to liquid scintillation solutions or to scintillation liquids that are polymerized to solid plastics. This allows a wide range of scintillator sizes and shapes. The properties of the scintillation materials, e.g. light yield, scintillation efficiency, transparency or temperature stability, can be very different so that the choice of the appropriate scintillation material depends strongly on the field of application. Further information to the scintillation process as well as to the variety of scintillation materials, their properties and their field of application can be found in [10] and in [12].

3.4   RADOS RTM 661/440 lnc Clearance Monitor

The RADOS RTM 661/440 lnc, denoted as RADOS RTM 661, is a total gamma counting device for clearance measurements (for the definition of *clearance*, see Ch. 4). The device, shown in Fig. 3.2, is produced by the manufacturer Mirion Technologies (RADOS) GmbH, denoted as RADOS.

Figure 3.2: RADOS RTM 661/440 lnc installed in the CERN ISR (Intersecting Storage Rings) clearance facility of the Radioactive Waste Section of the CERN Radiation Protection Group.

3.4.1   Technical Details

The characteristics of the RADOS RTM 661 are:

Detectors: Six large area plastic scintillation detectors are installed in a $4\,\pi$ detector arrangement with a geometry effect, the ratio between the effective detector surface and the measurement chamber surface, of 60 %. The detector dimension of the top detector as well as of the bottom detector is $50 \,\mathrm{x}\, 50 \,\mathrm{x}\, 5 \,\mathrm{cm}^3$, whereas the detectors in the side walls measure each $80 \,\mathrm{x}\, 50 \,\mathrm{x}\, 5 \,\mathrm{cm}^3$.

Shielding: A lead shielding ensures a low radiation background inside the measurement chamber and thus allows short measurement times at low detection limits. The shielding has a thickness of $3 \,\mathrm{cm}$ in the chamber door as well as in the chamber bottom and a thickness of $5 \,\mathrm{cm}$ in the other chamber walls. Measurements with

the AUTOMESS AD-b showed an ambient dose rate inside the RADOS RTM 661 of 12-15 nSv h^{-1}. A set of MDA values can be found in Tab. 3.3.

Integration: A digital bar code reader is connected to the device and permits to read in objects identification codes to the exclusion of type errors. Furthermore the device can be integrated into the CERN traceability system due to a fast ethernet network connection. A remote network connection can be used to communicate with the device, which is running the operating system QNX 6.5, e.g. for the purpose of data exchange or backup.

Supplement: An integrated scale is used to determine the object mass that is needed to convert the detected activity in mass specific activity. In addition a report printer is connected.

Table 3.3: Minimum detectable activities (MDA) of the RADOS RTM 661/440 lnc for the following parameters (data provided by the manufacturer RADOS): Measurement time of background $t_0 = 180$ s, background radiation $= 0.15\,\mu$Sv h^{-1}, error quantiles $k_{1-\alpha} = k_{1-\beta} = 1.64$.

Radionuclide	MDA			Measurement
	mass < 50 kg	mass < 100 kg	mass < 150 kg	time t_M
	[Bq]	[Bq]	[Bq]	[s]
^{60}Co	60	70	75	30
	45	55	60	60
^{137}Cs	170	195	215	30
	130	150	165	60

3.4.2 Limitations

The following limits have to be considered for the use of the RADOS RTM 661:

Detection of gamma emission only: The scintillation detectors are surrounded by a thin metal housing and are installed behind a stainless steel plate. Therefore the device is neither sensitive to beta emission nor to alpha particles, i.e. a complete radionuclide inventory especially with reliable ratios of *difficult-to-measure radionuclides*[3] to gamma emitting *key radionuclides*[3] has to be provided.

---

[3]Classification into *key radionuclides* and *difficult-to-measure radionuclides* after ISO 21238 [17] (for further information see footnote[1] on page 8)

Total gamma counting: The photon signal is detected without a direct measurement of the photon energy spectra. This also creates the need that a reliable radionuclide inventory is provided by the user.

Homogeneous activity distribution: A homogeneous distribution of the present radioactivity within the object to be measured is assumed both for the default device calibration as well as for the conversion of the gamma signal into activity. This means that either the activity distribution has to be homogeneous or dedicated calibrations for inhomogeneous distributions have to be performed or correction factors for the present measurement situation have to be applied.

Sensitivity on background variations: The device is sensitive on variations of the ambient dose rate in its close vicinity. These variations can be caused e.g. by radon and its decay products, by activated air or by movements of radioactive material . If the presence of such variations is observed, their impact on the measurements has to be quantified.

Object mass limitation: For CERN personal the maximum weight to be lifted by hand is limited to 20 kg due to the CERN safety regulations. At the exit of the accelerators the RADOS RTM 661 measurement chamber has to be charged by hand, thus the maximum mass of the object to be measured is not supposed to exceed 20 kg.

3.4.3   Functionality

In the RADOS RTM 661, six large area plastic scintillation detectors are installed. Around the detectors, a lead shielding with a thickness of 3 cm in the front door as well as in the bottom and with a thickness of 5 cm in all other sides reduces the impact of background radiation on the measurement inside the measurement chamber. The direct measurement data, i.e. the gross count rates of the individual detectors minus the determined background count rates, is then converted in the (mass specific) activity. In order to ensure a reliable conversion, i.e. to allow a conclusion on the clearance or non-clearance of the measured object, several parameters have to be taken into account. Some of these parameters have to be set by the user as measurement input, others are determined by the device itself or are stored in the devices database structure. The combination of different parameters results into different calibration factors, which are used afterwards to convert the direct measurement data from counts per second in the (mass specific) activity.

The following parameters have to be set by the user as input:

Container type: The geometry, the material composition, the mass and the volume of the container influence the measurement signal as well as the reduction of the background signal. For each container type, an individual calibration has to be performed. The mass of the container can be tared and thus excluded from the calculation of the mass specific activity.

Filling level: The filling level indicates up to which height the object fills the container. The filling level can be set to 25 %, 50 %, 75 % or 100 %. For each filling level an individual calibration has to be performed.

Relative radionuclide inventory: A relative radionuclide inventory has to be specified to perform a clearance measurement. The mass fractions have to be normalized to 100 %. The resulting exemption limit (for the definition of *exemption*, see Ch. 4) of the specified radionuclide inventory is calculated automatically and the activity fractions for each radionuclide are provided in the final report.

Disposal path: The user has to specify the path of disposal for the object to be measured. For each path of disposal, different clearance values or safety factors can be assigned.

Material type: The material type of the object has to be set as well. With this information the device can assign a corresponding surface to mass ratio for surface contamination calculations and a natural activity value to be subtracted from the activity result.

The following parameters are determined by or saved in the device:

Radiation background: The count rate due to ambient background radiation and electrical noise.

Weight: The internal scale provides the object mass with a precision of $0.1\,\mathrm{kg}$.

Background reduction: The background reduction is the difference between the background signal detected whereby the measurement chamber is empty and the background signal with the object inside the measurement chamber. The reduction of the background signal can be ascribed to the additional shielding of the detectors by the object as well as to the reduction of the air volume in the measurement chamber due to the presence the object.

Further parameters that are needed for the determination of the calibration factors are partially given by the device manufacturer RADOS, partially provided by the user

and partially determined via individual calibration processes. The calibration of the device consists of a basic calibration and a height calibration. The basic calibration covers the individual detector responses, the measurement chamber geometry and shielding as well as the radiation background in the close vicinity of the device. The basic calibration has to be redone if the device is moved to another location or in case detectors or parts of the measurement electronics are exchanged. The height calibration covers the geometrical effects due to the geometry, the material composition and the material properties of the measurement object as well as of its container. The height calibration has to be performed for each container, material and filling level combination over the full mass range. The mass range spans from object masses of $20\,\mathrm{kg}$ to $400\,\mathrm{kg}$ divided in $20\,\mathrm{kg}$ steps. The calibration is performed with artificial radioactive sources of $^{60}\mathrm{Co}$. Other radionuclides relevant for the measurement are taken into account by using the Leading Nuclide Correlation (lnc) Method (see following paragraph).

The user can chose the norm used for error calculation, error propagation as well as determination of the detection limit. The two possible choices are the German norm DIN 25457 and the international norm ISO 11929. For use at CERN, the ISO 11929 is chosen. Therefore the minimum detectable activity, or detection limit, is calculated with the following equation (see Sec. 3.2 or device documentation)

$$y^{\#} \;=\; k_{1-\alpha}\,\tilde{\sigma}(0)\;+\;k_{1-\beta}\,\tilde{\sigma}(y^{\#}) \tag{3.4.1}$$

with

$$\tilde{\sigma}(y) = \sqrt{\left(\frac{\sigma_w}{w}\right)^2 y^2 + \left[\frac{w}{t_m} - 2\left(r_0\,\sigma_{fw} + \sigma_{qw}\right)\right] y + \sigma_H^2} \tag{3.4.2}$$

$$\sigma_H = w\,\sqrt{f\,\frac{r_0}{t_m} + f^2\,\frac{r_0}{t_0} + r_0^2\,\sigma_f^2 + \frac{q}{t_m} + \sigma_q^2 + 2\,r_0\,\sigma_{fq}} \tag{3.4.3}$$

where

$$r_0 = \text{Background count rate};$$
$$t_0 = \text{Measurement time of the background measurement};$$
$$t_m = \text{Measurement time};$$
$$w = \text{Calibration factor};$$
$$f = \text{Background reduction factor};$$
$$q = \text{NORM-activity count rate};$$
$$\sigma_w = \text{Uncertainty of the calibration factor};$$
$$\sigma_f = \text{Uncertainty of the background reduction factor};$$
$$\sigma_q = \text{Uncertainty of the NORM-activity count rate};$$
$$\sigma_{fw}, \sigma_{qw}, \sigma_{fq} = \text{Correlated uncertainties}.$$

As can be seen in Eq. 3.4.1, the detection limit depends on the background error propagation in combination with the measurement error propagation. For the uncertainty of the background measurement $\tilde{\sigma}(0)$ as well as for the uncertainty of the measurement $\tilde{\sigma}(y^{\#})$, the influence of the measurement time, of the calibration factor, of the background reduction factor as well as of the NORM-activity count rate is taken into account. An illustration of the minimum detectable activity as a function of the measurement time is given in Fig. 3.3. In practice, the RADOS RTM 661 measurement procedure sets the detection limit and the quantiles and calculates then the measurement time needed to achieve the desired detection limit. The detection limit is set to the clearance activity limit that is calculated for the given nuclide inventory. The user has to specify the three quantiles, i.e. the one to avoid the error of the 1$^{\text{st}}$ kind $k_{1-\alpha}$, the one to avoid the error of the 2$^{\text{nd}}$ kind $k_{1-\beta}$ as well as the one for the confidence interval $k_{1-\frac{\gamma}{2}}$. In addition the users sets a minimum and a maximum measurement time. After that, the necessary measurement time for the specified parameters is calculated by the device. If the calculated measurement time is higher than the maximum measurement time set by the user, the device aborts the measurement process and proposes a longer measurement time.
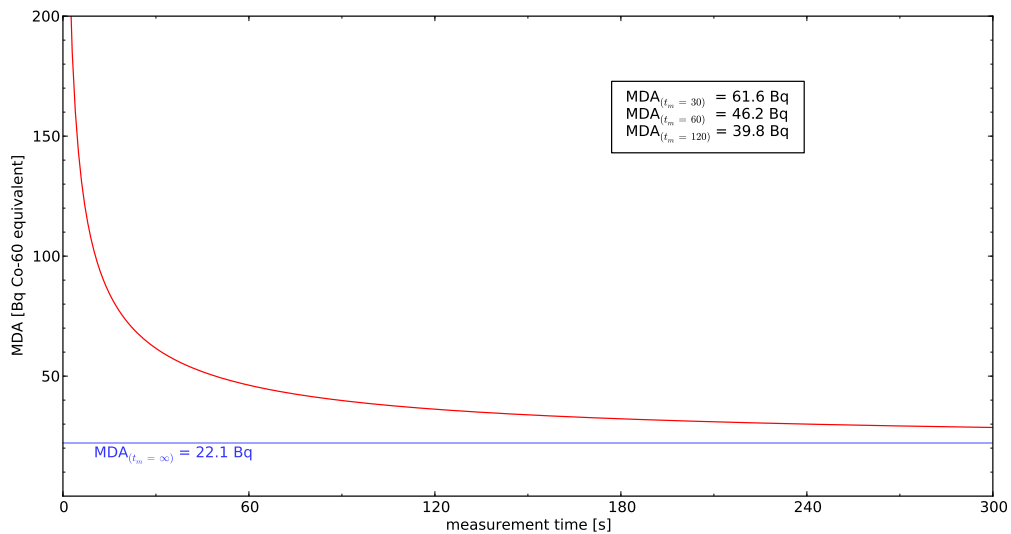
Figure 3.3: Minimum detectable activity (MDA) of the RADOS RTM 661 as a function of the measurement time calculated by using the Eq. 3.4.1 that originates from the norm ISO 11929 [25]. The following parameters, which can be regarded as representative for the present configuration, and a radionuclide inventory consisting of $100\,\%$ of ^{60}Co, were used: $t_0 = 180\,s$, background count rate $= 1000\,counts\,s^{-1}$, calibration factor $= 3.0$, $k_{1-\alpha} = k_{1-\beta} = 1.64$, background reduction factor $= 1.0$, NORM-activity count rate and the uncertainties $\sigma_w, \sigma_f, \sigma_q, \sigma_{fw}, \sigma_{qw}$ and $\sigma_{fq} = 0$. The resulting MDA values reproduce the ones provided by the manufacturer that are given in Tab. 3.3.

3.4.4   Leading Nuclide Correlation (*lnc*) Method

RADOS RTM lnc devices are calibrated with artificial ^{60}Co sources yielding calibration factors, to convert detected net count rates into ^{60}Co activities. Different calibration factors for different measurement conditions, i.e. object geometries, container filling levels, and object masses, are used. To determine the activity of other radionuclides, the Leading Nuclide Correlation (lnc) Method was developed by RADOS. As can be seen in Eq. 3.4.4, the *lnc* factor for the radionuclide b, denoted lnc_b, correlates the detector response in activity ^{60}Co equivalent to an activity of the given radionuclide b. With this method the device distributes the gamma signal fractions to activities for each radionuclide proportional to its gamma emission as well as activity fraction in the relative radionuclide inventory provided by the user. A set of *lnc* factors is delivered by RADOS for the most common radionuclides. In a discussion with RADOS, dedicated to the determination and use of the RADOS *lnc*-factors, the information was received, that the *lnc* factors are determined for an average volume/mass ratio. To ensure the validity over the entire range of geometry and density variety, an additional security factor is added [26]. For radionuclides without a significant γ-emission the *lnc* factor is set to zero. In these cases the activity for this radionuclide is determined by calculation and added to the measured activity. The formal description of the RADOS *lnc* factors is

$$A_b = \frac{M}{lnc_b} \,, \tag{3.4.4}$$

where

$$A_b = \text{Activity of radionuclide } b \left[Bq_b \right];$$
$$M = \text{Measurement result } \left[Bq\,^{60}\text{Co} \right]$$
$$\quad\quad (\text{net machine counts per second converted in activity } ^{60}\text{Co equivalent});$$
$$lnc_b = \text{Correlation factor for radionuclide } b \left[\frac{Bq\,^{60}\text{Co}}{Bq_b} \right].$$

3.4.5   Leading Nuclide Correlation Fitter

As shown in Sec. 7.2.4 and [27], the *lnc* factors are needed for the determination of the resulting gamma signal of a radionuclide inventory if the detector efficiency should be taken into account. For the large number of radionuclide inventories, especially for the wide variety of radionuclides, the *lnc* factors for a lot of radionuclides have to be known. As already mentioned in Sec. 3.4.4, the manufacturer RADOS provided a set of *lnc* factors. Unfortunately, this list of *lnc* factors is neither exhaustive nor covers

all the radionuclides needed for the calculations performed, i.e. the provided set includes radionuclides that are typically found in Nuclear Power Plants, but the set misses *lnc* factors of radionuclides that are specific to accelerator induced activation processes.

Therefore, a fitting method was developped [28] to determine a detector response curve over the photon energy span of interest. The fitting method calculates a mono-energetic efficiency function by using known *lnc* factors and optimizes the parameters of the mono-energetic efficiency function using the *Nelder-Mead simplex algorithm* [29]. Thus the mono-energetic efficiency value lnc_{mono}, as a function of the photon energy of interest, is available for further gamma signal calculations. As illustrated in Eq. 3.4.5, the *lnc* factors for the single radionuclides are determined by using the values of the fitted mono-energetic efficiency function as well as the nuclide specific photon emission probabilities per decay. Because of confidentiality reasons, the values of the single *lnc* factors as well as the fitted response function can not be presented in this public work. The fitting method, the resulting efficiency curve as well as a comparison between the manufacturer *lnc* factor values and the ones determined by the fitter method can be found in the CERN internal documentation of the fitting method [28].

$$lnc_b^* = \frac{\sum\limits_E \epsilon_{b,\,E}\, lnc_{mono}(E)}{\sum\limits_E \epsilon_{\mathrm{Co60},\,E}\, lnc_{mono}(E)} \qquad (3.4.5)$$

where

$$lnc_b^* = \text{Fitted correlation factor for the radionuclide } b \left[\frac{Bq_{\,^{60}\mathrm{Co}}}{Bq_{\,b}}\right];$$

$$E = \text{Photon energy } [\,\mathrm{keV}\,];$$

$$\epsilon_{b,\,E} = \text{Emission probability of a photon with the energy } E$$
$$\text{per decay of radionuclide } b\,;$$

$$\epsilon_{\mathrm{Co60},\,E} = \text{Emission probability of a photon with the energy } E$$
$$\text{per decay of } {}^{60}\mathrm{Co}\,;$$

$$lnc_{mono}(E) = \text{Detector efficiency of the RADOS RTM lnc}$$
$$\text{for the photon energy } E \left[\frac{Bq_{\,^{60}\mathrm{Co}}}{Bq_{\,b}}\right].$$

3.4.6   Sensitivity to Variations of the Radiation Background

Figure 3.4a shows the radiation background signal recorded with the RADOS RTM 661 in December 2012. In December 2012 the accelerator complex was in operation until mid of the month. During this period a variation of the background signal up to 40 %

of the mean was detected. The figure shows a sudden change of the signal height at the shut-down of the accelerator. This indicates clearly the correlation between the acceleration operation and the background variation. The RADOS RTM is located in the CERN ISR (Intersecting Storage Rings) clearance facility, which provides sufficient distance to the accelerator system, so that the detected variation of the background radiation cannot result from residual activity of the accelerator itself nor from the prompt radiation, but most probably from activated air that moves trough the complex tunnel system. Very low quantities of activated air, quite far below the legal clearance limits, can have a measurable influence due to the high sensibility of the RADOS RTM to air activation. In 2013, during the long shut down period of the CERN accelerator complex, constructional sealing works were performed in the tunnel system to ensure that air activation is no longer an issue to be considered for background measurements with the RADOS RTM devices. Figure 3.4b illustrates the radiation background signal recorded in August 2014, after the sealing works were done and the accelerator operations have been restarted. The variation in Fig. 3.4b is $\pm 3\,\%$ which is acceptable. The maximal change rate is in the order of $0.86\,\%$ per hour. Therefore, by repeating the measurement of the radiation background, while performing a measurement campaign, every 60 minutes the maximal associated error stays below $1\,\%$. The Fig. 3.4c shows an overlay of the first half of December 2012 with the second half of August 2014. During these periods the accelerator complex was operational and a direct comparison of the background signal variation is possible. The pattern that is visible even after the sealing works is probably related to the presence and decay of radon and its decay products. Within the two measurement periods the device has been moved some meters and rotated through $90°$. This can explain the change in the background signal height, which is today about $20\,\%$ higher.
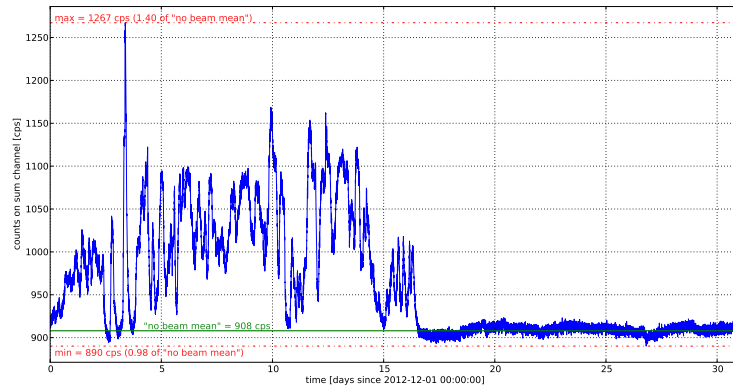
(a) Recorded radiation background signal in December 2012
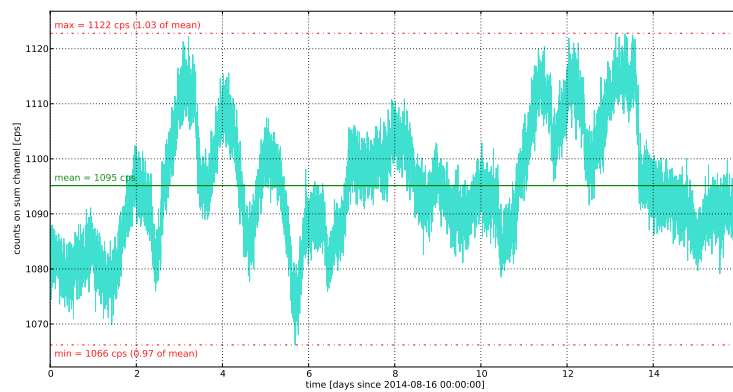
(b) Recorded radiation background signal in August 2014
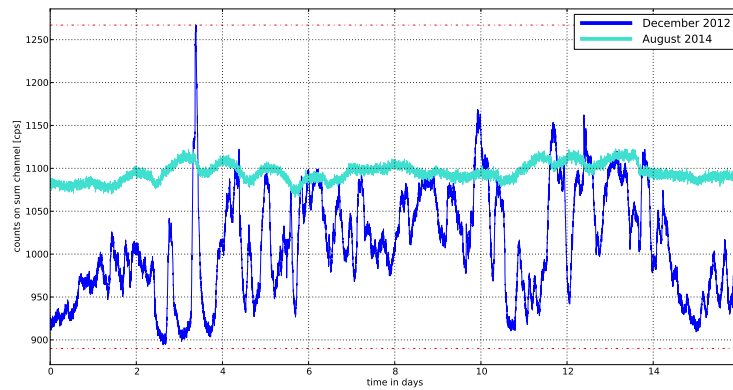
(c) Overlay of second half of August 2014 with first half of December 2012

Figure 3.4: Radiation background variation recorded by the RADOS RTM 661/440 lnc. Figure 3.4a illustrates the variation in December 2012 while shut-down of the accelerator complex and Fig. 3.4b in August 2014 after sealing works were performed in the tunnel system. The remaining background variation is moderate ($\pm 3\,\%$) and perfectly acceptable for the clearance measurements, even though the accelerator complex is operational. For a better comparison Fig. 3.4c shows a partial overlay of the two periods.

3.5   AUTOMESS 6150AD-b/H Dose Rate Meter

AUTOMESS 6150AD-b/H [30], denoted AD-b, is a plastic scintillator probe for the dose
rate meter AUTOMESS 6150AD6/H [31], denoted AD6. The AD-b probe is designed
for measuring the quantity ambient dose equivalent rate H*(10). The probe consists
of a cylindrical three by three inches organic scintillator. The device measures with an
accuracy of $\pm\,40\,\%$ at any direction and an energy within the range of $20\,\mathrm{keV}$ to $7\,\mathrm{MeV}$ as
well as with an accuracy of $\pm\,10\,\%$ in the typical energy range of interests of this work, i.e.
$350\,\mathrm{keV}$ to $2.5\,\mathrm{MeV}$ (see Fig. 3.6). Figure 3.6 shows the response curve of the device as
a function of the photon energy. This dose rate meter/scintillator probe combination is
sufficient sensitive to fulfil the dose rate criterion for the clearance of material according
to the Swiss legislation.

Figure 3.5:   AUTOMESS 6150AD6/H with the scintillation probe AUTOMESS
6150AD-b/H and the Bluetooth adapter AUTOMESS BlueCOM-Adapter 910.1.

A Bluetooth adapter, i.e. AUTOMESS BlueCOM-Adapter 910.1, is available and
allows a wireless connection between the dose rate meter and a computer. The detected
signal is either registered with a frequency of one signal per second or can be integrated
over a certain time interval. The results can be saved in a text file, handled and analysed
by the AUTOMESS software WINCOM as well as by dedicated software solutions. The
devices are shown in Fig. 3.5.
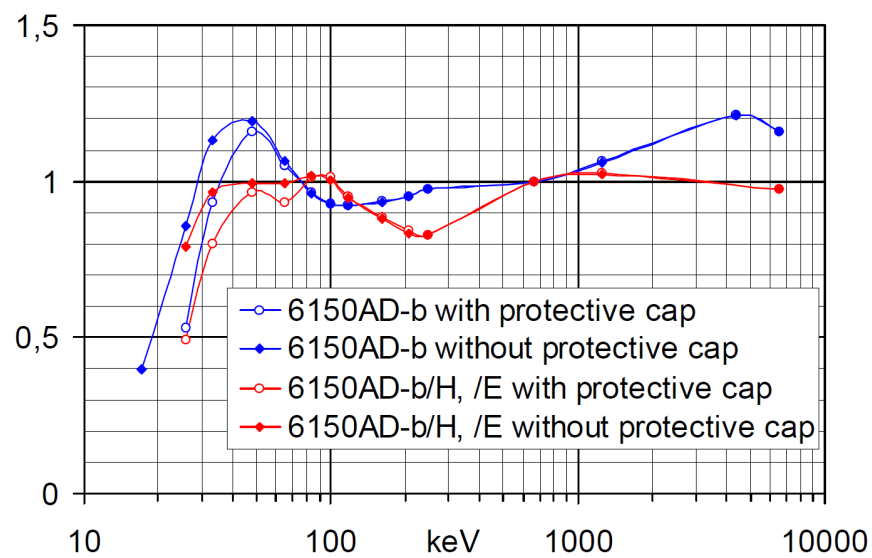
Figure 3.6: AUTOMESS AD-b (/H,/E) photon energy dependent response curves. The curves are normalized to the response value at the energy of ^{137}Cs, i.e. 662 keV. The graphic is taken from [30].

CHAPTER 4

Clearance from Regulatory Control

Due to its location at the boarder between France and Switzerland as well as to its status as an international organisation, CERN has to respect and to follow certain International, European, French and Swiss regulations. This chapters describes roughly the different regulations that exist and are applicable for CERN dealing with clearance from regulatory control of potential radioactive material.

In the context of practices with (potentially) radioactive material, it is essential to distinguish between two different concepts - exemption and clearance.

EXEMPTION On an international level, the International Atomic Energy Agency (IAEA) defines exemption in the Safety Guide RS-G-1.7 [32] and the Safety Series No.115 [33]: *Exemption determines a priori which practices and sources within practices may be freed from the requirements for practices on the basis of their meeting certain criteria. In essence, exemption may be considered a generic authorization granted by the regulatory body which, once issued, releases the practice or source from the requirements that would otherwise apply and, in particular, the requirements relating to notification and authorization.*
with
The criteria for exemption are that (a) the effective dose expected to be incurred by any member of the public due to the exempted practice or source is of the order of 10 μSv or less in a year, and (b) either the collective effective dose committed by one year of performance of the practice is no more than about 1 man Sv or an assessment for the optimization of protection shows that exemption is the optimum option.
and
No practice or source within a practice should be authorized unless the practice produces sufficient benefit to the exposed individuals or to society to offset the radiation

43

harm that it might cause; that is: unless the practice is justified, taking into account social, economic and other relevant factors.

On the European level, the European Commission (EC) does so with the guidance RP122 [34]. In this guidance the EC follows and refers to the definition of the IAEA.

CLEARANCE Definition of clearance by the IAEA in the Safety Guide RS-G-1.7 [32]: *Clearance is defined as the removal of radioactive materials or radioactive objects within authorized practices from any further regulatory control by the regulatory body.*

The EC distinguishes in the EC-RP12 [34] between clearance and exemption as follows: *While clearance levels may be defined generically the decision whether to apply clearance levels is an individual decision of the competent authorities on the basis of a case-by-case evaluation of the practice which gives rise to the contaminated or activated material. The undertaking can judge whether any of the waste streams comply with clearance levels and submit an application to the authorities, but it is for the authorities to decide. In the case of Exemption the holder/receiver makes the decision by looking into exemption rules. The receiver/holder must be in the position to unambiguously make the decision whether to notify his practice to the authorities based on published exemption rules. In the case of possible clearance the practice is already reported or authorised and therefore subject to regulatory control.*

November 5th 2010 CERN signed, in cooperation with the Swiss Federal Council and the French Government, the Tripartite Agreement RS/SR 0.814.592.2 [35]. With this document CERN binds itself to dispose radioactive materials within the possible disposal pathways of both host countries, Switzerland and France, on a fair share basis. The total activity of cleared material is been taking into account for the fair share calculation of this agreement. Clearance of potential activated or contaminated material is not present in French regulations. Thus clearance at CERN follows Swiss regulations, is supervised by the Swiss authorities (BAG/OFSP) and cleared material leaves CERN via Swiss recycle or waste streams. Hence CERN clearance levels have to conform to Swiss clearance levels given in [36]. The Swiss authorities announced that in the near future, the Swiss clearance levels will be revised. It can be expected that the Swiss clearance levels will be attuned with the International or European ones.

4.1 International Clearance Regulations

The International Atomic Energy Agency, IAEA, published the Safety Guide RS-G 1.7 [32] in 2004 and the Safety Report No44 [37] in 2005. Within these documents definitions and guidelines for practices with radioactive materials and sources within practices are given. These guidelines direct to National authorities, regulatory bodies and operating organizations. These guidelines represent the basis for future clearance procedures as well as clearance and exemption levels on European and National levels. In addition the IAEA released in 2012 the Safety Report No67 [38], that gives general and practical advices for the clearance process.

4.2 European Clearance Regulations

The European Communion, EC, released in 2000 the EC-RP122 [34] that is a development out of EC-RP89 [39] and EC-RP113 [40]. In this document the EC follows and refers to the IAEA regulations mentioned above. In the useful comparison study [41], the EC shows that International [32] and European [34] exemption and clearance levels show no major discrepancies.

4.3 National Clearance Regulation of Switzerland

Clearance in Switzerland, at CERN frequently denoted *free-release*, follows the ORaP [36] and ENSI-B04 [42]. For an object to be cleared the conformity with the three clearance criteria, namely with respect to *the ambient dose rate*, *the surface contamination* as well as *the mass specific activity* or *the total activity*, has to be proved. These criteria are explained more in detail in the following paragraphs. A set of common radionuclides with their corresponding Swiss exemption limits as well as their surface contamination limits can be found in the Appendix A.6.i in Tab. A.6.1. The Swiss regulations do not distinguish between clearance and exemption levels. Only one set of values is defined for both concepts. Furthermore no specific clearance is possible, i.e. no different clearance procedures and different clearance levels for different paths of disposal (see clearance concept distinguishing after [34]). Only a general clearance concept is allowed.

Ambient Dose Rate, the maximum allowed ambient dose rate defined in the ORaP [36] is $0.1\,\mu Sv^{-1}$. The dose rate has to be measured in a distance of $10\,cm$ from the surface and the background radiation has to be subtracted.

Surface Contamination, the complete object surface has to measured or a representative sample campaign has to be performed. In the ORaP [36], CS_i is defined as surface contamination limit $[Bq\,cm^{-2}]$ for the radionuclide i averaged over a surface area of $100\,cm^2$. If more than one radionuclide is present in the radionuclide inventory, the additive rule over all radionuclides i has to be applied.

$$CS < 1 \qquad\qquad (4.3.1)$$

with

$$CS \coloneqq CS^{\mathrm{sum}} = \sum_i CS_i^{\mathrm{frac}} = \sum_i \frac{a_i^{\mathrm{surf}}}{CS_i} \qquad\qquad (4.3.2)$$

where

$$
\begin{aligned}
CS_i &= \text{Surface contamination limit of radionuclide } i\ [Bq\,cm^{-2}]\,; \\
a_i^{\mathrm{surf}} &= \text{Surface activity of radionuclide } i\ [Bq\,cm^{-2}]\,; \\
CS_i^{\mathrm{frac}} &= \text{Fraction of the surface activity of radionuclide } i \text{ with} \\
&\qquad \text{respect to the corresponding surface contamination limit}\,; \\
CS^{\mathrm{sum}} &= \text{Fraction of the surface activity of a given radionuclide inventory} \\
&\qquad \text{with respect to the corresponding surface contamination limit}\,.
\end{aligned}
$$

Mass Specific Activity or Total Activity, the ORaP [36] specifies LE_i as clearance limit for mass specific activity $[Bq\,kg^{-1}]$ and $LE_{\mathrm{abs},i}$ as clearance limit for total activity $[Bq]$ for the radionuclide i. The $LE_{\mathrm{abs},i}$ value corresponds to the amount of activity of radionuclide i that, in case of ingestion, would lead to a committed effective dose of $10\,\mu Sv$. This activity related to a mass of $1\,kg$ results in the limit for mass specific activity LE_i. If more than one radionuclide is present in the radionuclide inventory, the additive rule has to be applied to prove compliance with clearance criterion (see Eq. 4.3.4 and Eq. 4.3.5). A proper definition and nomenclature is essential, due to the complexity of use and calculation of these limits and their fractions. The formalized criterion that has to be fulfilled for clearance is

$$LE < 1 \qquad \text{or} \qquad LE_{\mathrm{abs}} < 1\,, \qquad\qquad (4.3.3)$$

with

$$LE \coloneqq LE^{\mathrm{sum}} = \sum_i LE_i^{\mathrm{frac}} = \sum_i \frac{a_i}{LE_i}\,, \qquad\qquad (4.3.4)$$

$$LE_{\mathrm{abs}} \coloneqq LE^{\mathrm{SUM}} = \sum_i LE_i^{\mathrm{FRAC}} = \sum_i \frac{A_i}{LE_{\mathrm{abs},i}}\,, \qquad\qquad (4.3.5)$$

where

$$
\begin{aligned}
LE_i \text{ or } LE_{\text{abs},i} ={}& \text{Swiss exemption limit of radionuclide } i \\
& \left(\text{specific activity } \left[Bq\,kg^{-1}\right] \text{ or total activity } \left[Bq\right]\right); \\
a_i \text{ or } A_i ={}& \text{Specific or total activity of radionuclide } i \left[Bq\,kg^{-1}\right] \text{ or } \left[Bq\right]; \\
LE_i^{\text{frac}} \text{ or } LE_i^{\text{FRAC}} ={}& \text{Fraction of the specific or the total activity of radionuclide } i \\
& \text{with respect to the corresponding Swiss exemption limit}; \\
LE^{\text{sum}} \text{ or } LE^{\text{SUM}} ={}& \text{Fraction of the specific or the total activity of a given} \\
& \text{radionuclide inventory with respect to the corresponding} \\
& \text{Swiss exemption limit}.
\end{aligned}
$$

Equation 4.3.7 shows that the additive rule also has to be applied to determine the specific activity of a nuclide inventory with $LE = 1$ that indicates the activity threshold below which the clearance criterion for the specific activity is fulfilled. Mathematically expressed the activity threshold is written as

$$
a_{LE=1} = \frac{a}{LE}. \tag{4.3.6}
$$

With Eq. 4.3.4 the activity threshold can be calculated by

$$
a_{LE=1} = \frac{\sum\limits_i a_i}{\sum\limits_k \frac{a_k}{LE_k}}. \tag{4.3.7}
$$

Radiological Characterization Technique for Activated Material

Material flow out of the accelerator facilities and experimental zones originates from maintenance, repair and upgrade actions as well as from decommissioning. Due to beam losses during operation and the resulting particle interactions, radioactivity can be induced in certain accelerator components. For safe handling, transport and elimination of these components it is essential to perform a reliable radiological characterization already at the exit of the accelerator.

5.1 Characterization Process Description
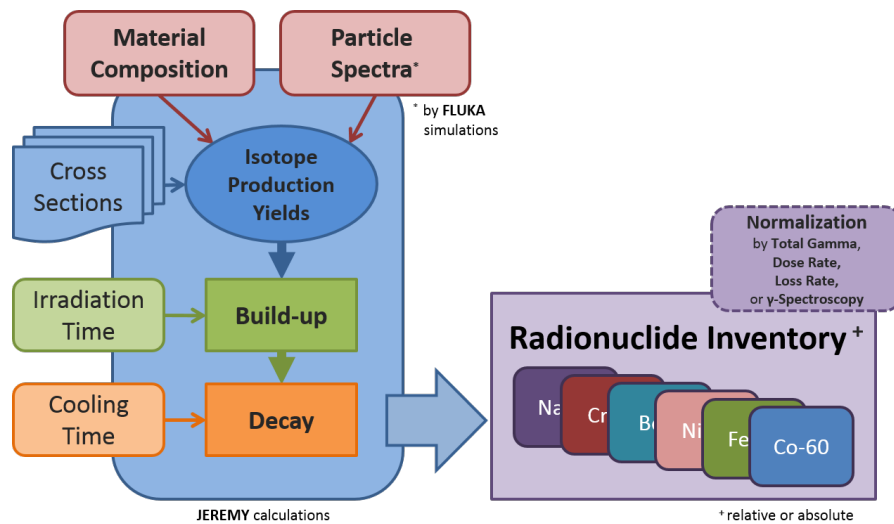
Figure 5.1: Scheme of a possible radionuclide inventory determination process.

The accelerator radiation induced activity can be calculated if certain parameters are

known. A possible way to compute induced activity is shown in Fig. 5.1. In a first step the radionuclide production yields are calculated by folding the particle spectra (particle fluence) with the radionuclide production cross sections as well as the chemical material composition of the component. In a second step, the radionuclide production yields together with the irradiation time profile (see Fig. 5.2) give the specific activities of the various radionuclides, also denoted as radionuclide inventory. In case a normalisation of the specific activities is needed, several different methods can be used to obtain an inventory with normalized activities (see Sec. 5.5).
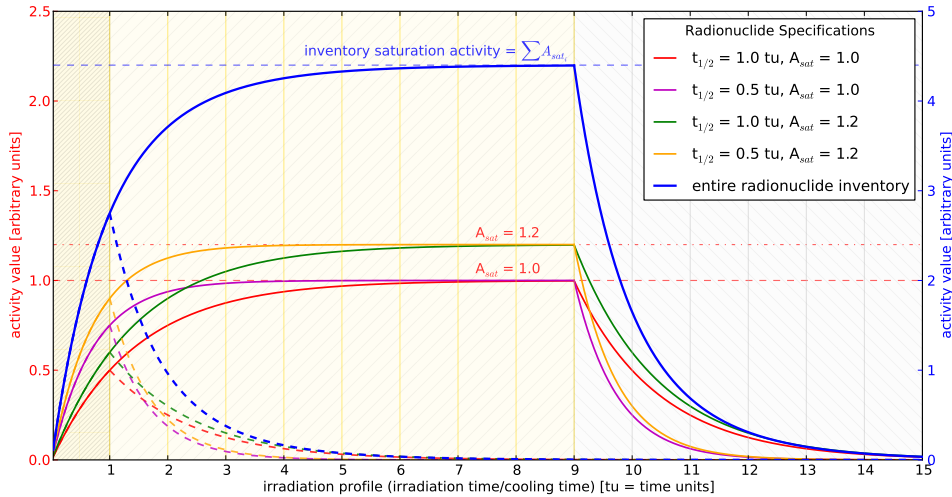
Figure 5.2: Activity evolution over irradiation and cooling time for a radionuclide inventory that consist of four radionuclides with different half-life periods as well as with different production yields for the given conditions. The graph shows an irradiation profile of nine half-life periods of irradiation time and up to six half-life periods of waiting time, whereas the dashed lines represent an irradiation profile of one half-life period of irradiation time and up to 14 half-life periods of waiting time.

5.2 FLUKA

FLUKA [43] [44] is a general purpose Monte Carlo code for calculations of particle transport and interactions with matter, covering an extended range of applications spanning from proton and electron accelerator shielding to target design, calorimetry, activation, dosimetry, detector design, Accelerator Driven Systems, cosmic rays, neutrino physics, radiotherapy, among others.

The FLUKA code can simulate with high accuracy the interaction and propagation of about 60 different particles in matter, including photons and electrons from 1 keV to

thousands of TeV, neutrinos, muons of any energy, hadrons of energies up to 20 TeV (up to 10 PeV by linking FLUKA with the Dpmjet code) and all the corresponding antiparticles as well as neutrons down to thermal energies and heavy ions. The program can also transport polarised photons (e.g., synchrotron radiation) and optical photons. Time evolution and tracking of emitted radiation from unstable residual nuclei can be performed on line.

In FLUKA, complex physics models are used, e.g., for hadron inelastic nuclear interactions, elastic scattering, nucleus-nucleus interactions, transport of charged hadrons and muons and for interactions and transport of low-energy neutrons (< 20 MeV), electrons, photons, optical photons and neutrinos.

Various biasing and scoring functions, the high accuracy and flexibility in the geometry handling as well as the graphical user interface FLAIR [45] can be seen as the strong points or even unique features offered by FLUKA.

For the presented characterization process, FLUKA can be used to simulate particle spectra for certain irradiation conditions. Parameters for these irradiation conditions are the primary particle type and energy, beam position and direction, beam interacting material, object position and materials and geometries of ambient structure.

5.3 ActiWiz

ActiWiz [46] is a CERN in-house developed mathematical model and an associated computer code with a graphical interactive user interface that allows fast and simple analysis of radionuclide production due to beam interactions in the CERN accelerator chain. Part of the ActiWiz project was the analysis and evaluation of common particle spectra of the CERN accelerator tunnel complex. This analysis and evaluation lead to seven irradiation positions that cover common activation situations at CERN. These positions are presented in Fig. 5.3.

5.4 JEREMY

JEREMY [48] [49] is a CERN in-house developed analytical activation calculation code. Following the scheme from Fig. 5.1, JEREMY can be used to determine radionuclide inventories for materials in known irradiation scenarios.

The JEREMY code computes the induced radioactivity from the fluence spectra of the radiation field to which the component of interest is exposed, from the irradiation
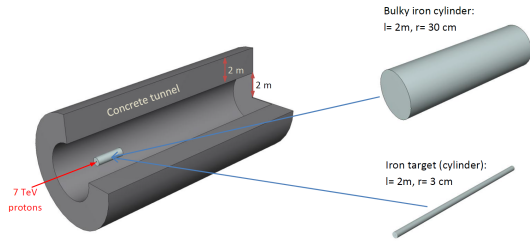
(a) General illustration of the simplified tunnel geometry used for the activation simulations within the ActiWiz [46] project.
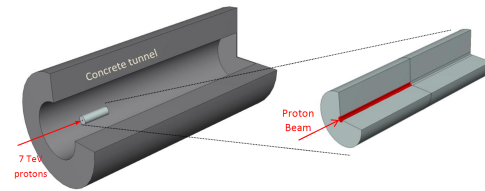
(b) Position #1: Activation occurring at the beam impact area.
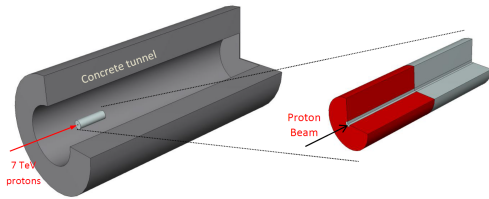
(c) Position #2: Activation occurring within bulky material (e.g. magnet) surrounding the beam impact area.
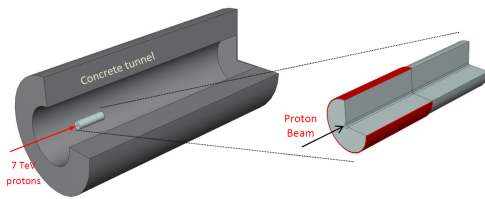
(d) Position #3: Activation occurring adjacent to bulky material (e.g. magnet) surrounding the beam impact area.
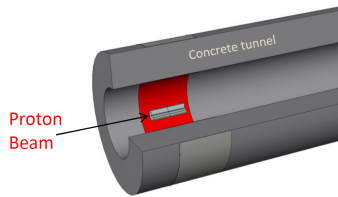
(e) Position #4: Activation occurring close to the concrete tunnel wall (beam loss in bulky material).
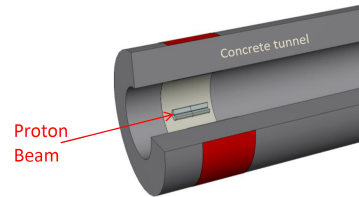
(f) Position #5: Activation occurring behind massive concrete shielding.
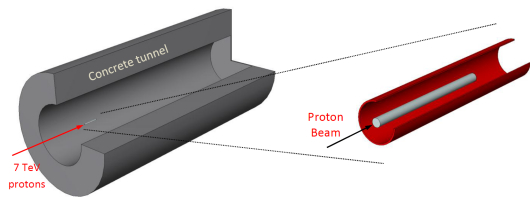
(g) Position #6: Activation occurring at 10 cm lateral distance to the target.
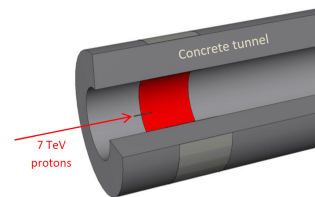
(h) Position #7: Activation occurring close to the concrete tunnel-wall (beam on target).

Figure 5.3: Common activation positions in CERN facilities, whereby the beam impact area (arrow) and the scoring volume (coloured in red) are illustrated in detail. These positions have been determined, analysed and evaluated within the CERN ActiWiz [46] project. Pictures are taken from [47].

history and from the chemical composition of the material. The approach chosen for the computation of the induced radioactivity with the JEREMY code is based on two steps. First, the particle spectra of the radiation environment are calculated via Monte Carlo simulations with codes like FLUKA (see Sec. 5.2), Geant4 [50] or MCNPX [51]. Given these fluence spectra as input, the radioactivity build-up and subsequent decay are calculated using the activation cross-section by the JEREMY code for each radionuclide of interest. The input of the chemical composition has to be in mass weight fractions for all present chemical elements. The fluence spectra for various secondary particles, mainly p, n, γ, π^+ and π^-, have to be provided per primary beam particle. To calculate the radionuclide production yields the JEREMY code needs, together with the chemical composition and the particle spectra as input, radionuclide production cross sections. For JEREMY, the radionuclide production cross sections for neutrons below 20 MeV have been extracted from the JEFF-3.1.1 library [52] including the energy dependent branching ratios between ground state and isomeric states when available. The radionuclide production cross sections for neutrons above 20 MeV as well as for p, π^+ and π^- have been calculated with FLUKA (see Sec. 5.2) where a branching ratio of 50 %/50 % between ground state and the first isomeric state has been assumed for radionuclides with isomeric states. The radionuclide production cross sections for photons up to 200 MeV have been extracted from the TENDL 2010 library [53] that is based on the TALYS code. The radionuclide production yields can be extracted for a direct use or for further calculations in various formats. With the JEREMY code the time evolution can be calculated as well. Therefore the irradiation time and the cooling time have to be specified and, from the radionuclide production yields, the radionuclide inventory is calculated. The decay data used in JEREMY has been extracted from the JEFF-3.1.1 library [52]. No time cut-off is applied in the time evolution, even for very short lived isotopes. Furthermore a normalization of the radionuclide inventory can be done to determine a radionuclide inventory with absolute activities.

5.5 Normalisation of the Calculated Radionuclide Inventory

This section provides a short description of the methods used to normalise the calculated radionuclide inventory to the present activity. A combination of multiple methods might be used depending on the complexity of the radionuclide inventory.

Gamma Spectroscopy

In the characterization process that has been developed in the last years gamma spectroscopy measurements, both in-situ measurements on entire objects or containers and laboratory measurements on taken samples, are used to determine the radionuclide inventory of the gamma emitters. Merging these radionuclide inventories with the ratios of *key radionuclides*[4] to *difficult-to-measure radionuclides*[4], the final radionuclide inventory is computed.

Dose Rate Correlation

For measurement campaigns with many measurement points or objects with repetitive or comparable geometry conditions, i.e. when the dose rate is proportional to the activity level, the radiological characterization can be based on a decision measurement with a dose rate meter. Therefore a transfer function from specific activity to dose rate has to be determined. To obtain the radionuclide inventory with absolute activities, the calculated radionuclide inventory will be normalised with the performed dose rate measurement for each point/object.

Detailed Irradiation Profile

If the full irradiation profile is available, i.e. the particle loss rate together with the corresponding irradiation profile or the absolute particle loss number, the final radionuclide inventory with absolute activities can be entirely obtained by calculations.

RADOS Integral Gamma Counter

The RADOS RTM performs a total gamma counting in a lead shielded measurement chamber with very low radiation background. The device uses a specific correlation factor to correlate the detected gamma signal into activity for the provided relative radionuclide inventory. The total activity as well as the activity fraction for each radionuclides of the inventory is calculated using this correlation factor. Further information about the RADOS RTM and its functionality can be found in Sec. 3.4.

---

[4]Classification into *key radionuclides* and *difficult-to-measure radionuclides* after ISO 21238 [17] (for further information see footnote[1] on page 8)

Radiochemical Analysis

Radionuclides without a significant gamma-ray emission, denoted *difficult-to-measure radionuclides*[4], are difficult to measure or at least it is quite difficult to quantify their activity. For certain radionuclides it is possible to perform a radiochemical analysis of a representative sample. The type of radiochemical analysis depends on the type of radionuclide, e.g. chemical dissolution and separation or pyrolyse both followed by liquid scintillation. These analysis are usually performed outside of CERN by accredited laboratories. Common radionuclides of interests detected by radiochemical analysis are ^{3}H, ^{14}C, ^{36}Cl, ^{55}Fe and ^{63}Ni.

Mathematical Description of the Developed Characterization Method

This chapter shall give a global understanding of the entire characterization process as well as a description of the mathematical structure of the developed method. The single calculation steps are mentioned, even if they and their equations are already explained in the dedicated chapters. In this chapter the explanation are less detailed but focused on the relation in between the different steps.

Exemption Limit Calculations

As explained in Sec. 4.3, one of the clearance criteria to fulfil for the clearance of an object is to prove that its specific activity does not exceed the exemption limit given in [36]. Mathematically this means that (see Eq. 4.3.3)

$$LE < 1 \quad \text{or} \quad LE_{\text{abs}} < 1 \,, \tag{6.0.1}$$

with

$$LE \coloneqq LE^{\text{sum}} = \sum_i LE_i^{\text{frac}} = \sum_i \frac{a_i}{LE_i} \,; \tag{6.0.2}$$

$$LE_{\text{abs}} \coloneqq LE^{\text{SUM}} = \sum_i LE_i^{\text{FRAC}} = \sum_i \frac{A_i}{LE_{\text{abs},i}} \,, \tag{6.0.3}$$

where

$$LE_i \text{ or } LE_{\text{abs},i} = \text{Swiss exemption limit of radionuclide } i$$
$$\text{(specific activity } [\text{Bq kg}^{-1}] \text{ or total activity } [\text{Bq}]) \,;$$
$$a_i \text{ or } A_i = \text{Specific or total activity of radionuclide } i \, [\text{Bq kg}^{-1}] \text{ or } [\text{Bq}] \,;$$
$$LE_i^{\text{frac}} \text{ or } LE_i^{\text{FRAC}} = \text{Fraction of the specific or the total activity of radionuclide } i$$
$$\text{with respect to the corresponding Swiss exemption limit} \,;$$
$$LE^{\text{sum}} \text{ or } LE^{\text{SUM}} = \text{Fraction of the specific or the total activity of a given radionuclide}$$
$$\text{inventory with respect to the corresponding Swiss exemption limit} \,.$$

Radionuclide Inventory Calculations

To be able to prove compliance with the mentioned criterion, a comprehensive knowledge of the composition of the given radionuclide inventory is essential. Therefore the radionuclide inventory for the present material composition and within the given irradiation conditions has to be calculated. The radionuclide inventory is calculated (as explained in Sec. 5.4) via a PHYTON script interfacing the JEREMY calculation engine. The calculation engine calculates a_b, the specific activity of a the radionuclide b, with the following approach

$$a_b = \sum_r \sum_e T_{br} \, P_{re} \, m_e \,, \tag{6.0.4}$$

where

$$a_b = \text{Specific activity of the radionuclide } b \,;$$
$$e = \text{Element of the material composition} \,;$$
$$r = \text{Directly produced radionuclide} \,;$$
$$m_e = \text{Weight fraction of the element } e \text{ in the material composition} \,;$$
$$P_{re} = \text{Production rate of the radionuclide } r \text{ from the element } e \text{ given the selected}$$
$$\text{particle spectra} \,;$$
$$T_{br} = \text{Time evolution matrix that describes the activity build-up and decay}$$
$$\text{of the radionuclide } b \text{ resulting from the production of the radionuclide } r \,.$$

The production rate P_{re}, for a loss rate of one primary beam particle per second, is given by the matrix

$$P_{re} = \frac{N_A}{M_e} \sum_{i=\text{p,n},\gamma,\pi^+,\pi^-} \int \Phi_i(E) \, \sigma_{i,e,r}(E) \, dE \,, \tag{6.0.5}$$

with

$$N_A = \text{Avogadro's constant};$$

$$M_e = \text{Atomic weight for the element } e;$$

$$\Phi_i(E) = \text{Radiation fluence for the various secondary particles}$$

$$\text{per primary beam particles};$$

$$\sigma_{i,e,r}(E) = \text{Abundances weighted average of the production cross sections}$$

$$\text{of the radionuclide } r \text{ produced of the element } e$$

$$\text{for the various secondary particles}.$$

The matrix T_{br} describes the time evolution of the specific activity of radionuclide b. This includes the activity build-up as well as the full decay chain leading to radionuclide b. The matrix T_{br} can be expressed by

$$
\begin{aligned}
T_{br}(t_{\text{irr}}, t_{\text{cool}}) &= \sum_{c,r \to b} \int_0^{t_{\text{irr}}} \sum_{m=1}^{j_c} c_m^c \, e^{-\lambda_m^c \left((t_{\text{cool}} + t_{\text{irr}}) - t_0\right)} \, dt_0 \\
&= \sum_{c,r \to b} \sum_{m=1}^{j_c} \frac{c_m^c}{\lambda_m^c} \left(e^{-\lambda_m^c \, t_{\text{cool}}} - e^{-\lambda_m^c \, (t_{\text{cool}} + t_{\text{irr}})} \right) \\
&= \sum_{c,r \to b} \sum_{m=1}^{j_c} \frac{c_m^c}{\lambda_m^c} e^{-\lambda_m^c \, t_{\text{cool}}} \left(1 - e^{-\lambda_m^c \, t_{\text{irr}}} \right),
\end{aligned}
\tag{6.0.6}
$$

where c runs over all decay chains starting from radionuclide r leading to radionuclide b, with

$$j_c = \text{number of radionuclides in a given decay chain } c;$$

$$\lambda_m^c = \text{total decay rate of the m}^{\text{th}} \text{ radionuclide in decay chain } c;$$

$$c_m^c = \textit{Bateman Coefficient} \text{ [54] [55] of the m}^{\text{th}} \text{ radionuclide in decay chain } c;$$

$$t_{\text{irr}} = \text{irradiation time, the period the object has been in the radiation field};$$

$$t_{\text{cool}} = \text{cooling time, the waiting time since the end of the irradiation period}.$$

Further details to the calculation engine can be found in [49]. The resulting radionuclide inventories include specific activities for a loss rate of one primary beam particle per second.

Inventory Visualisation and Analysis Calculations

The relative activity fractions are calculated to be able to compare radionuclide inventories regardless of the loss rate. The activity fraction a_b^{rel} of the specific radionuclide b,

as a function of the cooling time t_{cool}, is calculated by

$$a_b^{\mathrm{rel}}(t_{\mathrm{cool}}) = \frac{a_b(t_{\mathrm{cool}})}{\sum_i a_i(t_{\mathrm{cool}})} \ . \tag{6.0.7}$$

These values, plotted over the entire cooling time range, give an overview of the nuclide inventory evolution for a given irradiation scenario (see Sec. 7.2.1 or in [27]).

Another important parameter to be calculated is the activity threshold $a_{LE=1}$ that represents the activity below which the clearance criterion of specific activity for a certain radionuclide inventory is fulfilled . This activity can be calculated by (see Eq. 4.3.7)

$$a_{LE=1} = \frac{\sum_i a_i}{\sum_k \frac{a_k}{LE_k}} \ . \tag{6.0.8}$$

The significance of each radionuclide can be illustrated by calculating its fraction of the exemption limit. The relative fraction LE_b^{rel} of the exemption limit LE of a specific radionuclide b, as a function of the cooling time t_{cool}, is calculated by

$$LE_b^{\mathrm{rel}}(t_{\mathrm{cool}}) = \frac{\frac{a_b(t_{\mathrm{cool}})}{LE_b}}{LE(t_{\mathrm{cool}})} \ , \tag{6.0.9}$$

with

$$LE(t_{\mathrm{cool}}) = \sum_i \frac{a_i(t_{\mathrm{cool}})}{LE_i} \ . \tag{6.0.10}$$

As shown in Sec. 7.2.2 and in [27], these relative fractions, plotted over the cooling time, allow to evaluate the importances of the various radionuclides as well as their evolution over the time. Depending on the irradiation and cooling conditions, the list of present radionuclides can be very long. A reasonable cut off, without neglecting significant radionuclides, has to be applied. According to the Swiss guideline for clearance ENSI-B04 [42], the radionuclide inventory must include at least all radionuclides for which the sum of their fractions of the exemption limit equals or exceeds 90 %. Following this guideline, stacked bar plots of the exemption limit fractions were created (as explained in Sec. 7.2.3 as well as in [27]).

Inventory Evaluation Calculations

Beside the general analysis of the resulting radionuclide inventories, a goal of this work was also to integrate the detection efficiency of the RADOS RTM 661. As described in Sec. 3.4, the RADOS RTM 661 works with a single radionuclide calibration for ^{60}Co and efficiency correlation factors, denoted *lnc factors*[5], for all other radionuclides of the given

---

[5]A *lnc factor* correlates the detector response on a gamma-ray signal to the activity of a certain radionuclide. This *leading nuclide correlation* method is used by RADOS within its RTM lnc devices (see Sec. 3.4).

radionuclide inventory. Unfortunately the list of existing *lnc* factors is neither exhaustive
nor includes all radionuclides resulting out of the performed radionuclide inventory calcu-
lations. Therefore a mono-energetic detector efficiency function was computed. This was
done by a mathematical fitter method [28] and in agreement with the device manufac-
turer RADOS [26]. The resulting efficiency curve has to be confidential and for internal
use only. Combining the information of this efficiency curve with data from the nuclear
data base JEFF 3.1.1 [52] allows to calculate the resulting gamma-ray signal of all ra-
dionuclides of the given radionuclide inventories. The signal is calculated for an object
of 1 kg with the activity of $a_{LE=1}$ (see Eq. 6.0.8). The resulting dimension is *Becquerel*
^{60}Co *equivalent per kg*. Following this approach, the detectable gamma-ray signal for the
radionuclide S_b, as a function of the cooling time t_{cool}, can be expressed by

$$S_b(t_{\text{cool}}) = \frac{a_b(t_{\text{cool}}) \sum_E \epsilon_{b\,E}\, lnc_{\text{mono}}(E)}{LE(t_{\text{cool}})} \,, \qquad (6.0.11)$$

with the $LE(t_{\text{cool}})$ defined in Eq. 6.0.10. The total detectable signal S_{total} for the full
radionuclide inventory, as a function of the cooling time, is calculated by the following
formula

$$S_{\text{total}}(t_{\text{cool}}) = \sum_b S_b(t_{\text{cool}}) = \frac{\sum_b a_b(t_{\text{cool}}) \sum_E \epsilon_{b\,E}\, lnc_{\text{mono}}(E)}{LE(t_{\text{cool}})} \,, \qquad (6.0.12)$$

where

$$a_b = \text{Specific activity of the radionuclide } b\,;$$
$$E = \text{Photon energy}\,;$$
$$\epsilon_{b\,E} = \text{Emission probability of a photon with the energy E per decay}$$
$$\text{of radionuclide b}\,;$$
$$lnc_{\text{mono}}(E) = \text{Device efficiency of the RADOS RTM for the photon energy E.}$$

The resulting gamma-ray signal per Swiss exemption limit (see Eq. 6.0.12) condenses
all relevant parameters of a radionuclide inventory for a clearance measurement with
the RADOS RTM device. Hence, this characteristic can be used as classification and
comparison criterion for radionuclide inventories. So the most conservative radionuclide
inventory for a clearance measurement, and therefore the enveloping one for all the
other radionuclide inventories resulting from the same input parameter range, is the
radionuclide inventory that leads to the lowest gamma-ray signal per Swiss exemption
limit.

Detection Limit and Background Radiation Calculations

The device detection limit, denoted minimum detectable activity (MDA), as well as the
radiation background, i.e. photon signal inside the lead shielded measurement chamber

at the actual device location, have to be calculated or transformed into the used dimension Bq ^{60}Co equivalent. For the MDA, a conservative value of 60 Bq ^{60}Co equivalent was taken. This corresponds to the MDA for the detection of ^{60}Co in an object of up to 50 kg with a measurement time of $t_m = 30$ s. The radiation background in the measurement chamber, measured with an AD6/AD-b, corresponds to an ambient dose rate of $12\text{-}15$ nSv h^{-1}. For this radiation background the RADOS RTM 661 detects around 1000 counts s^{-1}, which correlates to 3170 Bq ^{60}Co equivalent by taking the corresponding calibration factor of 3.17 Bq ^{60}Co equivalent/counts s^{-1}.

Radionuclide Replacement Calculations

Under certain conditions it is possible to simplify the radionuclide inventories that serve as input data for the RADOS RTM 661. Therefore activity fractions of certain radionuclides can be replaced by activity fractions of other radionuclides. The goal is to minimise the number of radionuclides and hence the variety as well as total number of input radionuclide inventories as much as possible. The simplified radionuclide inventory has to be equal or more conservative in terms of detectable signal per exemption limit, i.e. the resulting gamma-ray signal per exemption limit of the simplified radionuclide inventory has to be lower than the signal of the initial radionuclide inventory. This condition can be proven by Eq. 6.0.13, which is composed of Eq. 3.4.5 and Eq. 6.0.12.

$$S_{\text{new}} \leqslant S_{\text{old}} \,, \tag{6.0.13}$$

with

$$S = \frac{\sum\limits_{i} a_i \ lnc_i^*}{\sum\limits_{k} \frac{a_k}{LE_k}} \,. \tag{6.0.14}$$

The replacement process consists of three possible cases.

Case A , where

$$lnc_{\text{new}}^* \cdot LE_{\text{new}} \ > lnc_{\text{old}}^* \cdot LE_{\text{old}} \,. \tag{6.0.15}$$

This replacement case leads to a radionuclide inventory that results in a higher gamma-ray signal per exemption limit, i.e. the simplified radionuclide inventory is less conservative. A replacement of this kind should be avoided or only be performed in combination with the introduction of a safety factor on the final exemption limit. The determination of this safety factor has to take the full radionuclide inventory into account.

Case B.1 , where

$$lnc^*_{\text{new}} \cdot LE_{\text{new}} \leqslant lnc^*_{\text{old}} \cdot LE_{\text{old}} \,, \tag{6.0.16}$$

with

$$lnc^*_{\text{new}} > lnc^*_{\text{old}} \,. \tag{6.0.17}$$

An example for this case would be the replacement of an activity fraction of ^{54}Mn by an activity fraction of ^{60}Co. A 'case B.1' radionuclide replacement can generally lead to a more conservative radionuclide inventory or, under certain conditions to a less conservative radionuclide inventory. The worst case scenario is present when the exemption limit of the initial radionuclide inventory is entirely dominated by radionuclides without a significant gamma-ray emission. In this constellation, the replacement of an activity fraction of a radionuclide with a significant gamma-ray emission will affect the resulting gamma-ray signal per exemption limit but has no influence on the exemption limit. As can be concluded out of Eq. 6.0.17, the replacement will evoke a higher signal per exemption limit. Thus it will lead to a less conservative radionuclide inventory. To avoid this extreme scenario, i.e. to ensure that the replacement leads in any case to an equal or more conservative radionuclide inventory, a reduction factor has to be introduced on the exemption limit of the simplified radionuclide inventory that will be used as input for the RADOS RTM device. This worst case reduction factor is equal to the ratio between the gamma-ray signal resulting from the initial radionuclide inventory to the gamma-ray signal resulting from the simplified radionuclide inventory. Mathematical this can be expressed by

$$S_{\text{new}} \cdot f_B = S_{\text{old}} \,, \tag{6.0.18}$$

where

$$f_{B,\,\text{min}} = \frac{lnc^*_{\text{old}}}{lnc^*_{\text{new}}} < 1 \,. \tag{6.0.19}$$

The factor $f_{B,\,\text{min}}$ is the lowest reduction factor for a 'case B.1' radionuclide replacement when the full variety of possible radionuclide inventories is considered. Therefore it guaranties the validity of the 'case B.1' radionuclide replacement. Equation 6.0.19 illustrates that $f_{B,\,\text{min}}$ corresponds to the ratio of the lnc^* factor of the initial radionuclide to the lnc^* factor of the replacing radionuclide. In conclusion, a 'case B.1' replacement can be performed provided that the exemption limit of the simplified radionuclide inventory will be lowered by the factor $f_{B,\,\text{min}}$.

Case B.2 , where

$$lnc^*_{\text{new}} \cdot LE_{\text{new}} \leqslant lnc^*_{\text{old}} \cdot LE_{\text{old}} \,, \tag{6.0.20}$$

with

$$lnc^*_{\text{new}} \leqslant lnc^*_{\text{old}} \,. \tag{6.0.21}$$

A replacement of an activity fraction of ^{22}Na by an activity fraction of ^{60}Co would be an example for this replacement case. Due to Eq. 6.0.20 and Eq. 6.0.21 a 'case B.2' replacement leads stringently to a more conservative radionuclide inventory. That means that the simplified radionuclide inventory has automatically a lower resulting gamma-ray signal per exemption limit. Thus an additional safety factor is not needed but the present activity A_{real} will be overestimated by the factor f'. As shown in Eq. 6.0.22 and Eq. 6.0.23, the maximum possible overestimation can be determined by the factor f'_{max}. This maximum possible overestimation takes place if the radionuclide inventory to be simplified consists only of the radionuclide that will be replaced.

$$\frac{A'_{\text{max}}}{A_{\text{real}}} = f'_{\text{max}} \,, \tag{6.0.22}$$

with

$$f'_{\text{max}} = \frac{lnc^*_{\text{old}} \cdot LE_{\text{old}}}{lnc^*_{\text{new}} \cdot LE_{\text{new}}} \geqslant 1 \,. \tag{6.0.23}$$

In conclusion, a 'case B.2' replacement can be performed without any restrictions and it will add an intrinsically additional safety factor of f' on the activity measurement.

For all replacement cases the lnc^* factors and the $lnc^* \cdot LE$ values play an important role. Therefore the lnc^* factors, the Swiss LE values as well as the $lnc^* \cdot LE$ values of common radionuclides are shown in Tab. 6.1.

Table 6.1: Common radionuclides with their corresponding lnc^* factor, their Swiss exemption limit LE as well as their $lnc^* \cdot LE$ value. The table is sorted by the last column $(lnc_i^* \cdot LE_i)$ in descending order. For confidential reasons it had to be agreed with the manufacturer RADOS that neither the lnc^* factors not the $lnc^* \cdot LE$ values are shown in the public version of this document. Nevertheless the order of the different radionuclides, and hence the eventual possibility for a radionuclide replacement, is well recognisable. The lnc^* factors can be found in [28].

Radionuclide	Half-life	lnc_i^* $[\frac{Bq\,^{60}Co}{Bq_i}]$	LE_i $[\frac{Bq_i}{g}]$	$lnc_i^* \cdot LE_i$ $[\frac{Bq\,^{60}Co}{g}]$
^{44}Ti$^{\#}$	60.0 a	0	2	0.00
^{36}Cl$^{\#}$	302000 a	0	10	0.00
^{55}Fe$^{\#}$	2.75 a	0	30	0.00
^{63}Ni$^{\#}$	98.7 a	0	70	0.00
^{3}H$^{\#}$	12.31 a	0	200	0.00
^{49}V$^{\#}$	330 d	0	600	0.00
^{137}Cs	30.05 a	—	0.8	—
^{65}Zn	244.01 d	—	3	—
^{57}Co	270.9 d	—	50	—
^{60}**Co**	**5.27 a**	**1.000**	**1**	**1.00**
^{22}Na	2.60 a	—	3	—
^{152}Eu	13.33 a	—	7	—
^{56}Co	78.76 d	—	4	—
^{54}Mn	312.13 d	—	10	—
^{110m}Ag	249.78 d	—	4	—
^{58}Co	70.85 d	—	10	—
^{51}Cr	27.70 d	—	300	—
^{64}Cu	12.70 h	—	80	—
^{24}Na	15 h	—	20	—
^{7}Be	53.22 d	—	400	—
^{44}Sc	3.97 h	—	30	—

$^{\#}$ Radionuclide that does not have a significant gamma emission and therefore has a lnc^* factor equal to zero.

Radionuclide Inventories

A comprehensive knowledge of the radionuclide inventories, their evolution over the time, their resulting gamma-ray signal and most important their dependency on the material composition and the irradiation condition, is essential for a reliable radiological characterization for clearance. As illustrated in Fig. 5.1, the following parameters have to be defined for a radionuclide inventory calculation.

Material composition, a list of the chemical elements and their weight fractions of the irradiated object;

Particle spectra, the description of the radiation field at the object position, i.e. particle types, energies and fluences;

Irradiation time, the period the object has been in the radiation field;

Cooling time, the waiting time since the end of the irradiation period.

The choice of the parameter range used in this work is explained in the Sec. 7.1.

7.1 Parameter Description

7.1.1 Material Compositions

The radionuclide inventories resulting from accelerator radiation induced activation vary strongly with the chemical material composition of the irradiated object. Therefore a detailed knowledge of the present chemical material composition and its variation is obligatory. To gain an overview over the variety of different materials present at CERN, a study dedicated to materials used at CERN was performed by Francesco La Torre and the author. On one hand this study was part of the CERN materials guideline project that resulted in the *CERN Materials Guideline Catalogue* [47]. On the other hand this study served to create a knowledge database for materials used at CERN [56]. For this work, reference materials were determined by the use of this knowledge database. The reference materials are representative compounds of the main metal families *steel*, *copper* and *aluminium*. These compounds include all common impurities for each material family. The element weight fraction of the single elements correspond to the maximum allowed in the given norm. All values smaller than ten percent are rounded up to the next larger power of ten. The balance is made with the main component iron, copper or aluminium. Table 7.1 shows the chemical material compositions of these reference materials. The following materials are used as reference materials for the radionuclide inventory calculations of the present work:

- *Common Steel* (Tab. 7.1a);

- *Common Copper* (Tab. 7.1b);

- *Common Aluminium* (Tab. 7.1c);

- *Pure Iron* (100 % Fe).

Pure Iron was used additionally for the inventory calculations. Even if *Pure Iron* is a rather hypothetical material composition, the resulting radionuclide inventories for the reference materials can give an overview of the ratios between certain *difficult-to-measure radionuclides*[6], e.g. ^{55}Fe or ^{63}Ni to corresponding *key radionuclides*[6], e.g. ^{54}Mn or ^{60}Co. A list of common radionuclides and their classification can be found in the Appendix A.6.i in Tab. A.6.1. A further reason for including *Pure Iron* is the wide compound variety in steel and iron compositions. Here the weight fraction of the element cobalt is of peculiar interest (as discussed in the paragraph 'Cobalt Content in Steel' on page 69). So the

---

[6]Classification into *key radionuclides* and *difficult-to-measure radionuclides* after ISO 21238 [17] (for further information see footnote[1] on page 8)

hypothetical material *Pure Iron* can be seen as an extreme composition for the material family steel and iron.

Table 7.1: Determined chemical material compositions of the reference materials *Common Copper*, *Common Steel* and *Common Aluminium*.

(a) *Common Steel*		(b) *Common Copper*		(c) *Common Aluminium*	
Element	Weight [%]	Element	Weight [%]	Element	Weight [%]
Fe	67.6	Cu	86.2	Al	93.5
Cr	18.0	Ni	10.0	Si	1.0
Ni	10.0	Fe	1.0	Cr	1.0
Ti	1.0	Be	1.0	Cu	1.0
Mn	1.0	Mn	1.0	Fe	1.0
Si	1.0	Al	0.1	Mg	1.0
Mo	1.0	Co	0.1	Mn	1.0
Co	0.1	Cr	0.1	Ti	0.1
C	0.1	P	0.1	Ni	0.1
P	0.1	S	0.1	V	0.1
S	0.1	Pb	0.1	Zn	0.1
		Si	0.1	Zr	0.1
		Zr	0.1		

Cobalt Content in Steel

The weight fraction of the element cobalt in steel alloys plays an important role for accelerator radiation induced activation calculations. The resulting radionuclide ^{60}Co that is mainly produced by activation reactions with the element cobalt, is frequently used as *key radionuclide*[6], i.e. used for correlation purposes with *difficult-to-measure radionuclides*[6] due to its well detectable gamma-ray emission. Cobalt is a metal that can be added while producing steel alloys. There is no process-related cobalt content in the steel production process, i.e. if a proper steel production is wanted, no cobalt content has to be present. In some special alloys cobalt is added artificially to improve its physical properties. Steel alloys with added cobalt can reach cobalt contents up to 40 % (e.g. CERN Phynox Steel [56]). In literature research as well as during the project work for the *CERN Materials Guideline Catalalogue* [47] cobalt content notation of < 0.2 % was found frequently within the norm data sheets of steel alloys. This limit can be seen

as the upper limit for high-alloyed steels, where no cobalt is added artificially. Cobalt contents up to the limit of $< 0.2\,\%$ can be explained by the fact that nowadays recycled metals represent a high percentage of the raw material for the steel production. The exact material composition of theses recycled materials is often unknown or below the declaration limits specified in the correspondent standards. For the calculation of ^{60}Co as *key radionuclide*[6] a minimum cobalt content level is required. As already explained, there is no process-related cobalt content in the steel production process. To find a reference value for the minimum cobalt weight fraction in steel a measurement campaign on a set of steel samples was performed to determine the average cobalt content of this set. The results of the entire measurement campaign can be found in the Appendix 7.1.1, whereas an extract of the cobalt weight fractions as well as the iron weight fractions can be found in Tab. 7.2. An average cobalt weight fraction of $0.096\,\%$ has been determined. This value agrees well with the opinion of two material specialists (see [57] [58]). Both specialists mentioned cobalt weight fractions between $0.1\,\%$ and $0.15\,\%$ as common values for cobalt in austenite steel. Therefore, $0.1\,\%$ was included as weight fraction of the element cobalt in the reference material *Common Steel* (see Tab. 7.1a).

7.1.2   Particle Spectra

The particle spectra, consisting the particle type and particle energy distribution are a major parameter for induced radioactivity calculations. The spectra are strongly dependent on the position in the accelerator, the surrounding material, the beam type (particle type) as well as the beam energy. The particle spectra determined within the ActiWiz [46] project were taken as representative particle spectra for common irradiation scenarios at CERN. The ActiWiz spectra, which are calculated by the Monte-Carlo code FLUKA [43] [44], are combinations of the object position and the nominal beam energy of the accelerator facility. In the ActiWiz spectra, neutrons, protons, and charged pions are taken into account. For the present work, a set of seven common ActiWiz positions was taken (see Fig. 5.3). The nominal beam energies of the main CERN accelerator facilities were considered for the radionuclide inventory calculations, i.e.:

- PSB, with $1.4\,\mathrm{GeV}$;

- PS, with $14\,\mathrm{GeV/c}$;

- SPS, with $400\,\mathrm{GeV/c}$;

- LHC, with $7\,\mathrm{TeV}$.

Table 7.2: Iron and cobalt weight fractions in a set of stainless steel samples sorted by the cobalt content in descending order. The weight fractions were determined by optical emission spectroscopy (OES) by a device denoted 'PMI-MASTER Pro' (Oxford Instruments). The full determined sample compositions as well as pictures of the samples can be found in the Appendix A.4.

ID	Fe [%]	Co [%]
X04	69.6	0.015
4B	68.0	0.031
4A	68.7	0.032
1B	69.3	0.051
1A	69.8	0.054
X01	69.4	0.056
2B	67.6	0.089
2A	67.7	0.091
6A	69.1	0.110
6B	69.0	0.110
5B	69.6	0.135
5A	69.7	0.141
X03	70.2	0.146
X02	70.6	0.154
3B	68.9	0.156
3A	69.5	0.161
mean	69.2	0.096

7.1.3   Inventory Time Evolution - Activity Build-up and Decay

Specific irradiation and cooling times have to be set to determine the evolution of the radionuclide inventories over time. The irradiation times are used to calculate the activity build-up during irradiation and the cooling times are required to calculate the radioactive decay after beam stop up to the time of interest. The following periods were chosen as irradiation times to cover common situations for CERN material.

60 days, a very short irradiation period that is the typical time span between two technical stops;

1 year, a short irradiation period, e.g. a typical interval between shut-downs;

3 years, a medium-length irradiation period that corresponds to a typical short technical life time of an object placed in the accelerator;

10 years, a long irradiation period, e.g. a typical medium technical life time of an object placed in the accelerator;

30 years, a very long irradiation period that represents the typical nominal life time of the CERN accelerators.

Together with the irradiation positions and the accelerator beam energies, this results in 7 *positions* x 4 *energies* x 5 *irradiation times* = 140 *irradiation scenarios* per material composition that have to be calculated.

   To cover the entire radiological characterization of materials that are taken out of the machines during urgent technical interventions up to materials with long storage periods for clearance purposes, a wide span of cooling times has to be taken into consideration. For this work, a cooling time range from 1 day up to 30 years was considered to be adequate. To cope the evolution of the initial radionuclide inventory over the mentioned cooling time span, the following 51 cooling times were set explicitly,

   • 1 to 7 day(s), i.e. for maintenance interventions;

   • 1 to 5 week(s), i.e. administrative time before immediate shipping or tooling;

   • 1 to 12 month(s), i.e. non time-critical shipping or tooling;

   • 1 to 30 year(s), i.e. maximal waiting period for clearance.

For the given 140 irradiation scenarios, this leads to 7140 radionuclide inventories per considered material composition that have to be calculated.

7.1.4 Calculation Engine - the JEREMY Code

The radionuclide inventories are calculated with a script written in the programming language PYTHON interfacing the analytical code JEREMY [48]. The JEREMY code calculates the activity for each radionuclide for the given parameters with the mathematical approach (see Sec. 5.4). Further explanations of the JEREMY code can be found in Sec. 5.4 as well as in [48] and [49].

7.2   Radionuclide Inventory Calculation and Visualisation

The enormous amount of 28560 radionuclide inventories had to be calculated, i.e. 7140 radionuclide inventories for each of the four selected reference materials. Therefore the calculations were automatised and performed by a PYTHON script. Additional, to facilitate the use and the understanding, a clear illustration of the calculation results is needed. Thus, four plot types were developed to illustrate the calculation results. In these four plots, the values of interest are plotted over the cooling time span. This allows a full overview of the entire time evolution. These plots were produced for each of the 140 irradiation scenarios per considered reference material and are published as a result catalogue in a CERN technical report [27], a 600-page document. The different plot types, i.e. the *Activity Fraction Plot*, the *LE Fraction Plot*, the *LE Fraction Stack Plot* and the *Gamma Signal Plot*, are explained in detail in the following sections, whereby the plots were calculated for *Common Aluminium*, which was irradiated for *30 years* in the *PSB* at the *ActiWiz position #4*.

7.2.1 Activity Fraction Plot
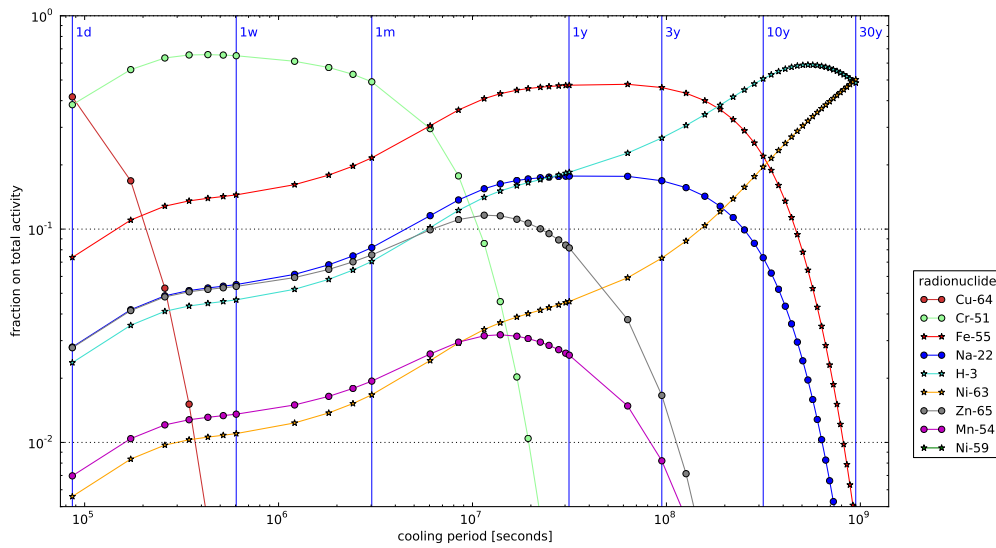
Figure 7.1: Activity fractions over the cooling time.

Figure 7.1 illustrates the fraction of the specific activity for the various radionuclides. One plot is made per irradiation scenario and the inventory time evolution is plotted over the cooling time. The line markers used for activities of *key radionuclides*[7] are circles whereas for activities of *difficult-to-measure radionulides*[7] stars are used as line markers. The activity fraction $a_b^{\text{rel}}(t_{\text{cool}})$ of the radionuclide b for the cooling time t_{cool} is calculated by (see Eq. 6.0.7)

$$a_b^{\text{rel}}(t_{\text{cool}}) = \frac{a_b(t_{\text{cool}})}{\sum_i a_i(t_{\text{cool}})} \, . \tag{7.2.1}$$

_____

[7]Classification into *key radionuclides* and *difficult-to-measure radionuclides* after ISO 21238 [17] (for further information see footnote[1] on page 8)

7.2.2 Exemption Limit (LE) Fraction Plot
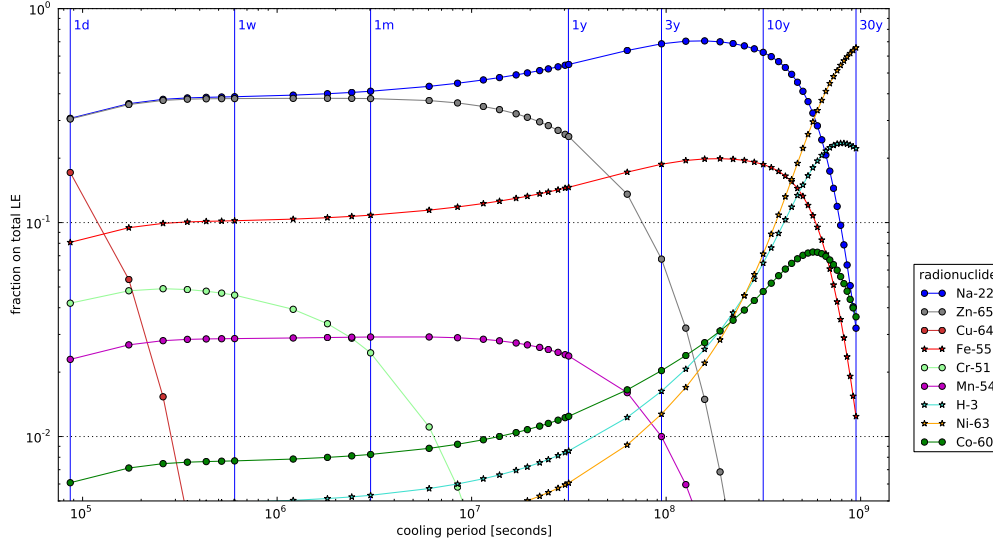
Figure 7.2: LE fractions over the cooling time.

The LE_i value, i.e. the Swiss exemption limit for the specific activity of the radionuclide i, is taken from [36]. The LE fraction plot(see Fig. 7.2) shows for each radionuclide its fraction of the corresponding LE of the entire radionuclide inventory. This permits an evaluation of the importance of each radionuclide for the clearance of the chosen material under the given irradiation and cooling conditions. The relative fraction LE_b^{rel} on the LE of a specific radionuclide b for a cooling time t_{cool} is calculated by (see Eq. 6.0.9)

$$LE_b^{\mathrm{rel}}(t_{\mathrm{cool}}) = \frac{\frac{a_b(t_{\mathrm{cool}})}{LE_b}}{LE(t_{\mathrm{cool}})} , \qquad (7.2.2)$$

with (see Eq. 6.0.10)

$$LE(t_{\mathrm{cool}}) = \sum_i \frac{a_i(t_{\mathrm{cool}})}{LE_i} . \qquad (7.2.3)$$

7.2.3   Exemption Limit (LE) Fraction Stack Plot
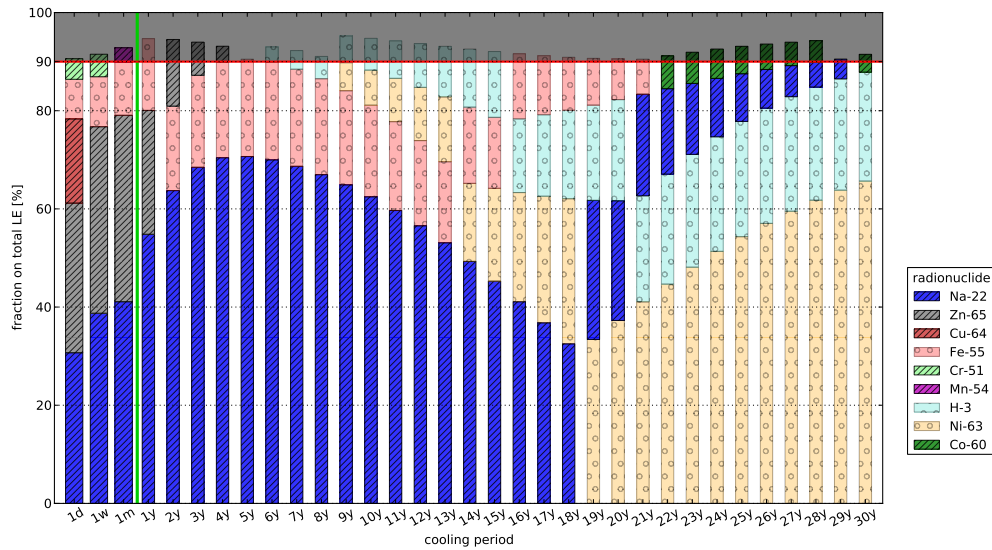
Figure 7.3: LE fractions stacked up to at least 90 % over the cooling time.

Following the ENSI guideline B-04 [42], all radionuclides that contribute together to more than 90 % to the fraction of the clearance limit LE (sum of all contributions) have to be taken into account for the activity determination. Therefore the fractions of LE (see fraction plot Fig. 7.2 and Eq. 7.2.2) were sorted and plotted up to a total value of $LE \geqslant 0.9$. Figure 7.3 shows the stacked LE fraction plot whereby the hatch of the color bar indicates for each radionuclide if the radionuclide can be classified as *key radionuclide*[8], i.e. indicated by lines as hatch with intensive colors, or as *difficult-to-measure radionuclide*[8] which are indicated by small circles as hatch and plotted with pastel colors.

---

[8]Classification into *key radionuclides* and *difficult-to-measure radionuclides* after ISO 21238 [17] (for further information see footnote[1] on page 8)

7.2.4   Gamma Signal Plot
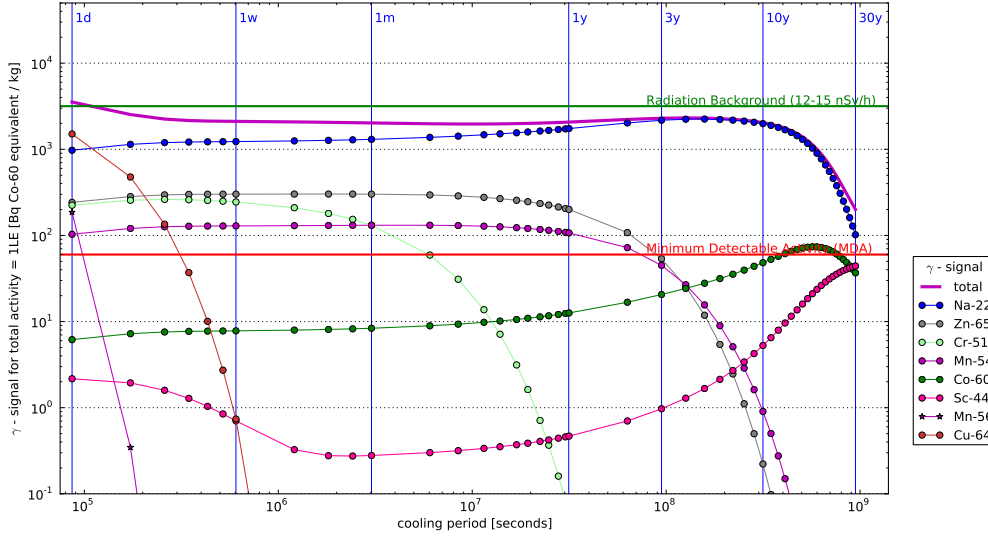
Figure 7.4: Resulting gamma-ray signal over the cooling time.

Figure. 7.3 shows the detectable gamma-ray signal for each single radionuclide as well as for the entire radionuclide inventory for a given irradiation scenario and cooling time combination. The signal is calculated by taking into account the detector efficiency of the RADOS RTM 661/440 lnc device. The determination of the mono-energetic detector efficiency curve is explained more in detail in 3.4.5 and in [28]. The signal is calculated for an object of $1\,kg$ with the activity of $1\,LE$. So the resulting dimension is $Becquerel\,^{60}\mathrm{Co}\,equivalent\,per\,kg$. The detectable signal for the radionuclide S_b, depending on the cooling time t_{cool}, can be expressed as (see Eq. 6.0.11)

$$S_b(t_{\mathrm{cool}}) = \frac{a_b(t_{\mathrm{cool}}) \sum_E \epsilon_{b\,E}\, lnc_{\mathrm{mono}}(E)}{LE(t_{\mathrm{cool}})}\,, \qquad (7.2.4)$$

with the $LE_{t_{\mathrm{cool}}}$ defined in Eq. 7.2.3. The total signal S_{total} is calculated with the following formula (see Eq. 6.0.12)

$$S_{\mathrm{total}}(t_{\mathrm{cool}}) = \sum_b S_b(t_{\mathrm{cool}}) = \frac{\sum_b a_b(t_{\mathrm{cool}}) \sum_E \epsilon_{b\,E}\, lnc_{\mathrm{mono}}(E)}{LE(t_{\mathrm{cool}})}\,, \qquad (7.2.5)$$

where

$$a_b = \text{Specific activity of the radionuclide } b\,;$$
$$E = \text{Photon energy}\,;$$
$$\epsilon_{b\,E} = \text{Emission probability of a photon with the energy } E \text{ per decay of}$$
$$\text{radionuclide } b\,;$$
$$lnc_{\mathrm{mono}}(E) = \text{Mono-energetic device efficiency of the RADOS RTM for the photon}$$
$$\text{energy } E\,.$$

The device MDA as well as the radiation background, i.e. the photon signal inside the lead shielded measurement chamber at actual device location, are integrated as additional lines in the plot. For the MDA, a conservative value of $60\,Bq\,^{60}$Co *equivalent* was taken. This corresponds to the MDA for the detection of ^{60}Co in an object of up to $50\,kg$ with a measurement time of $t_m = 30\,s$. The plotted radiation background corresponds to an ambient dose rate of $12-15\,nSv\,h^{-1}$. Under this background conditions the device detects around $1000\,counts\,s^{-1}$, which correlates to $3170\,Bq\,^{60}$Co *equivalent* by using the correspondent calibration factor of 3.17.

7.2.5   Visualisation Plot Catalogue

The four plots, i.e. the *Activity Fraction Plot*, the *LE Fraction Plot*, the *LE Stack Plot* and the *Gamma Signal Plot*, were produced for each of the 140 irradiation scenarios per considered reference material. All visualisation plots have been put together in a 600-page CERN technical report. This report is available as [27]. Furthermore, the visualisation plot set per reference material that includes the most conservative resulting radionuclide inventory[9] is shown in Appendix A.3.i, for the four considered materials calculated over the full parameter range and in Appendix A.3.ii, for all considered materials calculated over a limited parameter range. The limited parameter range, defined more in detail in Sec. 7.3, sets the upper limit for the cooling time range to two years of cooling.

---

[9]The most conservative radionuclide inventory in terms of the lowest resulting gamma-ray signal per Swiss exemption limit for an activity of $LE = 1$ and for object masses up to one kilogram, by taking the detector efficiency of the RADOS RTM 661 into account.

7.3   Synthesis of the Radionuclide Inventory Calculations

The resulting gamma-ray signal per Swiss exemption limit, which is explained more in detail in Chapter 6 as well as in Sec. 7.2.4, condenses the major parameters of a radionuclide inventory. Hence, this characteristic can be used as classification and comparison criterion for radionuclide inventories. So the most conservative[10] one among a selection of radionuclide inventories, i.e. the enveloping one while using it as input radionuclide inventory for the RADOS RTM 661, is the radionuclide inventory that leads to the lowest gamma-ray signal per Swiss exemption limit for the given selection. Therefore, the dependency of the resulting gamma-ray signal on the different input parameters as well as its evolution over the time were studied more in detail. The results of these studies are illustrated in this section. Within this work, the result span for two sets of input parameters were calculated and evaluated.

First the analysis was performed over the complete parameter range, which is defined in Sec. 7.1 for each reference material. This gives a global view of the entire subject and works out the limits of the characterization method used. The resulting gamma-ray signal values per exemption limit for each reference material as well as the corresponding radionuclide inventory for the most conservative[10] and therefore enveloping case are shown in Sec. 7.3.1.

Out of the results from this first analysis a second parameter range was defined. The goal of a second parameter range was to find the parameter restrictions that lead to radionuclide inventories that result, for all considered scenarios as well as for all considered materials, in a gamma-ray signal per exemption limit that is higher than the device detection limit of the RADOS RTM 661. So by analysing the resulting gamma-ray signal tables, especially Tab. 7.6, the parameter span was decreased. To be more exact, the cooling time range was reduced to cooling times not longer than two years in comparison to cooling times up to 30 years of the full parameter range. For this limited parameter range, the resulting gamma-ray signal values per exemption limit for each reference material as well as the corresponding radionuclide inventory for the enveloping case are shown in Sec. 7.3.2.

Tables 7.3 - 7.6 show the analysis results of the radionuclide inventory study for the four considered materials for full parameter range, whereas Tab. 7.8 - 7.11 include the analysis results for the modified parameter range.

The tables include the resulting gamma-ray signal as function of the irradiation time as well as of the ActiWiz irradiation position (see Fig. 5.3). Each shown minimum

---
[10]See footnote[9] on page 79.

gamma-ray signal value is taken over all 51 selected cooling times (see Sec. 7.1.3) and all considered accelerator beam energies. The beam energies of the four main CERN accelerators PSB, PS, SPS and LHC (see Sec. 7.1.2) were taken into account. Thus each matrix element indicates the lowest resulting gamma-ray signal of $51 \times 4 = 204$ calculated radionuclide inventories. The gamma-ray signal value is accompanied by the cooling time for that this value is reached. The absolute minimum for each reference material is shown in the lower right corner. This value represents the lowest resulting gamma-ray signal of 7140 calculated radionuclide inventories. A red colour font indicates a calculated resulting gamma-ray signal that is lower than the device MDA. For these calculations the device MDA was assumed to be 60 Bq ^{60}Co $equivalent$, which is a rather conservative device MDA of the RADOS RTM 661 (see Sec. 3.4 and Tab. 3.3). If the resulting gamma-ray signal value is below the device MDA, the accompanying value in parentheses represents the cooling time for that the resulting gamma-ray signal of the corresponding radionuclide inventory falls for the first time below the MDA.

At the end of each section, a table can be found including the weight fractions for the most conservative radionuclide inventory[11] per reference material. Hence, Tab. 7.7 shows the most conservative radionuclide inventories[11] for the entire study and Tab. 7.12 shows the corresponding ones for the limited parameter range. These radionuclide inventories can be used as enveloping input inventories for the RADOS RTM 661 to cover the selected reference materials within the chosen parameter range.

---

[11]See footnote[9] on page 79.

7.3.1 Detectable Gamma Signals per Exemption Limit and Corresponding Radionuclide Inventories

Table 7.3: Minimum resulting gamma-ray signal of radionuclide inventories with an activity of $LE = 1$, for the reference material *Common Copper* (for the chemical material composition see Tab. 7.1b) as function of the irradiation time and irradiation position. The presented minimum value is taken over all cooling times and all accelerator beam energies. The values are given in *Becquerel* ^{60}Co *equivalent per kg*. The value in the parentheses is the cooling time in years, for which the minimum is reached.

Position	Minimum gamma-ray signal for LE =1 $[Bq\ ^{60}\mathrm{Co}\ equivalent\ \mathrm{kg}^{-1}]$					Minimum $\leftrightarrow$
	60 days	1 year	3 years	10 years	30 years	
# 1	889 (30 y)	888 (30 y)	882 (30 y)	864 (30 y)	837 (30 y)	837
# 2	901 (30 y)	899 (30 y)	886 (30 y)	846 (30 y)	740 (30 y)	740
# 3	947 (30 y)	945 (30 y)	936 (30 y)	908 (30 y)	822 (30 y)	822
# 4	973 (30 y)	972 (30 y)	966 (30 y)	947 (30 y)	884 (30 y)	884
# 5	932 (30 y)	931 (30 y)	921 (30 y)	890 (30 y)	800 (30 y)	800
# 6	911 (30 y)	910 (30 y)	901 (30 y)	873 (30 y)	810 (30 y)	810
# 7	954 (30 y)	953 (30 y)	944 (30 y)	918 (30 y)	836 (30 y)	836
Minimum $\updownarrow$	889	888	882	846	740	**740**[‡]

[‡] For the given reference material and within the chosen parameter range, all resulting gamma-ray signal values are above the device MDA of 60 *Bq* ^{60}Co *equivalent*.

Table 7.4: Minimum resulting gamma-ray signal of radionuclide inventories with an activity of $LE = 1$, for the reference material *Common Aluminium* (for the chemical material composition see Tab. 7.1c) as function of the irradiation time and irradiation position. The presented minimum value is taken over all cooling times and all accelerator beam energies. The values are given in *Becquerel* ^{60}Co *equivalent per kg.* The value in the parentheses is the cooling time in years, for which the minimum is reached.

Position	Minimum gamma-ray signal for LE=1 $[Bq\ ^{60}\mathrm{Co}\ equivalent\ \mathrm{kg}^{-1}]$					Minimum $\leftrightarrow$
	60 days	1 year	3 years	10 years	30 years	
# 1	651 (30 y)	639 (30 y)	560 (30 y)	440 (30 y)	387 (30 y)	387
# 2	952 (30 y)	934 (30 y)	826 (30 y)	644 (30 y)	526 (30 y)	526
# 3	984 (30 y)	965 (30 y)	849 (30 y)	644 (30 y)	481 (30 y)	481
# 4	587 (30 y)	571 (30 y)	484 (30 y)	333 (30 y)	200 (30 y)	200
# 5	1034 (30 y)	1015 (30 y)	897 (30 y)	690 (30 y)	534 (30 y)	534
# 6	808 (30 y)	794 (30 y)	701 (30 y)	555 (30 y)	481 (30 y)	481
# 7	954 (30 y)	937 (30 y)	829 (30 y)	649 (30 y)	535 (30 y)	535
Minimum $\updownarrow$	587	571	484	333	200	**200**‡

‡ For the given reference material and within the chosen parameter range, all resulting gamma-ray signal values are above the device MDA of 60 *Bq* ^{60}Co *equivalent.*

Table 7.5: Minimum resulting gamma-ray signal of radionuclide inventories with an activity of $LE = 1$, for the reference material *Common Steel* (for the chemical material composition see Tab. 7.1a) as function of the irradiation time and irradiation position. The presented minimum value is taken over all cooling times and all accelerator beam energies. The values are given in *Becquerel* ^{60}Co *equivalent per kg*. The value in the parentheses is the cooling time in years, for which the minimum is reached.

Position	Minimum gamma-ray signal for LE =1 [Bq ^{60}Co *equivalent* kg^{-1}]					Minimum $\leftrightarrow$
	60 days	1 year	3 years	10 years	30 years	
# 1	597 (10 y)	596 (9 y)	603 (8 y)	646 (7 y)	758 (6 y)	596
# 2	792 (8 y)	791 (8 y)	796 (7 y)	823 (6 y)	855 (6 y)	791
# 3	901 (8 y)	901 (7 y)	904 (7 y)	917 (6 y)	911 (30 y)	901
# 4	939 (3 y)	940 (3 y)	941 (2 y)	949 (30 y)	891 (30 y)	891
# 5	785 (9 y)	786 (8 y)	790 (8 y)	814 (7 y)	844 (6 y)	785
# 6	593 (9 y)	594 (9 y)	600 (8 y)	643 (7 y)	726 (6 y)	593
# 7	925 (7 y)	925 (7 y)	927 (6 y)	938 (5 y)	921 (30 y)	921
Minimum $\updownarrow$	593	594	600	643	726	**593**[‡]

[‡] For the given reference material and within the chosen parameter range, all resulting gamma-ray signal values are above the device MDA of 60 *Bq* ^{60}Co *equivalent*.

Table 7.6: Minimum resulting gamma-ray signal of radionuclide inventories with an activity of $LE = 1$, for the reference material *Pure Iron* (100 % Fe) as function of the irradiation time and irradiation position. The presented minimum value is taken over all cooling times and all accelerator beam energies. The values are given in *Becquerel* ^{60}Co *equivalent per kg*. The value in the parentheses is the cooling time in years, for which the minimum is reached. Values below the device MDA are given in red.

Position	Minimum gamma-ray signal for LE$=$1 [Bq ^{60}Co *equivalent* kg^{-1}]					Minimum $\leftrightarrow$
	60 days	1 year	3 years	10 years	30 years	
# 1	320 (11 y)	320 (10 y)	326 (9 y)	368 (8 y)	498 (7 y)	320
# 2	73 (12 y)	74 (12 y)	76 (11 y)	100 (10 y)	172 (8 y)	73
# 3	18 (9 y†)	18 (9 y†)	18 (8 y†)	25 (7 y†)	45 (8 y†)	18
# 4	1 (5 y†)	1 (5 y†)	1 (4 y†)	2 (3 y†)	4 (3 y†)	1
# 5	45 (12 y†)	45 (11 y†)	47 (11 y†)	63 (11 y)	112 (9 y)	45
# 6	167 (11 y)	169 (11 y)	174 (10 y)	218 (8 y)	345 (7 y)	167
# 7	40 (10 y†)	40 (10 y†)	42 (9 y†)	55 (9 y†)	97 (8 y)	40
Minimum $\updownarrow$	1	1	1	2	4	1

† If the resulting gamma-ray signal is below the device MDA of 60 Bq ^{60}Co *equivalent*, the accompanying value in parentheses represents the shortest cooling time for which the resulting gamma-ray signal of the corresponding radionuclide inventory is below the device MDA.

Table 7.7: Most conservative radionuclide inventories resulting from the present study, i.e. the radionuclide inventories for the different reference materials that yield the lowest gamma-ray signal within the chosen parameter range. *Common Aluminium* has the radionuclide inventory with the lowest corresponding gamma-ray signal for an activity of $LE = 1$, apart from the hypothetical material *Pure Iron*.

Radionuclide	Activity fraction			
	Common Steel [%]	Common Copper [%]	Common Aluminium [%]	Pure Iron [%]
^{55}Fe	**74**[§]	–	0.41	**99**[§]
^{63}Ni	0.26	**67**[§]	**50**[§]	–
^{3}H	21	29	**48**[§]	0.69
^{60}Co	**2**[§‡]	**2.4**[§‡]	**0.04**[§‡]	–
^{54}Mn	**0.67**[‡]	–	–	**0.0046**[‡]
^{44}Sc	**0.27**[‡]	**0.25**[‡]	**0.045**[‡]	**0.0038**[‡]
^{22}Na	**0.25**[‡]	–	**0.11**[‡]	–

[§] Activity fraction that has to be taken into account because of its significant contribution to the exemption limit (according [42]).

[‡] Activity fraction of a radionuclide that should be included in the inventory because of its well detectable gamma emission, which can be used to infer the activity fraction of difficult-to-measure radionuclides.

7.3.2 Detectable Gamma Signals per Exemption Limit and Corresponding Radionuclide Inventories (Limited Parameter Range)

Table 7.8: Minimum resulting gamma-ray signal of radionuclide inventories with an activity of $LE = 1$, for the reference material *Common Copper* (for the chemical material composition see Tab. 7.1b) as function of the irradiation time and irradiation position. The presented minimum value is taken over all accelerator beam energies and a limited cooling time range compared to Tab. 7.3, whereby the present cooling time range is limited to a maximum cooling time of two years. The values are given in *Becquerel* ^{60}Co *equivalent per kg.* The value in the parentheses is the cooling time in years, for which the minimum is reached.

Position	Minimum gamma-ray signal for LE=1 $[Bq\ ^{60}\mathrm{Co}\ equivalent\ \mathrm{kg}^{-1}]$					Minimum $\leftrightarrow$
	60 days	1 year	3 years	10 years	30 years	
# 1	1495 (24 m)	1436 (24 m)	1242 (24 m)	1111 (24 m)	1071 (24 m)	1071
# 2	1139 (24 m)	1118 (24 m)	1059 (24 m)	1027 (24 m)	1018 (24 m)	1018
# 3	1041 (24 m)	1036 (24 m)	1022 (24 m)	1014 (24 m)	1011 (24 m)	1011
# 4	1014 (24 m)	1013 (24 m)	1012 (24 m)	1011 (24 m)	1009 (24 m)	1009
# 5	1210 (24 m)	1179 (24 m)	1088 (24 m)	1037 (24 m)	1023 (24 m)	1023
# 6	1405 (24 m)	1351 (24 m)	1179 (24 m)	1073 (24 m)	1045 (24 m)	1045
# 7	1069 (24 m)	1059 (24 m)	1031 (24 m)	1017 (24 m)	1011 (24 m)	1011
Minimum $\updownarrow$	1014	1013	1012	1011	1009	**1009** = **16.8 x MDA**

Table 7.9: Minimum resulting gamma-ray signal of radionuclide inventories with an activity of $LE = 1$, for the reference material *Common Aluminium* (for the chemical material composition see Tab. 7.1c) as function of the irradiation time and irradiation position. The presented minimum value is taken over all accelerator beam energies and a limited cooling time range compared to Tab. 7.4, whereby the present cooling time range is limited to a maximum cooling time of two years. The values are given in *Becquerel* ^{60}Co *equivalent per kg*. The value in the parentheses is the cooling time in years, for which the minimum is reached.

Position	Minimum gamma-ray signal for LE=1 $[Bq\ ^{60}\mathrm{Co}\ equivalent\ \mathrm{kg}^{-1}]$					Minimum ↔
	60 days	1 year	3 years	10 years	30 years	
# 1	3128 (24 m)	3123 (24 m)	3099 (24 m)	3053 (24 m)	2983 (24 m)	2983
# 2	2997 (10 m)	3000 (8 m)	3031 (6 m)	3036 (6 m)	3004 (24 m)	2997
# 3	2692 (7 m)	2700 (5 m)	2799 (3 m)	2864 (2 m)	2851 (3 m)	2692
# 4	1642 (8 m)	1653 (7 m)	1807 (4 m)	1955 (3 m)	1962 (3 m)	1642
# 5	3143 (24 m)	3138 (24 m)	3115 (24 m)	3081 (24 m)	3041 (24 m)	3041
# 6	3140 (24 m)	3135 (24 m)	3111 (24 m)	3071 (24 m)	3016 (24 m)	3016
# 7	3067 (11 m)	3066 (11 m)	3069 (24 m)	3046 (24 m)	3006 (24 m)	3006
Minimum ↕	1642	1653	1807	1955	1962	**1642** = **27.4 x MDA**

Table 7.10: Minimum resulting gamma-ray signal of radionuclide inventories with an activity of $LE = 1$, for the reference material *Common Steel* (for the chemical material composition see Tab. 7.1a) as function of the irradiation time and irradiation position. The presented minimum value is taken over all accelerator beam energies and a limited cooling time range compared to Tab. 7.5, whereby the present cooling time range is limited to a maximum cooling time of two years. The values are given in *Becquerel* ^{60}Co *equivalent per kg*. The value in the parentheses is the cooling time in years, for which the minimum is reached.

Position	Minimum gamma-ray signal for LE=1 $[Bq\ ^{60}\mathrm{Co}\ equivalent\ \mathrm{kg}^{-1}]$					Minimum ↔
	60 days	1 year	3 years	10 years	30 years	
# 1	2379 (24 m)	2276 (24 m)	1815 (24 m)	1423 (24 m)	1344 (24 m)	1344
# 2	1591 (24 m)	1521 (24 m)	1260 (24 m)	1096 (24 m)	1069 (24 m)	1069
# 3	1116 (24 m)	1094 (24 m)	1018 (24 m)	984 (24 m)	984 (24 m)	984
# 4	941 (24 m)	940 (24 m)	941 (24 m)	951 (11 m)	960 (11 m)	940
# 5	2088 (24 m)	1989 (24 m)	1565 (24 m)	1245 (24 m)	1182 (24 m)	1182
# 6	2331 (24 m)	2226 (24 m)	1752 (24 m)	1355 (24 m)	1285 (24 m)	1285
# 7	1214 (24 m)	1178 (24 m)	1054 (24 m)	992 (24 m)	987 (24 m)	987
Minimum ↕	941	940	941	951	960	**940** = **15.7 x MDA**

Table 7.11: Minimum resulting gamma-ray signal of radionuclide inventories with an activity of $LE = 1$, for the reference material *Pure Iron* $(100\,\%\ \text{Fe})$ as function of the irradiation time and irradiation position. The presented minimum value is taken over all accelerator beam energies and a limited cooling time range compared to Tab. 7.6, whereby the present cooling time range is limited to a maximum cooling time of two years. The values are given in *Becquerel* ^{60}Co *equivalent per kg*. The value in the parentheses is the cooling time in years, for which the minimum is reached.

Position	Minimum gamma-ray signal for LE=1 $[Bq\ ^{60}\text{Co}\ equivalent\ \text{kg}^{-1}]$					Minimum $\leftrightarrow$
	60 days	1 year	3 years	10 years	30 years	
# 1	2505 (24 m)	2396 (24 m)	1885 (24 m)	1439 (24 m)	1364 (24 m)	1364
# 2	2465 (24 m)	2354 (24 m)	1823 (24 m)	1361 (24 m)	1285 (24 m)	1285
# 3	1533 (24 m)	1433 (24 m)	1010 (24 m)	698 (24 m)	652 (24 m)	652
# 4	264 (24 m)	240 (24 m)	152 (24 m)	97 (24 m)	90 (24 m)	90
# 5	2635 (24 m)	2525 (24 m)	1989 (24 m)	1504 (24 m)	1419 (24 m)	1419
# 6	2533 (24 m)	2423 (24 m)	1899 (24 m)	1439 (24 m)	1361 (24 m)	1361
# 7	1748 (24 m)	1642 (24 m)	1181 (24 m)	830 (24 m)	780 (24 m)	780
Minimum $\updownarrow$	264	240	152	97	90	**90** = **1.5 x MDA**

Table 7.12: Most conservative radionuclide inventories of the present study, whereby the upper limit of the cooling time range was reduced to a maximum cooling time of two years (compared to 30 years of maximum cooling time for Tab. 7.7). Within this parameter range, *Common Steel* has the radionuclide inventory with the lowest corresponding gamma-ray signal for an activity of $LE = 1$, apart from the hypothetical material *Pure Iron*. But contrary to the full cooling time range, no radionuclide inventory results in a gamma-ray signal lower than the device MDA of the RADOS RTM 661.

Radionuclide	Activity fraction			
	Common Steel [%]	Common Copper [%]	Common Aluminium [%]	Pure Iron [%]
^{55}Fe	72	2.4	**34**[§]	**99**[§]
^{60}Co	**24**[§‡]	**74**[§‡]	**0.051**[‡]	–
^{65}Zn	–	–	**29**[§‡]	–
^{63}Ni	2	22	0.45	–
^{22}Na	–	–	**14**[§‡]	–
^{54}Mn	**1.4**[‡]	**0.12**[‡]	**5.4**[‡]	**0.67**[‡]
^{51}Cr	–	–	**6.4**[‡]	–
^{3}H	0.1	0.75	4	0.34
^{44}Sc	–	–	–	**0.0021**[‡]

[§] Activity fraction that has to be taken into account because of its significant contribution to the exemption limit (according [42]).

[‡] Activity fraction of a radionuclide that should be included in the inventory because of its well detectable gamma emission, which can be used to infer the activity fraction of difficult-to-measure radionuclides.

7.3.3   Synthesis of the Detectable Gamma Signals per Exemption Limit

The calculated radionuclide inventories for all three reference materials show, over the entire span of chosen input parameters, a sufficient detectable gamma-ray signal per exemption limit for the RADOS RTM 661, even for the limiting object weight of $1\,kg$ below which the LE_{abs} has to be considered.

For the reference material *Common Copper*, the resulting gamma-ray signal per exemption limit decreases both with longer irradiation times as well as with longer cooling times. For short cooling times, i.e. up to one year of cooling, the resulting radionuclide inventories include many radionuclides with well detectable gamma-ray emissions. For these cooling times, *difficult-to-measure radionuclides*[12] do not have a significant importance for the exemption limit. Therefore the gamma-ray signal per exemption limit is rather high for short cooling times. For intermediate cooling times, i.e. one to fifteen years, most of the radionuclides with short half-life periods have decayed and the only radionuclide with a significant importance for the exemption limit is ^{60}Co, which has a well detectable gamma-ray emission. Thus, this results in a well detectable gamma-ray signal per exemption limit for intermediate cooling times. Due to their considerable different half-life periods (see Tab. A.6.1), for longer cooling times (up to 30 years) the importance of ^{60}Co for the exemption limit decreases whereas the importance of ^{63}Ni successively increases. Hence, and because ^{63}Ni has no gamma-ray emission, the gamma-ray signal per exemption limit decreases with longer cooling times. A change in irradiation time shifts this phenomena, whereby shorter irradiation times result in a shift to higher fractions of radionuclides with short half-life periods, i.e. for this reference material to a higher resulting gamma-ray signal per exemption limit, and longer irradiation times shift the ratio to higher fractions of radionuclides with long half-life periods, i.e. for this reference material to a lower resulting gamma-ray signal per exemption limit. A significant variation in signal strength depending on the beam energy or the object position was not noted. The lowest gamma-ray signal per exemption limit for the reference material *Common Copper* is $740\,Bq$ ^{60}Co *equivalent* kg^{-1}, which even for a $1\,kg$ object is well above the device MDA of $60\,Bq$ ^{60}Co *equivalent* (see Tab. 7.3). The corresponding radionuclide inventory is illustrated in Tab. 7.7 and the visualisation plots of the corresponding irradiation scenario, including the most conservative radionuclide inventory for the reference material *Common Copper*, can be found in the Appendix A.3.i in Fig. A.3.1.

Apart from a notable gamma-ray signal variation depending on the object position, the resulting gamma-ray signal for the reference material *Common Aluminium* shows the

---

[12]Classification into *key radionuclides* and *difficult-to-measure radionuclides* after ISO 21238 [17] (for further information see footnote[1] on page 8)

same characteristics as for *Common Copper*. For *Common Aluminium*, the radionuclide with the well detectable gamma-ray emission and the shorter half-life period is ^{22}Na and the radionuclides without gamma-ray emission and a longer half-life period are ^{3}H and ^{63}Ni. The dependency on the object position of the resulting gamma-ray signal for *Common Aluminium* can be explained by the different production yields of the radionuclides that are important for the exemption limit, i.e. ^{3}H, ^{22}Na and ^{63}Ni, for the different positions. These production yields are strongly dependent on the composition of the radiation field which changes with the different positions. Hence, it is important whether the particle spectra for a certain position is dominated by low energy neutrons or by high energy particles. Beside other influences, it can be stated for *Common Aluminium* that with higher fractions of high energy particles, the production of ^{3}H and ^{22}Na by spallation reactions on aluminium is favoured, whereby with higher fractions of low energy neutrons the production of ^{63}Ni by (n, γ) reactions on nickel impurities gains importance. Additional weighting factors for the importance of these three radionuclides are their different exemption limits (see Tab. A.6.1). So the different radiation fields for the different object positions result in varying activity fractions with varying importances for the exemption limit for the various radionuclides and therefore also in a varying gamma ray-signal per exemption limit of the entire radionuclide inventory. The lowest gamma-ray signal per exemption limit for the reference material *Common Aluminium* is $200\,Bq$ ^{60}Co *equivalent* kg^{-1}, which even for a $1\,kg$ object is above the device MDA of $60\,Bq$ ^{60}Co *equivalent* (see Tab. 7.4). The corresponding radionuclide inventory is illustrated in Tab. 7.7 and the visualisation plots of the corresponding irradiation scenario, including the most conservative radionuclide inventory for the reference material *Common Aluminium*, can be found in the Appendix A.3.i in Fig. A.3.2.

For the resulting detectable gamma-ray signal of the reference material *Common Steel*, the trend over the irradiation or the cooling time, over the beam energies or over the object positions, is not as simple as for the other reference materials. Generally, the resulting gamma-ray signal for a given irradiation scenario, which is rather high for short cooling times compared with the signal for the other reference materials, decreases with increasing cooling times towards a certain minimum value, which is based on the decay of ^{54}Mn. For the considered irradiation conditions, this minimum can be found between six and nine years of cooling time. With a further increase of the cooling time the importance for the exemption limit of ^{44}Ti/^{44}Sc increases and due to the well detectable gamma-ray signal of ^{44}Sc the gamma-ray signal per exemption limit consequently increases again. For short cooling times many radionuclides have a considerable importance for the exemption limit. Due to the successive longer half-life periods of the radionuclides ^{54}Mn, ^{55}Fe, ^{60}Co and ^{44}Ti, they dominate successively the exemption limit of the reference

material *Common Steel*. Among these radionuclides, ^{55}Fe is the only *difficult-to-measure radionuclide*. The lowest gamma-ray signal per exemption limit for *Common Steel* is 593 Bq ^{60}Co *equivalent* kg^{-1}, which is even for a 1 kg object well above the device MDA of 60 Bq ^{60}Co *equivalent* (see Tab. 7.5). The corresponding radionuclide inventory is illustrated in Tab. 7.7 and the visualisation plots of the corresponding irradiation scenario, including the most conservative radionuclide inventory for the reference material *Common Steel*, can be found in the Appendix A.3.i in Fig. A.3.3.

Within the three reference materials, *Common Aluminium* has the lowest detectable gamma-ray signal over the entire input parameter range. Hence, the worst case radionuclide inventory of *Common Aluminium* (see Tab. 7.7) can be taken as enveloping input radionuclide inventory for the RADOS RTM 661 when performing clearance measurements of objects made of materials that correspond to the chosen reference materials.

By considering, in addition to the reference materials, the hypothetical material *Pure Iron* as possible object material, a resulting gamma-ray signal below the device detection limit is possible (see Tab. 7.6). The characteristics of the gamma-ray signal per exemption limit for *Pure Iron* is very similar to the characteristics of the signal for *Common Steel*. Based on the decay of ^{54}Mn, the resulting gamma-ray signal decreases with increasing cooling times to a minimum. Contrary to *Common Steel* and due to the missing variety of gamma-ray emitting radionuclides that results in *Common Steel* from chemical elements other than iron such as e.g. cobalt, this minimum can be far below the detection limit of the RADOS RTM 661. The lowest gamma-ray signal per exemption limit for *Pure Iron* is 1.87 Bq ^{60}Co *equivalent* kg^{-1}, which for a 1 kg object is far below the device MDA of 60 Bq ^{60}Co *equivalent* (see Tab. 7.6). The corresponding radionuclide inventory is illustrated in Tab. 7.7 and the visualisation plots of the corresponding irradiation scenario, including the most conservative radionuclide inventory for the reference material *Pure Iron*, can be found in the Appendix A.3.i in Fig. A.3.4.

To verify if clearance of this hypothetical material is possible and to determine the parameter range for which this would be the case, an adaptation of the input parameter range was performed. The shortest cooling time, for which a resulting gamma-ray signal below the RADOS RTM 661 device MDA is possible, can be determined from Tab. 7.6. By limiting the cooling time range to a maximum cooling time of two years, the resulting gamma-ray signal of all calculated radionuclide inventories, i.e. for all considered materials, even for the hypothetical material *Pure Iron*, is above the device MDA (see Tab. 7.8 - 7.11). The lowest gamma-ray signal per exemption limit results from *Pure Iron* and is, even for a 1 kg object, with 90 Bq ^{60}Co *equivalent* kg^{-1} well above the device MDA of 60 Bq ^{60}Co *equivalent*. So the most conservative radionuclide inventory covering

all considered materials is the most conservative radionuclide inventory for the limited parameter range of the material *Pure Iron* (see Tab. 7.12). The visualisation plots for the worst case irradiation scenarios for the limited parameter range for all considered materials are illustrated in the Appendix A.3.ii.

CHAPTER 8

Geometry Effects

The results of Chapter 7 show that, for the considered parameter range, the resulting detectable gamma signal for all considered reference materials, apart from the hypothetical material *Pure Iron*, is higher than the detection limit of the RADOS RTM 661 device and therefore clearance by mean of a RADOS RTM 661 measurement is feasible. As explained in Sec. 3.4, for a reliable clearance measurement both the geometry and the density of the object to be cleared have to be covered by the device calibration. Normally, a general calibration of the measurement device is performed assuming a homogeneous activity distribution. The object geometry as well as the relative object density of items present in the CERN facilities vary strongly. Also the activity distribution can be quite complex. To evaluate the range of applicability of the general calibration, a dedicated geometry study was included into this work. Therefore Monte-Carlo simulations for different geometry and density combinations, which are not covered by the general calibration, were performed and compared to the general calibration results. The simulations were performed with the FLUKA Monte-Carlo code (see Sec. 5.2) whereby a sphere was taken as object geometry[13] and placed in an abstract model of the RADOS RTM 661 (see Fig. 8.1). The simulations were performed for a $20\,kg$ object due to the CERN safety regulations (see Sec. 3.4). To quantify the self-absorption impact not only for the maximum mass, an intermediate mass of $10\,kg$ was simulated additionally.

As explained in Sec. 3.4, the general calibration of the RADOS RTM 661 is performed with a nearly homogeneous mass distribution for relative material densities[14] up to $1\,g\,cm^{-3}$. Hence, the material densities chosen for the simulations had to be in the range from $1\,g\,cm^{-3}$ up to the nominal material density of the material considered. The

---

[13]A spherical geometry shape was chosen for the object to be cleared because this represents the worst case scenario for self-absorption effects.

[14]The maximum mass for the calibration with a steel plate calibration phantom is $400\,kg$. The phantom volume is almost $400\,cm^3$. This leads to a relative material density of $1\,g\,cm^{-3}$.
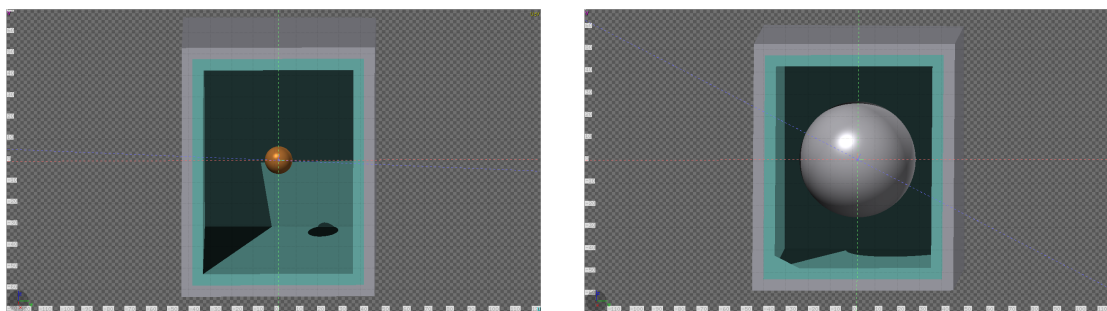
(a) Smallest Sphere in RADOS RTM 661   (b) Largest Sphere in RADOS RTM 661

Figure 8.1: Figure (a) shows the smallest ($10\,\mathrm{kg}$, copper, $\rho_{100} = \rho_{(\mathrm{Cu})}$) and Fig. (b) the largest ($20\,kg$, aluminium, $\rho_{10} = 0.1\,\rho_{(\mathrm{Al})}$) sphere model of the performed Monte-Carlo simulations. The figures as well as the simulations were produced by the use of FLAIR [45] interfacing the FLUKA Monte-Carlo particle transport code (Sec. 5.2).

simulations include three relative material densities ρ_{10}, ρ_{50} and ρ_{100}, i.e. corresponding to 10 %, 50 %, and 100 % of the nominal material density of the three material families *Copper*, *Iron* and *Aluminium*. The 10 % fraction, with $\rho = 0.1\,\rho_{(\mathrm{mat})}$, was chosen because this corresponds, e.g. for the material families *Copper* and *Iron*, to the maximum relative material density covered by the general RADOS RTM 661 device calibration. So this fraction is used as reference point for the families *Iron* and *Copper*. The 50 % fraction, with $\rho = 0.5\,\rho_{(\mathrm{mat})}$, was chosen because this represents a quite common material density, e.g. the average density of shredded iron or copper, and in addition it corresponds to the maximum relative material density covered by the general RADOS RTM 661 device calibration for the material family *Aluminium*. Therefore this fraction is used as reference point for the material family *Aluminium*. The full material (100 % density fraction) was chosen to cover the worst case self-absorption scenario, i.e. a massive metal sphere with $\rho = \rho_{(\mathrm{mat})}$.

The performed radionuclide inventory study of this work identifies the *key radionuclides* for the different reference materials. For *Common Copper* and *Common Steel* the *key radionuclide* is ^{60}Co, whereas for *Common Aluminium* it is ^{22}Na (see Tab. 7.7 and Tab. 7.12). Therefore the simulations were performed with the radionuclide ^{60}Co as activity for the spheres made of iron or copper and with the radionuclide ^{22}Na as activity for the aluminium spheres. A summary of the simulation results at peak energies is shown in Tab. 8.1. A more detailed presentation of the simulation plots can be found in Appendix Sec. A.5, whereby Sec. A.5.i shows the simulated photon spectra for the considered scenarios and Sec. A.5.ii illustrates the residual dose rates emitted by the simulated metal spheres for reference.

Assuming that the simulation scenario of the $20\,kg$ spheres with a homogeneous
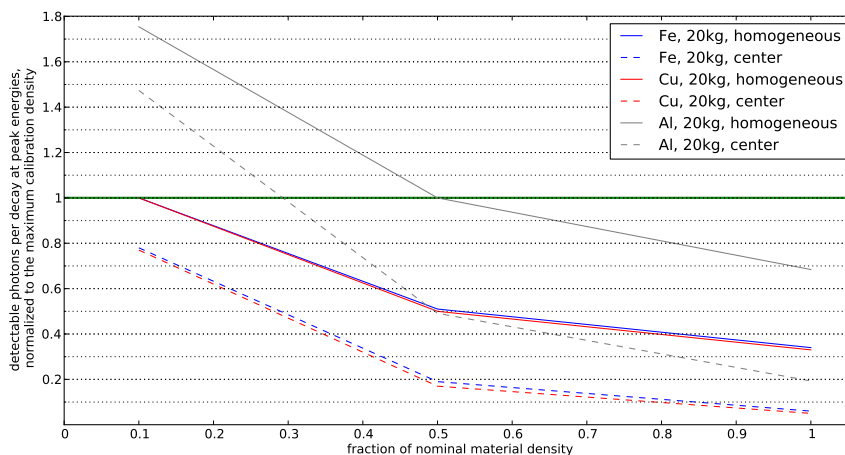
Figure 8.2: Synthesis of detectable photons per decay at peak energies for the three chosen material families *Copper*, *Iron* and *Aluminium* normalized to the scenario of homogeneous activity distribution and maximum calibration density. Results of homogeneous activity distribution as well as of centred radioactivity are illustrated for a metal sphere of $20\,kg$ with varying material density fractions, i.e. $10\,\%$, $50\,\%$ and $100\,\%$ of the nominal material density.

activity distribution is the coherent continuation of the general calibration of the RA-DOS RTM 661 device, the resulting relative number of photons of the 'ρ_{100}' scenarios[15] can be interpreted as required safety factor in case of an object density that is not covered by the general calibration. This safety factor is $33\,\%$ for *Copper*, $34\,\%$ for *Iron* and $69\,\%$ for *Aluminium*. The safety factors are illustrated in Fig. 8.2 together with the worst case factors, i.e. in case of radioactivity concentrated in the center of the sphere instead of homogeneously distributed. The worst case factor is $5\,\%$ for *Copper*, $6\,\%$ for *Iron* and $19\,\%$ for *Aluminium*. So the appropriate safety factor has to be chosen dependent to the relative density as well as the activity distribution for each object. A measurement, whereby the exemption limit is lowered to the fraction of the safety factor, covers the self-absorption effects for a material with a nominal material density and is therefore enveloping for all lower relative material densities.

---

[15]For the material families *Iron* and *Copper* also the 'ρ_{50}' scenario represents a measurement situation that is not covered by the general device calibration.

Table 8.1: Monte-Carlo simulated photon emission for the three material families *Copper*, *Iron* and *Aluminium*. The sphere mass, the material density as well as the activity distribution are varied. The photons are scored at the sphere surface and the values are normalized. Detailed photon spectra can be found in the Appendix A.5.i.

(a) Relative Numbers of Photons at Peak Energies Emitted from Copper Spheres.

Sphere Mass	Activity Distribution	Density Fraction[#]		
		ρ_{10}	ρ_{50}	ρ_{100}
10 kg	homogeneous	1.00	0.55	0.37
10 kg	centred	0.82	0.25	0.09
20 kg	homogeneous	**1.00**	**0.50**	**0.33**
20 kg	centred	0.77	0.17	0.05

[#] Values are normalized to scenario 'homogeneous, $\rho_{10} = 0.1\,\rho_{(\mathrm{Cu})}$'.

(b) Relative Numbers of Photons at Peak Energies Emitted from Iron Spheres.

Sphere Mass	Activity Distribution	Density Fraction[§]		
		ρ_{10}	ρ_{50}	ρ_{100}
10 kg	homogeneous	1.00	0.56	0.38
10 kg	centred	0.83	0.27	0.10
20 kg	homogeneous	**1.00**	**0.51**	**0.34**
20 kg	centred	0.78	0.19	0.06

[§] Values are normalized to scenario 'homogeneous, $\rho_{10} = 0.1\,\rho_{(\mathrm{Fe})}$'.

(c) Relative Numbers of Photons at Peak Energies Emitted from Aluminium Spheres.

Sphere Mass	Activity Distribution	Density Fraction[‡]		
		ρ_{10}	ρ_{50}	ρ_{100}
10 kg	homogeneous	1.64	1.00	0.72
10 kg	centred	1.44	0.59	0.28
20 kg	homogeneous	**1.75**	**1.00**	**0.69**
20 kg	centred	1.46	0.49	0.19

[‡] Values are normalized to scenario 'homogeneous, $\rho_{50} = 0.5\,\rho_{(\mathrm{Al})}$'.

Summary

Task

For material originating from high-energy accelerator facilities, the clearance from regulatory control performed at the exit of the facility is particular in certain ways. Due to the restricted infrastructural conditions and a quite limited time span for the clearance measurements at the exit of the accelerator, radiation background sensitive and time intensive gamma spectroscopy measurements for all components are prohibitively difficult to perform. Additionally, the measurement has to be non-destructive in most cases, e.g. due to the missing possibility to disassemble an object or due to the need to reuse or test an object in the unmodified present condition. Thus, measurements of disassembled subcomponents or sampling works for detailed mechanical, chemical or radiochemical analysis cannot be performed on a component-by-component basis. Furthermore the given situation can be rather challenging because of lack of certain information important for the determination of the complete activation process, e.g. the irradiation time profile, the chemical material composition or the object location when it has been in the accelerator facility.

This leads to a complex characterization situation with a large possible input parameter range. The present work tried to tackle this challenge by defining enveloping conditions and parameter sets that allow to perform material clearance measurements, even without a detailed knowledge of the object conditions and radiological history.

Strategy

According to the Swiss legislation for clearance of material from regulatory control, an object to be cleared has to fulfil three clearance criteria, i.e. the ambient dose rate criterion, the surface contamination criterion as well as the mass specific activity criterion. This works is focused on the mass specific activity criterion, because ambient dose rate determination is a well understood subject and surface contamination is not a significant issue at most CERN facilities.

A RADOS RTM 661/440 lnc clearance monitor, a well known device for clearance measurements in the nuclear industry, is operated in the Radioactive Waste Section of the CERN Radiation Protection Group. The main goal of this work was to evaluate if this kind of devices fit the needs for clearance measurements at the exit of accelerators, i.e. if the detection limit is sufficient low to robustly detect the radioactivity amount that corresponds to the exemption limit resulting of any irradiation scenario.

A comprehensive knowledge of the radionuclide inventory variety resulting from accelerator radiation induced activation at CERN is important for two reasons. On the one hand, the radionuclide inventories are a necessary input for the RADOS RTM 661 device. Thus, they have to be specified to be able to perform the clearance measurements. On the other hand, the resulting detectable gamma-ray signal can be calculated and compared to the device detection limit by combining the radionuclide inventories with the device efficiency. Hence, it can be verified that the device is able to detect the activity corresponding to the exemption limit over all irradiation scenarios resulting from the chosen input parameters.

Certain restrictions had to be set to define the field of validity of this work. The maximum mass of the object to be cleared, which has to be put in the measurement chamber by hand, is limited to 20 kg. According to the CERN safety regulation, the 20 kg limit corresponds to the maximum weight allowed to be lifted by hand. The dimensions of the measurement chamber are the limitation for the maximum size of the object to be cleared. In addition, the object characteristics as well as the present measurements parameters have to be part of the input parameter span.

The following input parameters were set for the calculation of the accelerator radiation induced activities. The chemical material composition of the object to be released was limited to three reference materials, i.e. *Common Steel*, *Common Copper* and *Common Aluminium*. The reference material compositions were determined in a material study that was part of this work. Additionally, the hypothetical material composition of 100 % Fe, denoted *Pure Iron*, was considered to evaluate the extreme case of complete absence of the chemical element cobalt. Due to its significant proportion on the production of the *key radionuclide* ^{60}Co, the mass fraction of the chemical element cobalt is of particular importance for the activation process. Also the radiation fields had to be specified. For this work, particle spectra, that had been determined and evaluated within the CERN ActiWiz project, were taken as representative spectra. The number of particle spectra sets was limited to 28 spectra per selected material composition and per selected irradiation period, i.e. seven selected object positions in the accelerator tunnel for each of the nominal beam energies of the four main CERN accelerators.

Results

One of the first parts of this work was to evaluate and describe the legal framework for clearance of material from regulatory control in Switzerland. During the preparation time of the thesis, the CERN Radioactive Waste Section started to establish the clearance process of potential radioactive waste. Therefore various procedures and concepts had to be created or adapted. This work was part of this creation process and theoretical approaches as well as ideas for practices could be tested and implemented immediately. The installation and calibration of three RADOS RTM devices in the framework of the characterization of radioactive waste for clearance helped to gain a profound knowledge of the clearance monitors, their use as well as their limitations. The evaluation of the influences of the radiation background variations as well as the determination of an energy dependent detector efficiency function for the RADOS RTM devices are results of the intensive work with these measurement devices. The participation in as well as the outcome of the project work for the CERN Material Guidelines Catalogue provided the basis data for the material study performed in this work. Goal and result of this study was the determination of the chemical material composition of representative reference materials.

The multiplicity of chosen input parameters lead to the enormous number of 28560 radionuclide inventories that had to be calculated. Therefore the calculations, the analysis as well as the data management were performed and automatised by PYTHON scripts. For the analysis of the calculation results, four plot types were developed that allow to visualize and evaluate the resulting radionuclide inventories and their characteristics. All visualisation plots are condensed in a 600-page report that can be used to facilitate future material characterization projects.

Another outcome of this work is the formal description of the entire radiological characterization process and the mathematical relations between the single steps and their various and often complex parameters. Especially the resulting gamma-ray signal per exemption limit of the calculated radionuclide inventories, combined with the device efficiency, can be seen as an important result that serves to evaluate radionuclide inventories and as decision parameter for a simplification of the input radionuclide inventories. A simplification process was developed and explained with the goal to reduce the variety of radionuclide inventories as input for the RADOS RTM devices and to create enveloping inventory families. The calculation and evaluation process of this work is focused on the use of a RADOS RTM device. The formulation of the process is general enough to be applied to the device efficiency of other detection devices. So the response of other devices, e.g. AUTOMESS AD6/AD-b, Thermo Scientific FH 40/BGO or certain HPGe detectors,

for the resulting gamma-ray signal could be determined and analysed by implementing a dedicated detector efficiency curve.

The resulting detectable gamma-ray signal per Swiss exemption limit was studied and analysed in detail for all resulting radionuclide inventories of this work, i.e. the gamma-ray signal per exemption limit was folded with the RADOS RTM device efficiency by the use of the previously determined mono-energetic detector efficiency function. The resulting detectable gamma-ray signal per Swiss exemption limit was compared to the device detection limit. Thus, the different radionuclide inventories were compared and evaluated. The most conservative ones, i.e. the ones with the lowest detectable gamma-ray signal per exemption limit, were identified and categorised by material as well as by irradiation conditions.

The calculated radionuclide inventories for all three reference materials show, over the entire span of chosen input parameters, a sufficiently detectable gamma-ray signal per exemption limit for the RADOS RTM 661, even for the limiting object weight of $1\,\mathrm{kg}$ below which the LE_{abs} has to be considered. For the reference material *Common Copper*, the resulting gamma-ray signal per exemption limit decreases both with longer irradiation times as well as with longer cooling times. A significant variation in signal strength depending on the beam energy or the object position was not noted. The *key radionuclide* ^{60}Co as well as the *difficult-to-measure radionuclide* ^{63}Ni are the major contributors to the exemption limit. For short and intermediate cooling times the exemption limit is dominated by ^{60}Co. Due to their considerably different half-life periods, for longer cooling times the importance of ^{60}Co for the exemption limit decreases whereas the importance of ^{63}Ni successively increases. Therefore the gamma-ray signal per exemption limit decreases as well. Apart from a notable gamma-ray signal variation depending on the object position, the resulting gamma-ray signal for the reference material *Common Aluminium* show the same characteristics as for *Common Copper*. For *Common Aluminium*, the *key radionuclide* with a shorter half-life period is ^{22}Na and the difficult-to-measure radionuclides with longer half-life periods are ^{3}H and ^{63}Ni. The dependency on the object position can be explained by different production yields for the different positions for each of the three radionuclides. These different production yields lead both to varying activity fractions of the important radionuclides as well as to varying resulting gamma-ray signals. For the resulting detectable gamma-ray signal of the reference material *Common Steel*, the trend over the irradiation or the cooling time, over the beam energies or over the object positions, is not as simple as for the other reference materials. Generally, the resulting gamma-ray signal for a given irradiation scenario, which is rather high for short cooling times compared to the signal for

the other reference materials, decreases with increasing cooling times towards a certain minimum value, which is based on the decay of ^{54}Mn. With a further increase of the cooling time the importance for the exemption limit of ^{44}Ti$/^{44}$Sc increases and due to the well detectable gamma-ray signal of ^{44}Sc the gamma-ray signal per exemption limit consequently increases again. Due to the successive longer half-life periods of the radionuclides ^{54}Mn, ^{55}Fe, ^{60}Co and ^{44}Ti, they dominate successively the exemption limit of the reference material *Common Steel*. Among these radionuclides, ^{55}Fe is the only *difficult-to-measure radionuclide*.

Within the three reference materials, *Common Aluminium* has the lowest detectable gamma-ray signal over the entire input parameter range. Hence, the worst case radionuclide inventory of *Common Aluminium* can be taken as enveloping input radionuclide inventory for the RADOS RTM 661 when performing clearance measurements of objects made of materials that correspond to the chosen reference materials.

In addition, activation calculations were performed with the hypothetical material *Pure Iron*, that consists of 100 % of the element iron and can therefore be seen as an extreme composition for the material family steel and iron. The characteristics of the gamma-ray signal per exemption limit for *Pure Iron* is very similar to the characteristics of the signal for *Common Steel*. Based on the decay of ^{54}Mn, the resulting gamma-ray signal decreases with increasing cooling times to a minimum. Contrary to *Common Steel* and due to the missing variety of gamma-ray emitting radionuclides that results in *Common Steel* from chemical elements other than iron such as e.g. cobalt, this minimum can be far below the detection limit of the RADOS RTM 661. To verify if clearance of this hypothetical material is possible and to determine the parameter range for which this would be the case, an adaptation of the input parameter range was performed. By limiting the cooling time range to a maximum cooling time of two years, the resulting gamma-ray signal of all calculated radionuclide inventories, i.e. for all considered materials, even for the hypothetical material *Pure Iron*, is above the device MDA of the RADOS RTM 661. Another possible parameter restriction is the total time since installation in the accelerator, i.e. adding the irradiation time and the cooling time. It can be stated that in case of a total time less than five years of an object in the accelerator, all resulting radionuclide inventories lead to a detectable gamma-ray signal that is above the device detection limit.

Due to these promising results, the combination of the total gamma counter with a gamma spectroscopy device was discarded for a standard clearance procedure. The additional gamma spectroscopy measurements, which were an initial idea when defining the goals for this work, should be used to determine *key radionuclides* and thereby to

distinguish certain radionuclide inventory groups from others. With the obtained results, an additional gamma spectroscopy measurement is not necessary to achieve a detectable gamma-ray signal above the device MDA.

Self-absorption effects of the object can have an important impact on the clearance measurement. These effects are included in the device calibration of the RADOS RTM 661 up to a certain geometry and density variety of the object. For the foreseen use at the exit of the accelerator and with the large range of object geometry and density variations, a dedicated calibration for each object is not possible. Monte-Carlo simulations were performed to determine and quantify the influence of object geometry and relative material density. The simulations were performed for different weights, relative material densities and activity distributions for the three material families *Iron*, *Copper* and *Aluminium*. For the different conditions different safety factors were determined. The clearance measurements will take the possible self-absorption effects into account, even for material densities and geometries that are not covered by the general calibration, when the exemption limits are lowered to these safety factors. A reasonable choice for a safety factor for homogeneous activity distribution is 33% and 5% for an activity concentrated as hot-spot in the center of the object.

In summary, this work demonstrates that under the specified conditions, the resulting gamma-ray signal per Swiss exemption limit from common materials, activated by accelerator radiation induced activation at CERN, is always above the device detection limit of the RADOS RTM 661/440 lnc. Consequently, by using the developed characterization method, the RADOS RTM 661 can be used for the clearance from Swiss regulatory control of material from CERN's accelerator facilities.

Appendices

A.1   Neutron Reaction Cross Sections
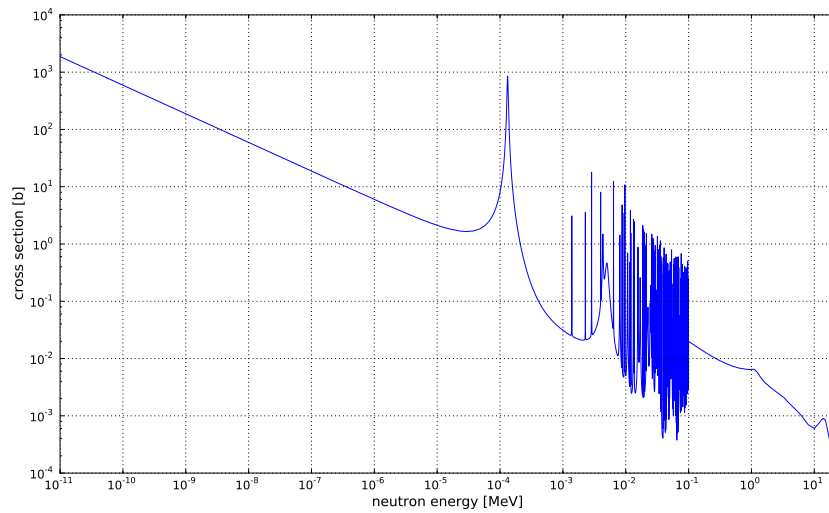
(a) Reaction cross section for $^{59}\mathrm{Co}(\mathrm{n},\gamma)^{60}\mathrm{Co}$ as a function of the neutron energy. Data taken from [59].
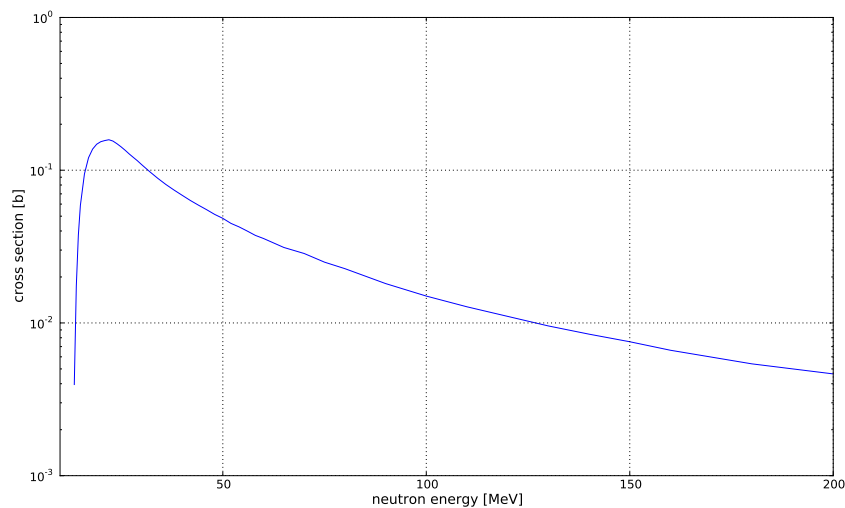
(b) Reaction cross section for $^{23}\mathrm{Na}(\mathrm{n},2\mathrm{n})^{22}\mathrm{Na}$ as a function of the neutron energy. Data taken from [60].

Figure A.1.1: Graph (a) illustrates the low energy (n,γ) radiative capture cross section on $^{59}\mathrm{Co}$ and the graph (b) displays the fast neutron $(\mathrm{n},2\mathrm{n})$ reaction cross section on $^{23}\mathrm{Na}$.

A.2   Photon Half-Value Layer Thicknesses

Table A.2.1: Photon half-value layer thicknesses [cm] calculated for common materials for various photon energies. Table taken from [14].

Energy (MeV)	Lead (11.35 g/cm^3)	Iron (7.874 g/cm^3)	Aluminum (2.699 g/cm^3)	Water (1.00 g/cm^3)	Air (0.001205 g/cm^3)	Stone concrete (2.30 g/cm^3)
0.1	0.011	0.237	1.507	4.060	3.726×10^3	1.734
0.3	0.151	0.801	2.464	5.843	5.372×10^3	2.747
0.5	0.378	1.046	3.041	7.152	6.600×10^3	3.380
0.662	0.558	1.191	3.424	8.039	7.420×10^3	3.806
1.0	0.860	1.468	4.177	9.802	9.047×10^3	4.639
1.173	0.987	1.601	4.541	10.662	9.830×10^3	5.044
1.332	1.088	1.702	4.829	11.342	1.047×10^4	5.368
1.5	1.169	1.802	5.130	12.052	1.111×10^4	5.698
2.0	1.326	2.064	5.938	14.028	1.293×10^4	6.612
2.5	1.381	2.271	6.644	15.822	1.459×10^4	7.380
3.0	1.442	2.431	7.249	17.456	1.604×10^4	8.141
3.5	1.447	2.567	7.813	19.038	1.747×10^4	8.828
4.0	1.455	2.657	8.270	20.382	1.868×10^4	9.366
5.0	1.429	2.798	9.059	22.871	2.094×10^4	10.361
7.0	1.348	2.924	10.146	26.860	2.449×10^4	11.846
10.0	1.228	2.940	11.070	31.216	2.817×10^4	13.227
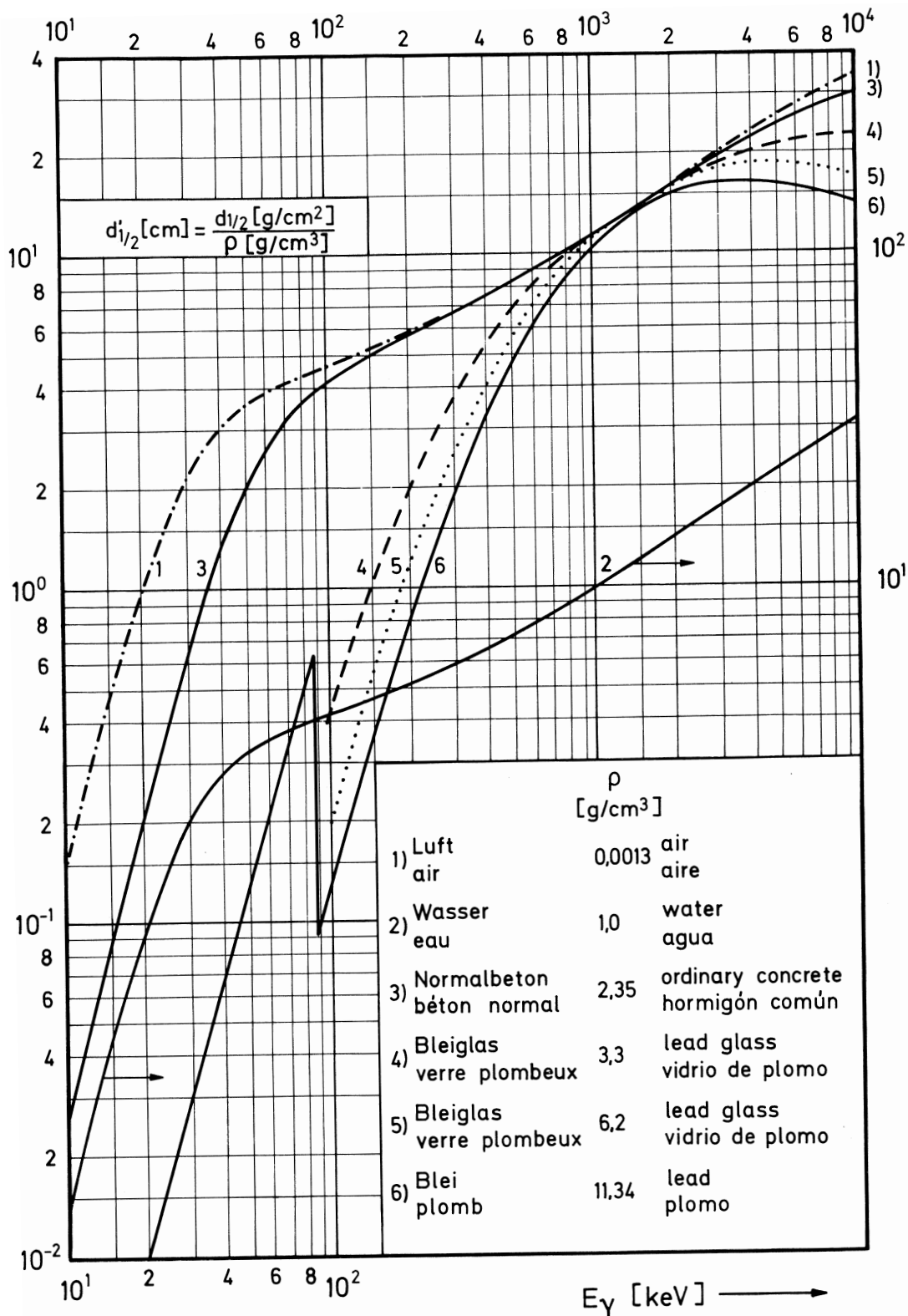
Figure A.2.1: Graphical presentation of half-value layer thicknesses for common materials as a function of the photon energy. Taken from [61]

A.3   Visualisation Plots of Worst Case Irradiation Scenarios

A.3.i   Plots for the Full Parameter Range

Common Copper (30 years, SPS, position 2)
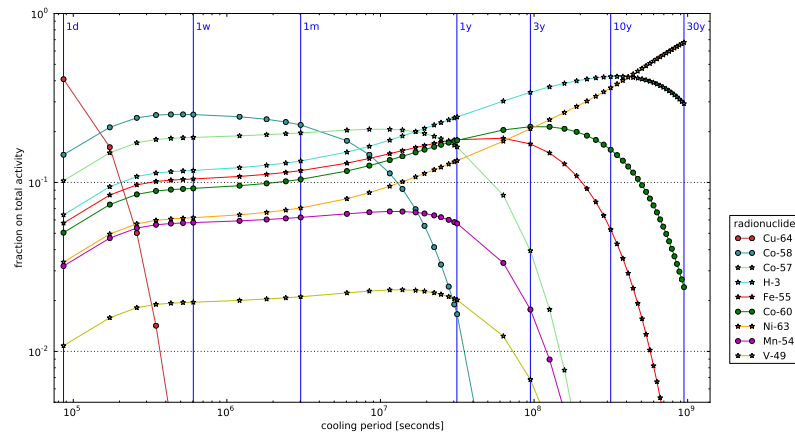
(a) Fractions of Activity
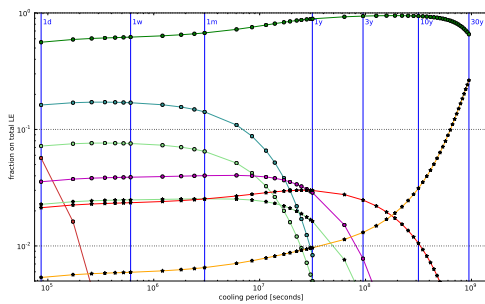
(b) Fractions of LE
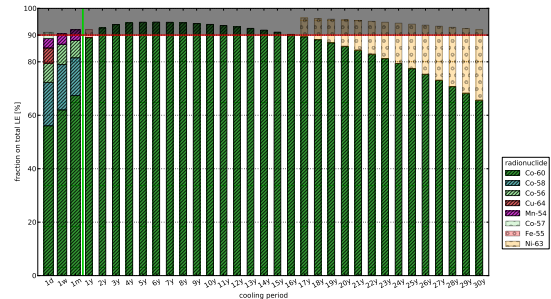
(c) LE Fractions stacked up to at least 90%
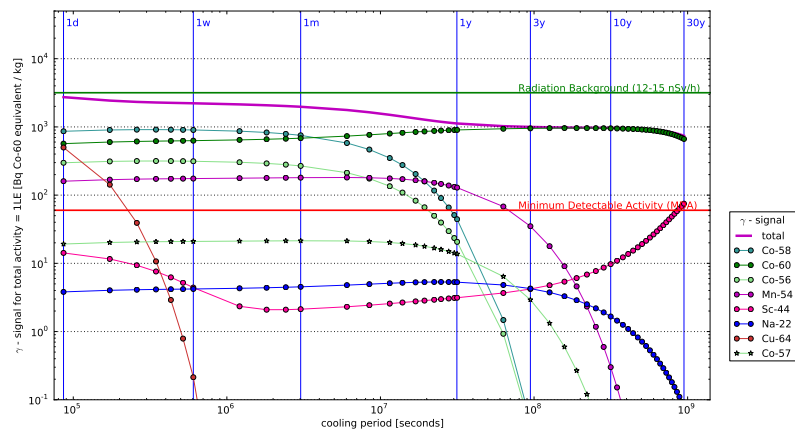
(d) Resulting Gamma Photon Signal

Figure A.3.1: Visualisation plots of the radionuclide inventories for the most conservative irradiation scenario for *Common Copper* (as defined in Sec. 7.2). The radionuclide inventory after 30 years of cooling has the lowest resulting gamma-ray signal.

Common Aluminium (30 years, PSB, position 4)
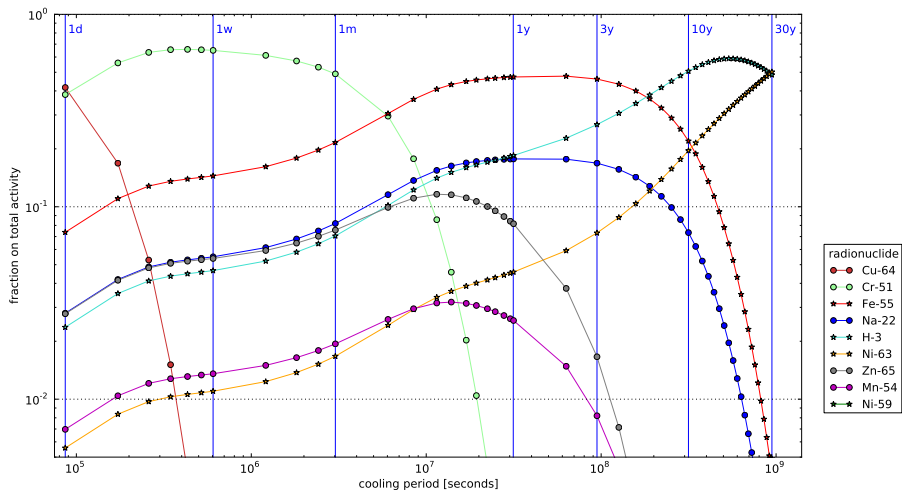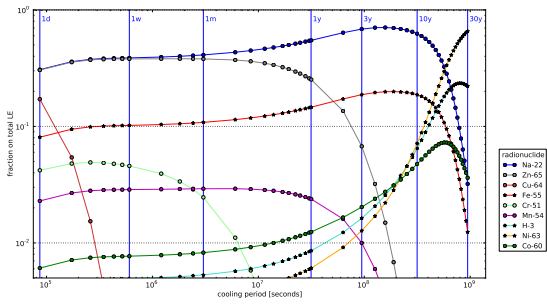
(a) Fractions of Activity

(b) Fractions of LE
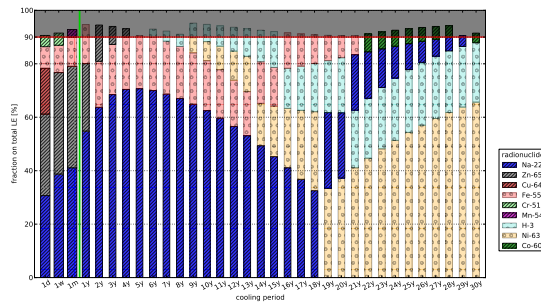
(c) LE Fractions stacked up to at least 90%
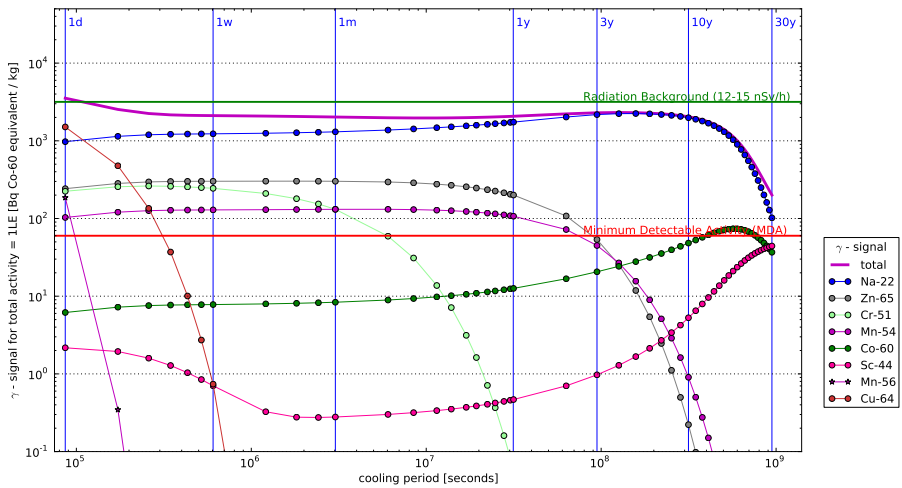
(d) Resulting Gamma Photon Signal

Figure A.3.2: Visualisation plots of the radionuclide inventories for the most conservative irradiation scenario for *Common Aluminium* (as defined in Sec. 7.2). The radionuclide inventory after 30 years of cooling has the lowest resulting gamma-ray signal.

Common Steel (60 days irradiation, PSB, position 6)
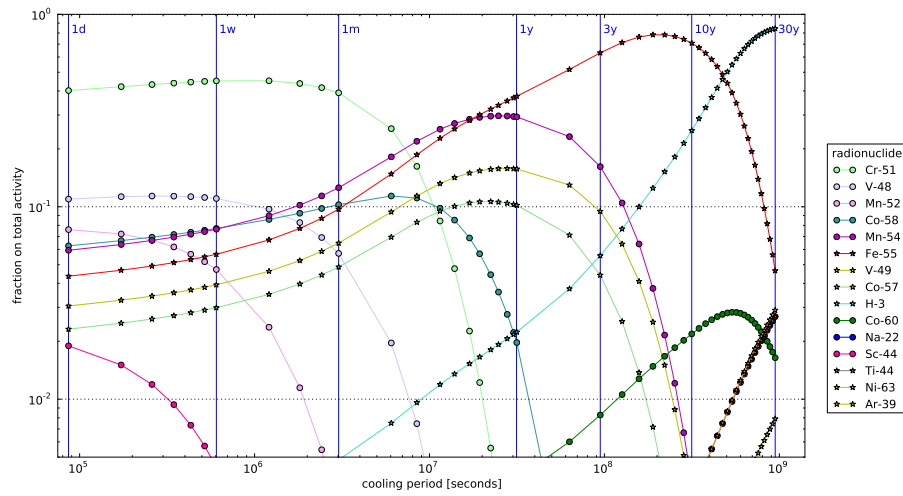
(a) Fractions of Activity
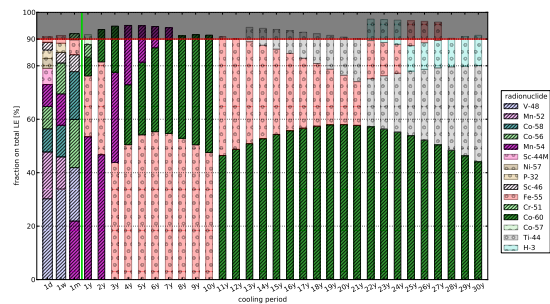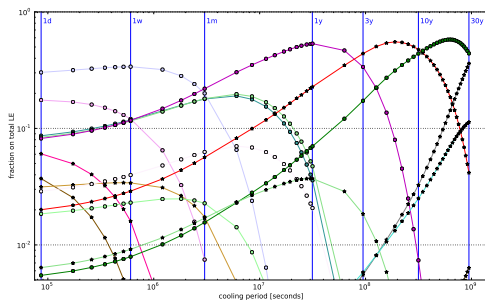
(b) Fractions of LE

(c) LE Fractions stacked up to at least 90%
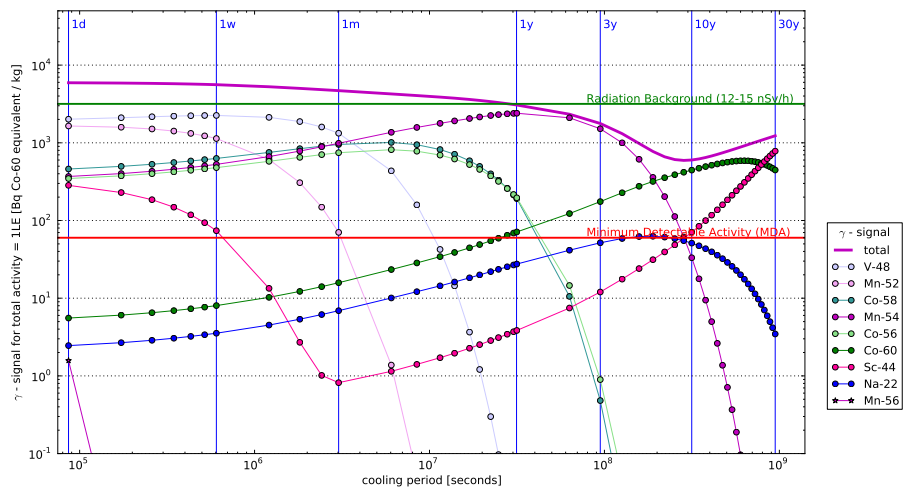
(d) Resulting Gamma Photon Signal

Figure A.3.3: Visualisation plots of the radionuclide inventories for the most conservative irradiation scenario for *Common Steel* (as defined in Sec. 7.2). The radionuclide inventory after 9 years of cooling has the lowest resulting gamma-ray signal.

Pure Iron (1 year, PSB, position 4)
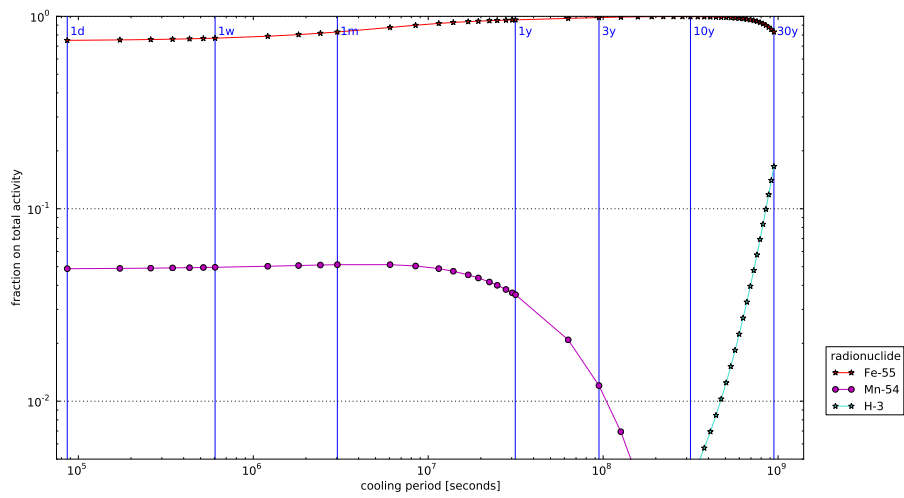
(a) Fractions of Activity
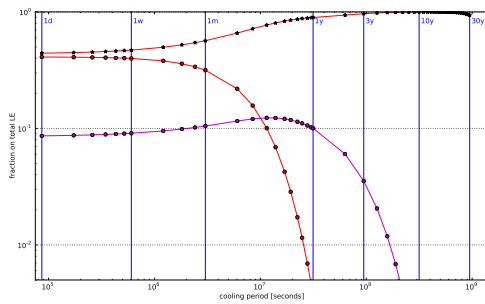
(b) Fractions of LE
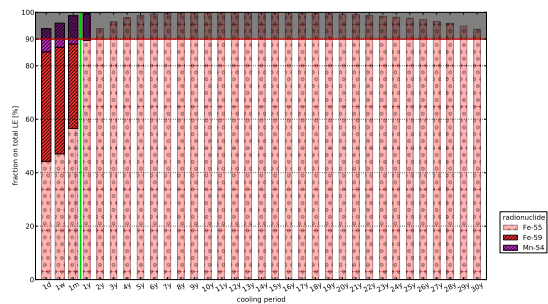
(c) LE Fractions stacked up to at least 90%
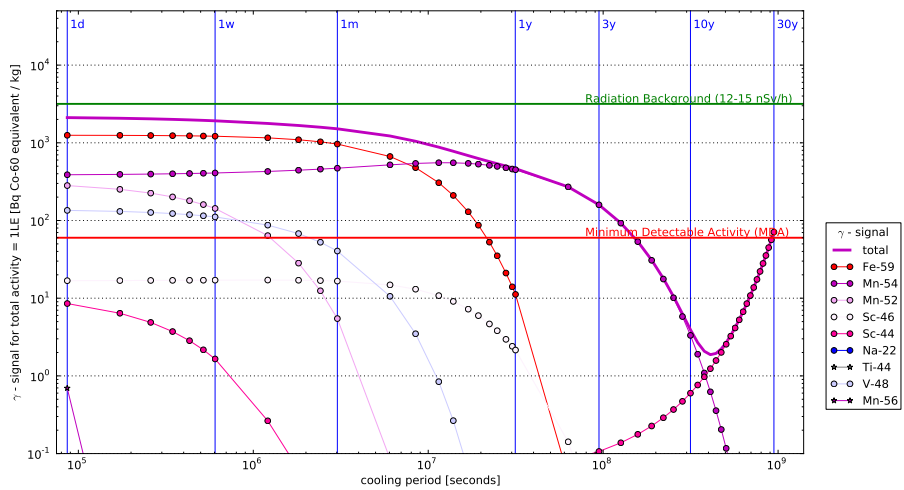
(d) Resulting Gamma Photon Signal

Figure A.3.4: Visualisation plots of the radionuclide inventories for the most conservative irradiation scenario for _Pure Iron_ (as defined in Sec. 7.2). The radionuclide inventory after 13 years of cooling has the lowest resulting gamma-ray signal.

A.3.ii   Plots for the Limited Parameter Range

Common Copper (30 years, PSB, position 4)
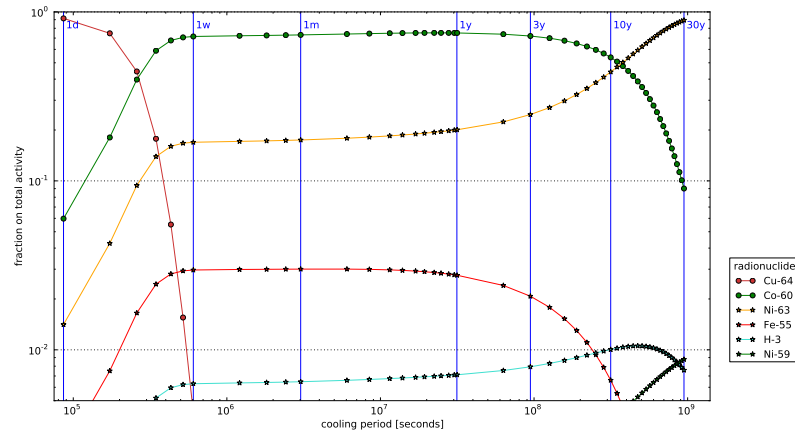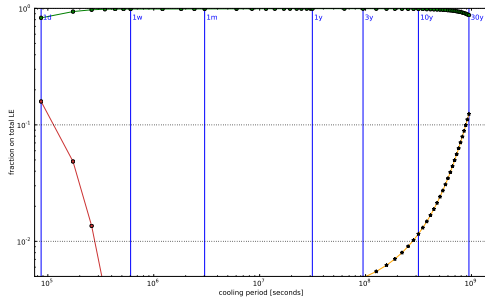
(a) Fractions of Activity

(b) Fractions of LE
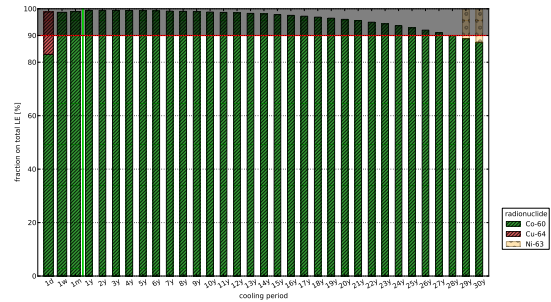
(c) LE Fractions stacked up to at least 90%
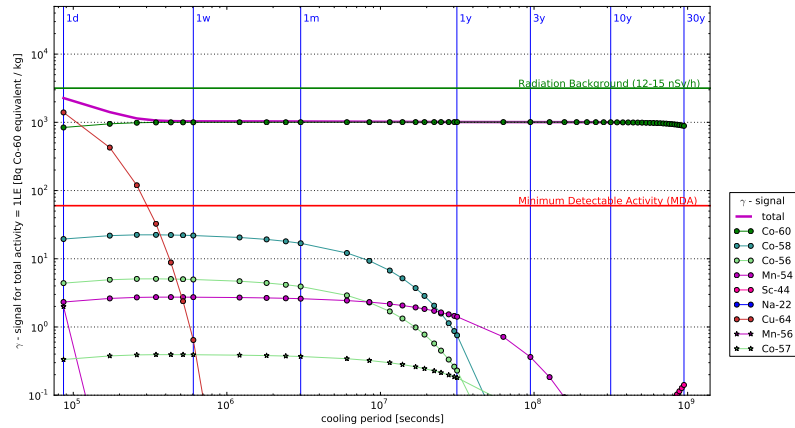
(d) Resulting Gamma Photon Signal

Figure A.3.5: Visualisation plots of the radionuclide inventories for the most conservative irradiation scenario for *Common Copper* (as defined in Sec. 7.2). Considering a cooling time range up to a maximum cooling time of 2 years, the radionuclide inventory after 2 years of cooling has the lowest resulting gamma-ray signal.

Common Aluminium (60 days, PS, position 4)
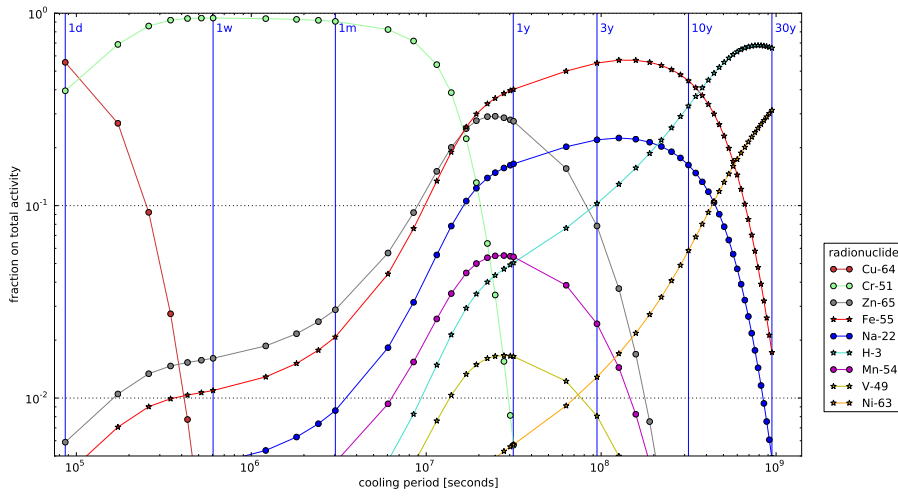
(a) Fractions of Activity
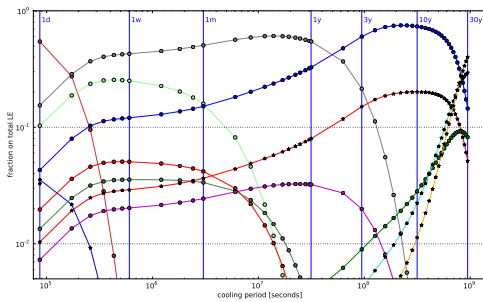
(b) Fractions of LE
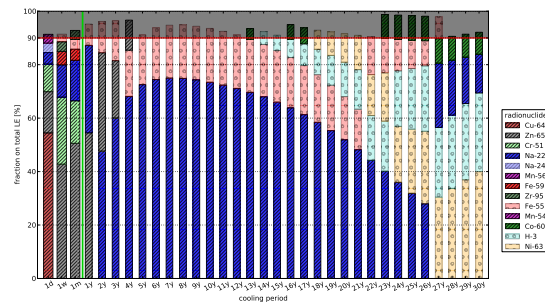
(c) LE Fractions stacked up to at least 90%
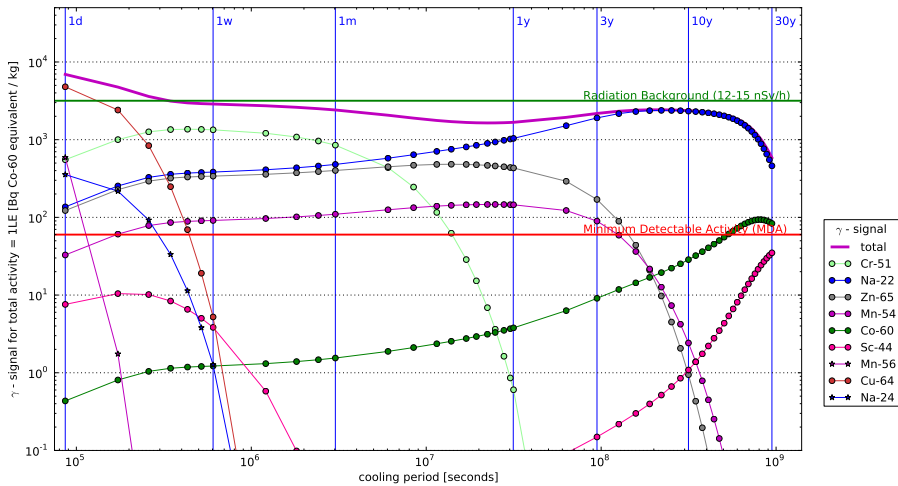
(d) Resulting Gamma Photon Signal

Figure A.3.6: Visualisation plots of the radionuclide inventories for the most conservative irradiation scenario for *Common Aluminium* (as defined in Sec. 7.2). Considering a cooling time range up to a maximum cooling time of 2 years, the radionuclide inventory after 8 months of cooling has the lowest resulting gamma-ray signal.

Common Steel (1 year, PS, position 4)
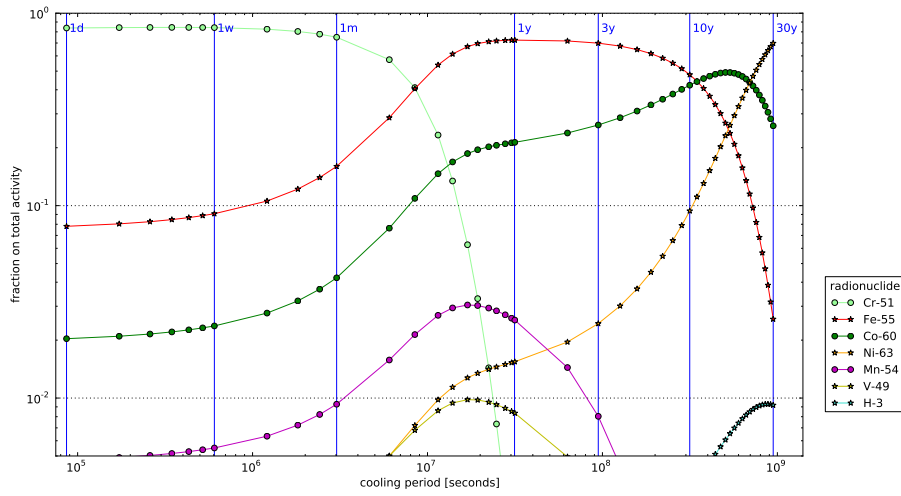
(a) Fractions of Activity
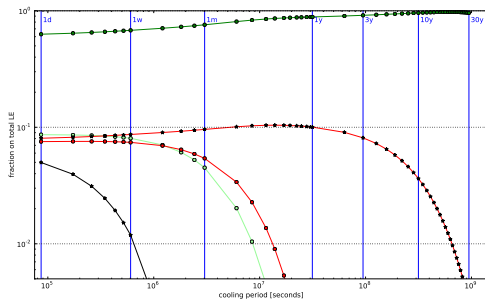
(b) Fractions of LE
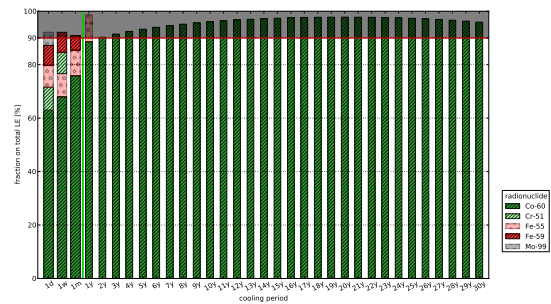
(c) LE Fractions stacked up to at least 90%
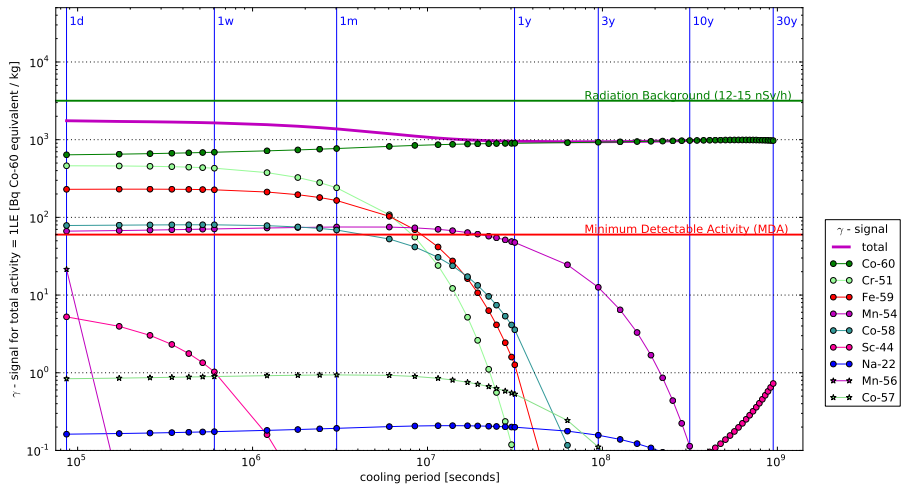
(d) Resulting Gamma Photon Signal

Figure A.3.7: Visualisation plots of the radionuclide inventories for the most conservative irradiation scenario for *Common Steel* (as defined in Sec. 7.2). Considering a cooling time range up to a maximum cooling time of 2 years, the radionuclide inventory after 2 years of cooling has the lowest resulting gamma-ray signal.

Pure Iron (30 years, PS, position 4)
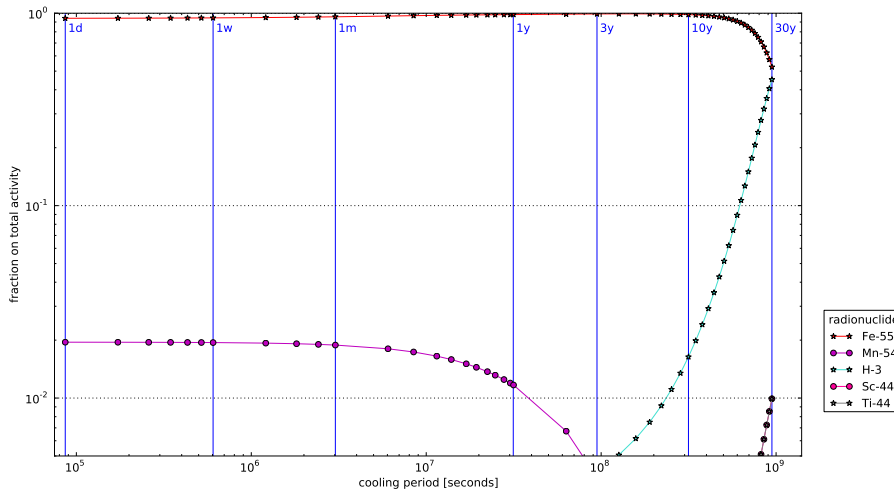
(a) Fractions of Activity
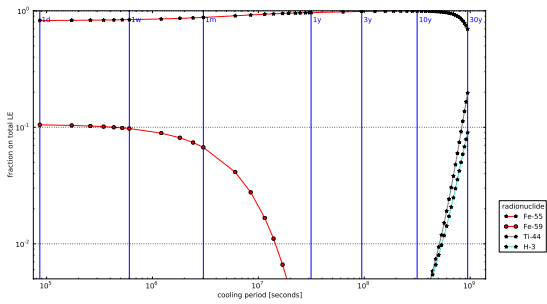
(b) Fractions of LE
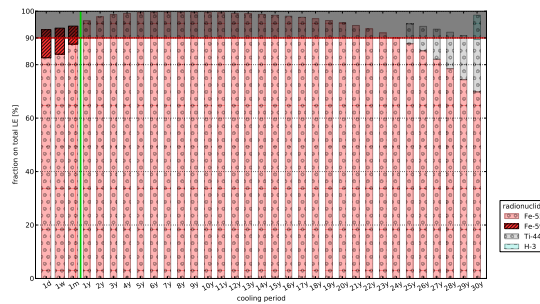
(c) LE Fractions stacked up to at least 90%
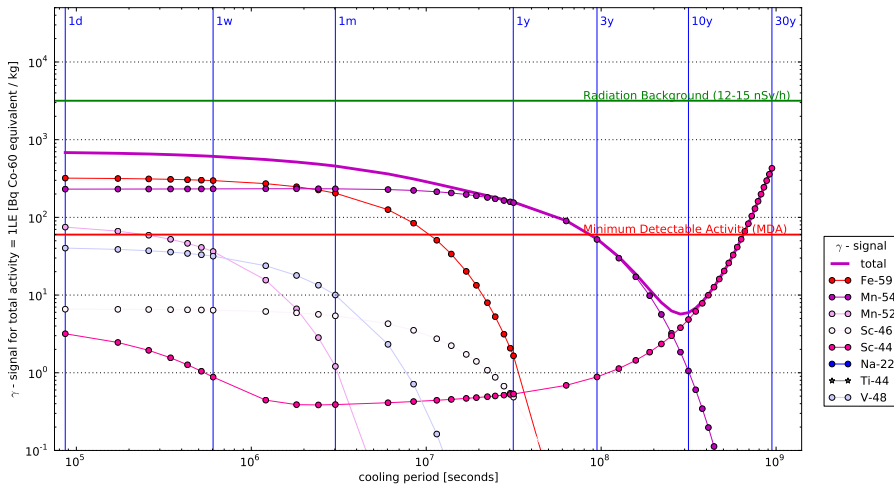
(d) Resulting Gamma Photon Signal

Figure A.3.8: Visualisation plots of the radionuclide inventories for the most conservative irradiation scenario for *Pure Iron* (as defined in Sec. 7.2). Considering a cooling time range up to a maximum cooling time of 2 years, the radionuclide inventory after 2 years of cooling has the lowest resulting gamma-ray signal.

A.4   Steel Material Sampling Campaign

(a) Steel Sample 'X01'

(b) Steel Sample 'X02'

(c) Steel Sample 'X03'

(d) Steel Sample 'X04'

(e) Steel Samples '1A', '1B', '2A', '2B', '3A', '3B', '4A', '4B', '5A', '5B', '6A' and '6B'

Figure A.4.1: Stainless steel pipes prepared for a sampling campaign to evaluate the chemical material composition of the reference material *Common Steel*. The determined chemical material composition of these samples can be found in Tab. A.4.1.

Table A.4.1: Chemical material compositions of the samples from the performed measurement campaign. The material compositions were determined by optical emission spectroscopy (OES) by a device denoted 'PMI-MASTER Pro' (Oxford Instruments). Pictures of the steel samples are shown in Fig. A.4.1.

	1A	1B	2A	2B	3A	3B	4A	4B	5A	5B	6A	6B	X01	X02	X03	X04
Fe	69.800	69.300	67.700	67.600	69.500	68.900	68.700	68.000	69.700	69.600	69.100	69.000	69.400	70.600	70.200	69.600
C	0.038	0.037	0.035	0.047	0.028	0.040	0.065	0.059	0.038	0.036	0.041	0.043	0.062	0.062	0.055	0.088
Si	0.303	0.314	0.537	0.533	0.608	0.548	0.488	0.466	0.336	0.344	0.334	0.372	0.454	0.732	0.591	0.623
Mn	1.370	1.390	1.100	1.070	1.040	1.130	0.366	0.369	1.300	1.320	1.830	1.810	1.330	0.951	0.955	0.827
Cr	17.800	17.900	18.200	18.200	18.000	18.100	17.700	17.900	17.900	17.900	17.600	17.400	18.500	17.500	17.700	17.500
Mo	0.095	0.097	0.232	0.226	0.151	0.151	0.119	0.117	0.177	0.169	0.283	0.275	0.164	0.115	0.146	0.111
Ni	10.200	10.500	11.700	11.900	10.200	10.600	11.400	11.900	10.000	10.000	10.100	10.300	9.660	9.590	9.910	10.100
Al	<0.001	0.002	0.003	0.004	0.002	0.005	0.064	0.063	<0.001	<0.001	0.003	0.003	0.003	0.004	0.003	0.082
Co	0.054	0.051	0.091	0.089	0.161	0.156	0.032	0.031	0.141	0.135	0.110	0.110	0.056	0.154	0.146	0.015
Cu	0.137	0.146	0.139	0.130	0.060	0.055	0.196	0.188	0.157	0.165	0.416	0.412	0.127	0.058	0.087	0.141
Nb	<0.0014	0.002	0.003	0.004	<0.0014	0.005	0.003	0.003	0.002	0.002	<0.0014	0.003	0.004	0.006	0.003	<0.0014
Ti	0.005	0.005	0.005	0.005	0.017	0.016	0.726	0.729	0.009	0.01	0.021	0.024	0.005	0.010	0.007	0.681
V	0.047	0.046	0.039	0.035	0.066	0.087	0.035	0.033	0.026	0.027	0.053	0.057	0.055	0.077	0.077	0.042
W	<0.030	<0.030	<0.030	<0.030	<0.030	<0.030	<0.030	<0.030	0.052	0.065	<0.030	0.077	0.039	0.053	<0.030	<0.030
Pb	<0.100	<0.100	<0.100	<0.100	<0.100	<0.100	<0.100	<0.100	<0.100	<0.100	<0.100	<0.100	<0.100	<0.100	<0.100	<0.100
Grade#	1.4301	1.4301	1.4303	1.4303	1.4306	1.4301	1.4541	1.4541	1.4301	1.4301	1.4305	1.4305	–	–	–	–

EN steel number, according to the Register of European Steels (Stahl-Eisen-Liste), proposed by
the mobile optical emission spectroscopy (OES) device 'PMI-MASTER Pro' (Oxford Instruments).

A.5   FLUKA Simulations of Self-Absorption Effects

A.5.i   Photon Spectra

Photon Spectra, Iron Sphere of 10 kg
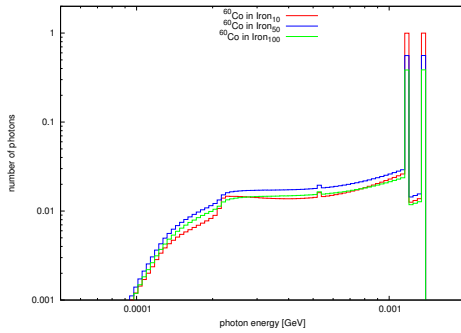
(a) Sphere, Homogeneous Activity
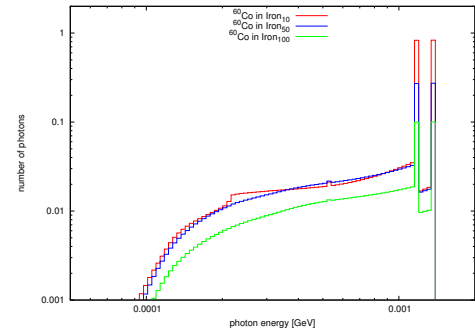
(b) Sphere, Centred Activity
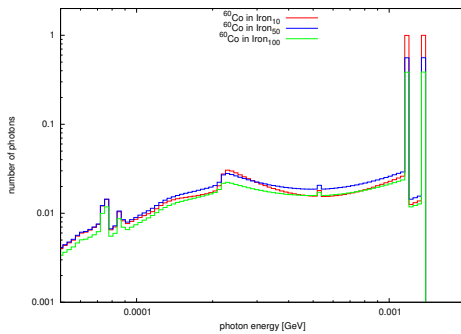
(c) Detector, Homogeneous Activity
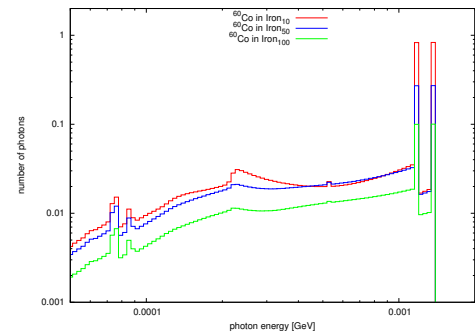
(d) Detector, Centred Activity
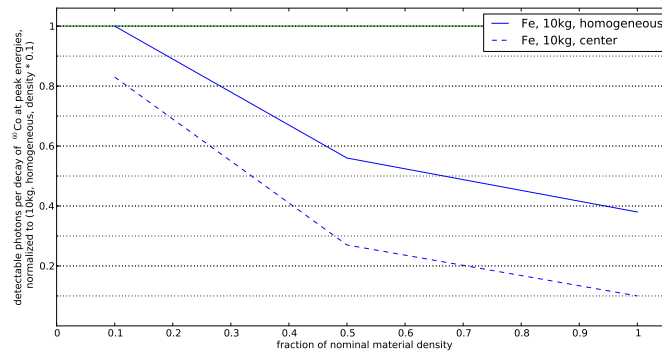
(e) Synthesis of Numbers of Photons at Peak Energies

Figure A.5.1: Photon spectra emitted from an iron sphere by the decay of ^{60}Co. Activity is homogeneously distributed in Fig. (a, c) and centred in Fig. (b, d). The sphere mass is 10 kg with a material density of $0.1\,\rho_{(\mathrm{Fe})}$, $0.5\,\rho_{(\mathrm{Fe})}$ or $\rho_{(\mathrm{Fe})}$. The photons are scored at the sphere surface in Fig. (a, b) and at the detector wall in Fig. (c, d). The numbers of photons are normalized to the scenario 'homogeneous, $\rho = 0.1\,\rho_{(\mathrm{Fe})}$' at peak energies. Figure (e) illustrates a synthesis of the numbers of photons at peak energies of Fig. (a, b).

Photon Spectra, Iron Sphere of 20 kg

(a) Sphere Surface, Homogeneous Activity

(b) Sphere Surface, Centred Activity

(c) Detector Wall, Homogeneous Activity

(d) Detector Wall, Centred Activity

(e) Synthesis of Numbers of Photons at Peak Energies
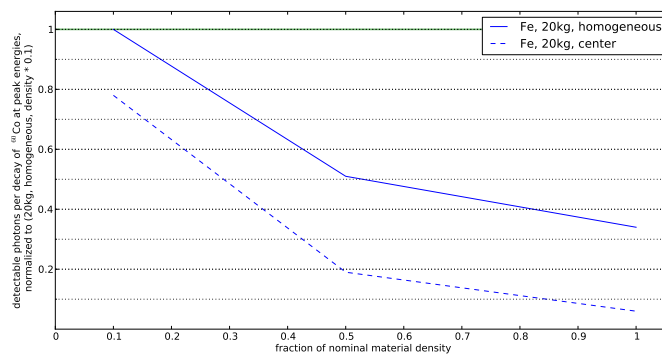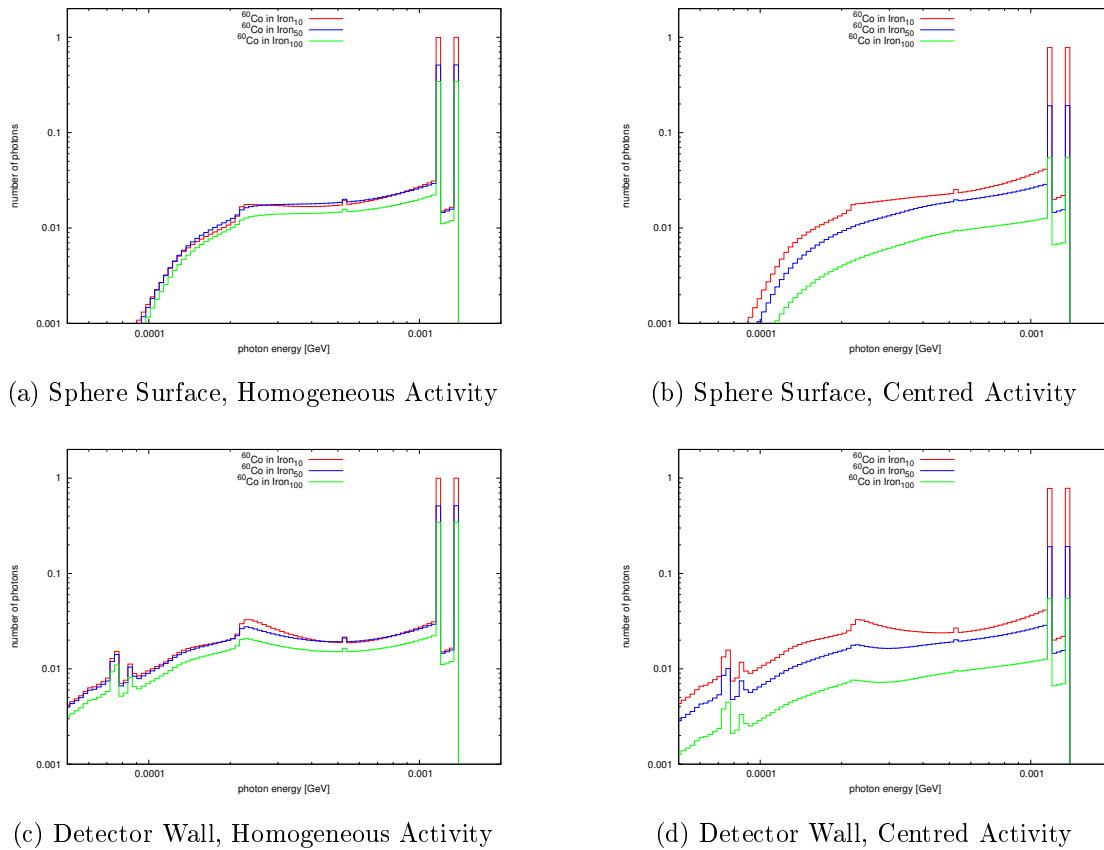
Figure A.5.2: Photon spectra emitted from an iron sphere by the decay of ^{60}Co. Activity is homogeneously distributed in Fig. (a,c) and centred in Fig. (b,d). The sphere mass is 20 kg with a material density of $0.1\,\rho_{(Fe)}$, $0.5\,\rho_{(Fe)}$ or $\rho_{(Fe)}$. The photons are scored at the sphere surface in Fig. (a, b) and at the detector wall in Fig. (c, d). The numbers of photons are normalized to the scenario 'homogeneous, $\rho = 0.1\,\rho_{(Fe)}$' at peak energies. Figure (e) illustrates a synthesis of the numbers of photons at peak energies of Fig. (a, b).

Photon Spectra, Copper Sphere of 10 kg
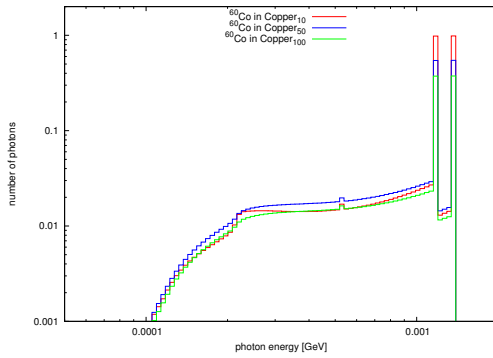
(a) Sphere Surface, Homogeneous Activity
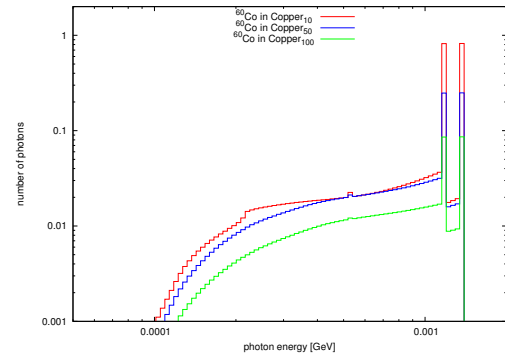
(b) Sphere Surface, Centred Activity

(c) Detector Wall, Homogeneous Activity

(d) Detector Wall, Centred Activity

(e) Synthesis of Numbers of Photons at Peak Energies

Figure A.5.3: Photon spectra emitted from a copper sphere by the decay of ^{60}Co. Activity is homogeneously distributed in Fig. (a, c) and centred in Fig. (b, d). The sphere mass is 10 kg with a material density of $0.1\,\rho_{(Cu)}$, $0.5\,\rho_{(Cu)}$ or $\rho_{(Cu)}$. The photons are scored at the sphere surface in Fig. (a, b) and at the detector wall in Fig. (c, d). The numbers of photons are normalized to the scenario 'homogeneous, $\rho = 0.1\,\rho_{(Cu)}$' at peak energies. Figure (e) illustrates a synthesis of the numbers of photons at peak energies of Fig. (a, b).

Photon Spectra, Copper Sphere of 20 kg

(a) Sphere Surface, Homogeneous Activity

(b) Sphere Surface, Centred Activity

(c) Detector Wall, Homogeneous Activity

(d) Detector Wall, Centred Activity

(e) Synthesis of Numbers of Photons at Peak Energies
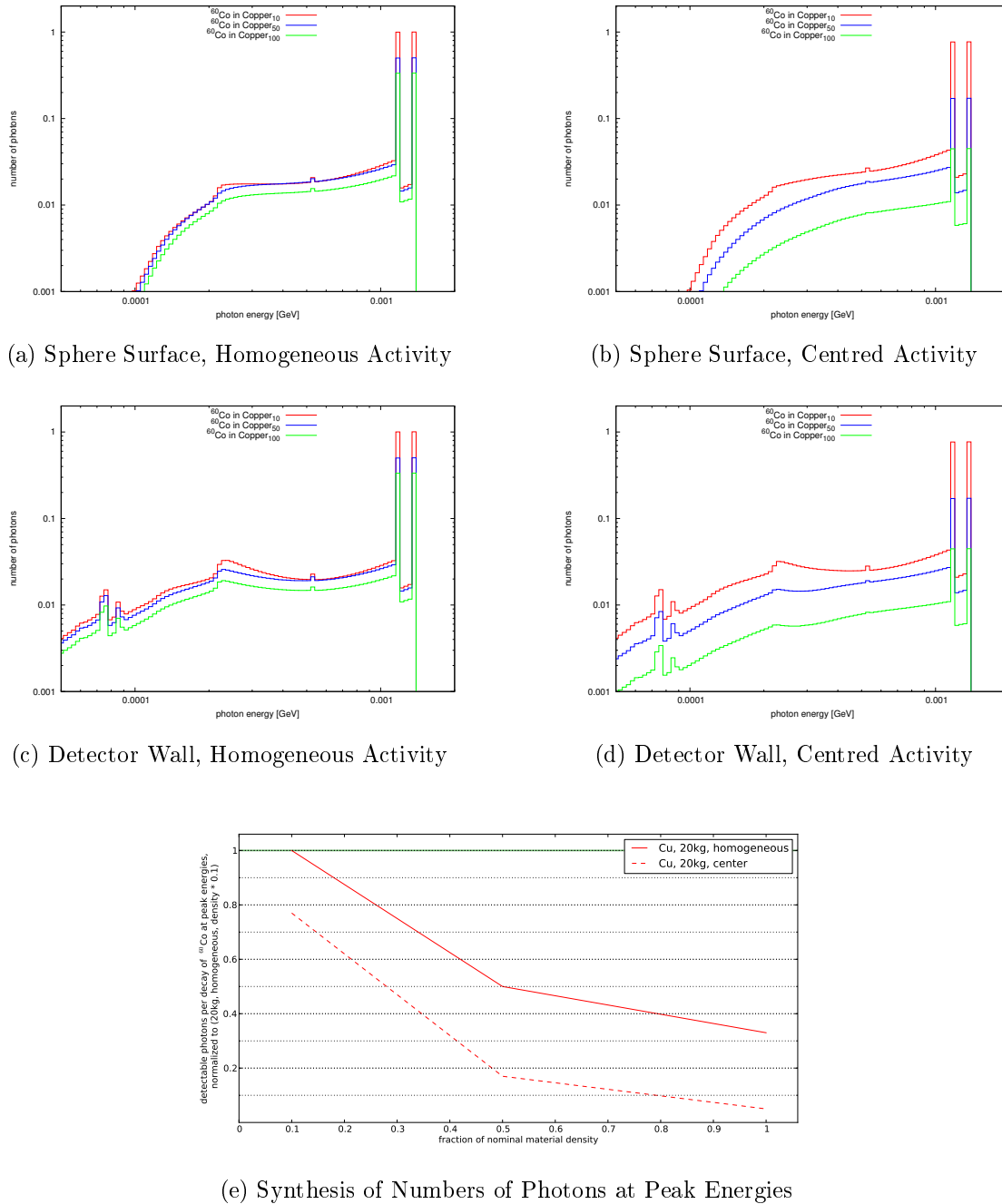
Figure A.5.4: Photon spectra emitted from a copper sphere by the decay of ^{60}Co. Activity is homogeneously distributed in Fig. (a, c) and centred in Fig. (b, d). The sphere mass is 20 kg with a material density of $0.1\,\rho_{(Cu)}$, $0.5\,\rho_{(Cu)}$ or $\rho_{(Cu)}$. The photons are scored at the sphere surface in Fig. (a, b) and at the detector wall in Fig. (c, d). The numbers of photons are normalized to the scenario 'homogeneous, $\rho = 0.1\,\rho_{(Cu)}$' at peak energies. Figure (e) illustrates a synthesis of the numbers of photons at peak energies of Fig. (a, b).

Photon Spectra, Aluminium Sphere of 10 kg
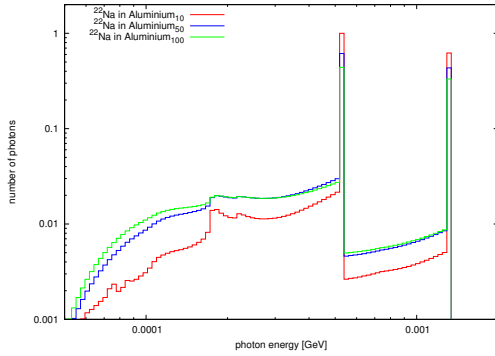
(a) Sphere Surface, Homogeneous Activity

(b) Sphere Surface, Centred Activity

(c) Detector Wall, Homogeneous Activity

(d) Detector Wall, Centred Activity

(e) Synthesis of Numbers of Photons at Peak Energies

Figure A.5.5: Photon spectra emitted from an aluminium sphere by the decay of ^{22}Na. Activity is homogeneously distributed in Fig. (a, c) and centred in Fig. (b, d). The sphere mass is 10 kg with a material density of $0.1\,\rho_{(Al)}$, $0.5\,\rho_{(Al)}$ or $\rho_{(Al)}$. The photons are scored at the sphere surface in Fig. (a, b) and at the detector wall in Fig. (c, d). The numbers of photons are normalized to the scenario 'homogeneous, $\rho = 0.1\,\rho_{(Al)}$' at peak energies. Figure (e) illustrates a synthesis of the numbers of photons at peak energies of Fig. (a, b) with a re-normalization to the scenario 'homogeneous, $\rho = 0.5\,\rho_{(Al)}$' at peak energies.

Photon Spectra, Aluminium Sphere of 20 kg

(a) Sphere Surface, Homogeneous Activity

(b) Sphere Surface, Centred Activity

(c) Detector Wall, Homogeneous Activity

(d) Detector Wall, Centred Activity

(e) Synthesis of Numbers of Photons at Peak Energies
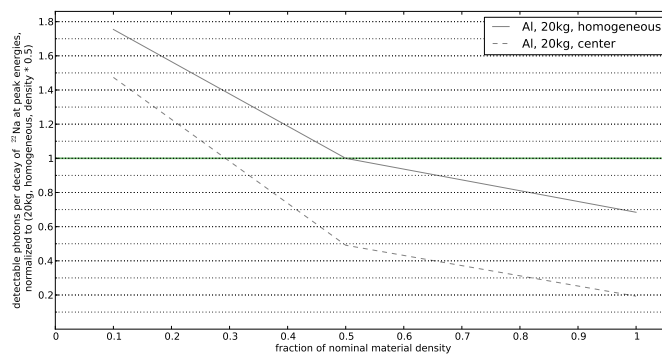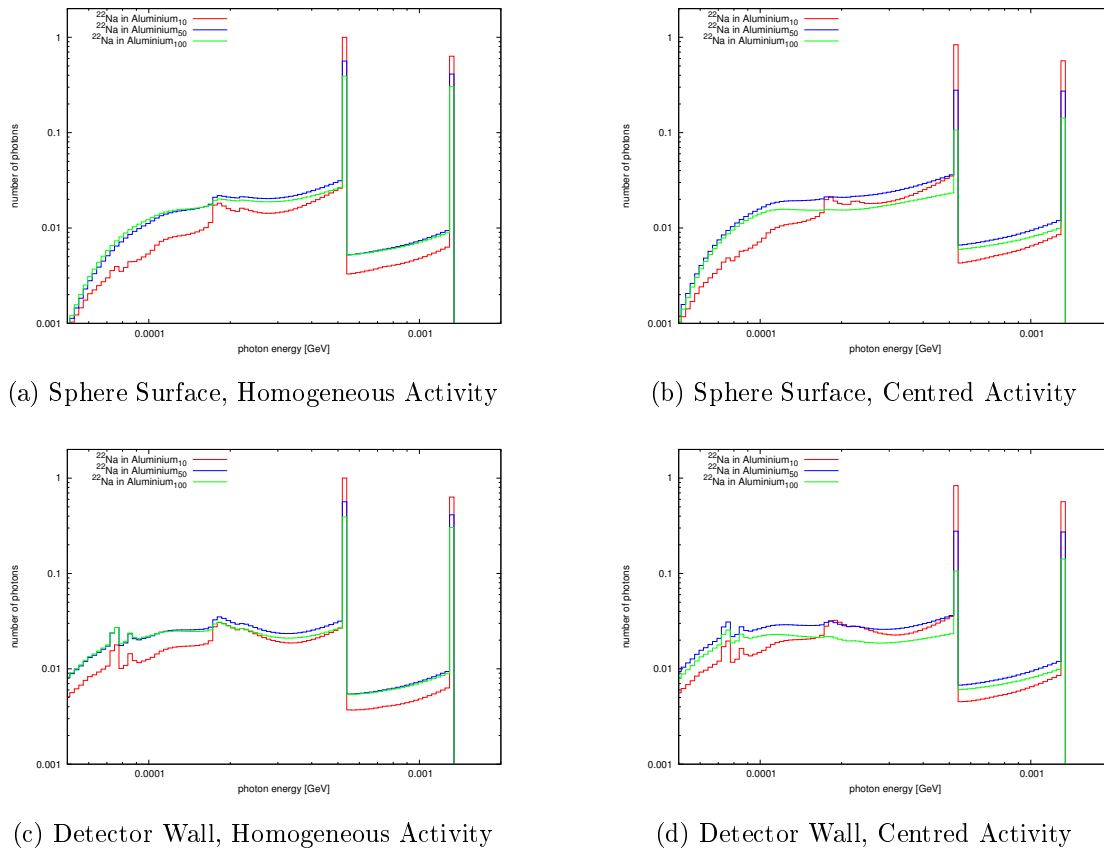
Figure A.5.6: Photon spectra emitted from an aluminium sphere by the decay of ^{22}Na. Activity is homogeneously distributed in Fig. (a, c) and centred in Fig. (b, d). The sphere mass is 20 kg with a material density of $0.1\,\rho_{(Al)}$, $0.5\,\rho_{(Al)}$ or $\rho_{(Al)}$. The photons are scored at the sphere surface in Fig. (a, b) and at the detector wall in Fig. (c, d). The numbers of photons are normalized to the scenario 'homogeneous, $\rho = 0.1\,\rho_{(Al)}$' at peak energies. Figure (e) illustrates a synthesis of the numbers of photons at peak energies of Fig. (a, b) with a re-normalization to the scenario 'homogeneous, $\rho = 0.5\,\rho_{(Al)}$' at peak energies.

A.5.ii Residual Dose Rate

Residual Dose Rate, Iron Sphere of 10 kg

(a) $\rho = 0.1\,\rho_{(Fe)}$, Homogeneous Activity

(b) $\rho = 0.1\,\rho_{(Fe)}$, Centred Activity

(c) $\rho = 0.5\,\rho_{(Fe)}$, Homogeneous Activity

(d) $\rho = 0.5\,\rho_{(Fe)}$, Centred Activity

(e) $\rho = \rho_{(Fe)}$, Homogeneous Activity

(f) $\rho = \rho_{(Fe)}$, Centred Activity
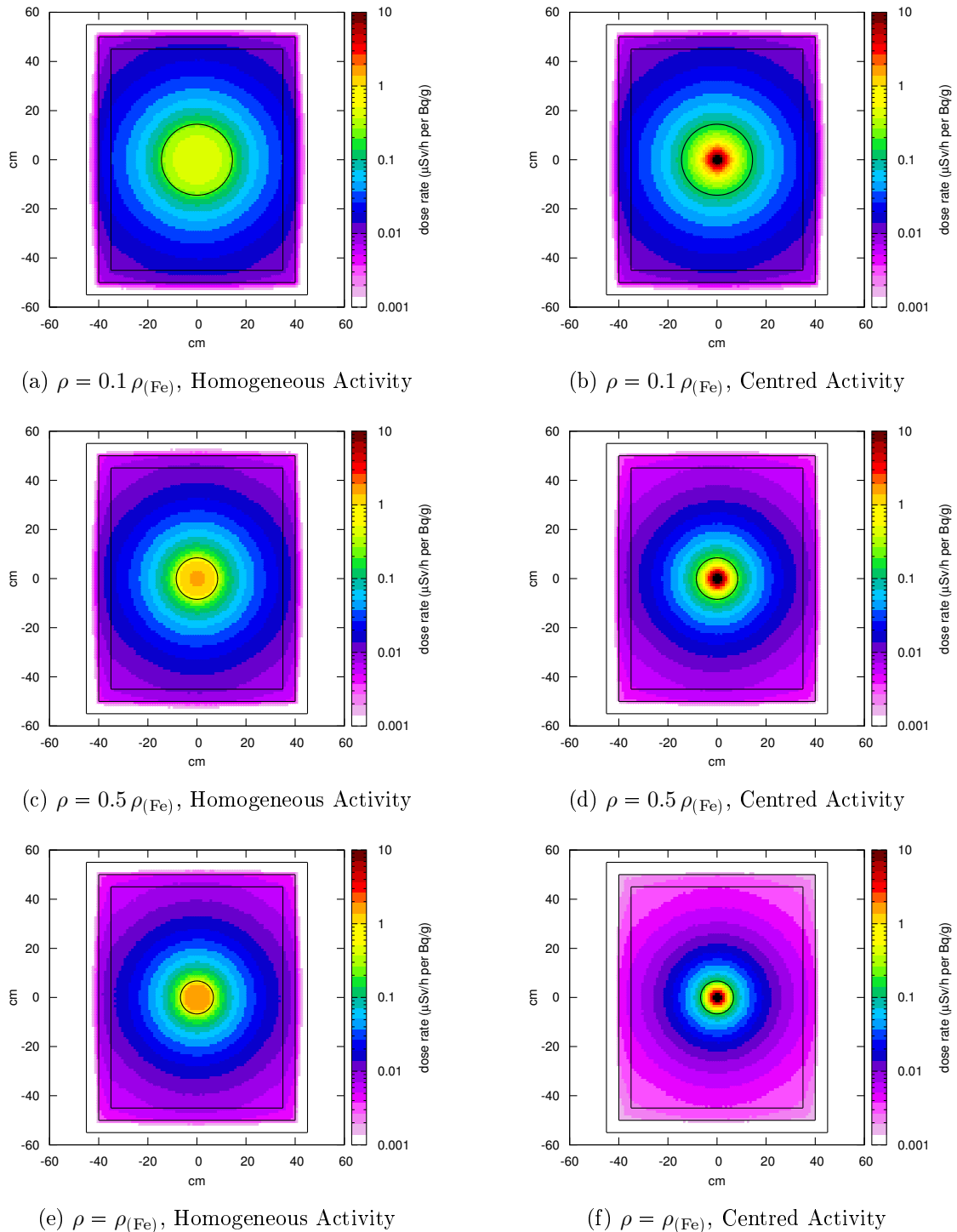
Figure A.5.7: Residual dose rate distribution of an activated iron sphere placed in the center of the RADOS RTM 661. The dose rate is calculated per $\mathrm{Bq\,g^{-1}}$ of $^{60}\mathrm{Co}$ for different material densities of a 10 kg sphere as well as for different activity distributions.

Residual Dose Rate, Iron Sphere of 20 kg

(a) $\rho = 0.1\,\rho_{(\mathrm{Fe})}$, Homogeneous Activity

(b) $\rho = 0.1\,\rho_{(\mathrm{Fe})}$, Centred Activity

(c) $\rho = 0.5\,\rho_{(\mathrm{Fe})}$, Homogeneous Activity

(d) $\rho = 0.5\,\rho_{(\mathrm{Fe})}$, Centred Activity

(e) $\rho = \rho_{(\mathrm{Fe})}$, Homogeneous Activity

(f) $\rho = \rho_{(\mathrm{Fe})}$, Centred Activity
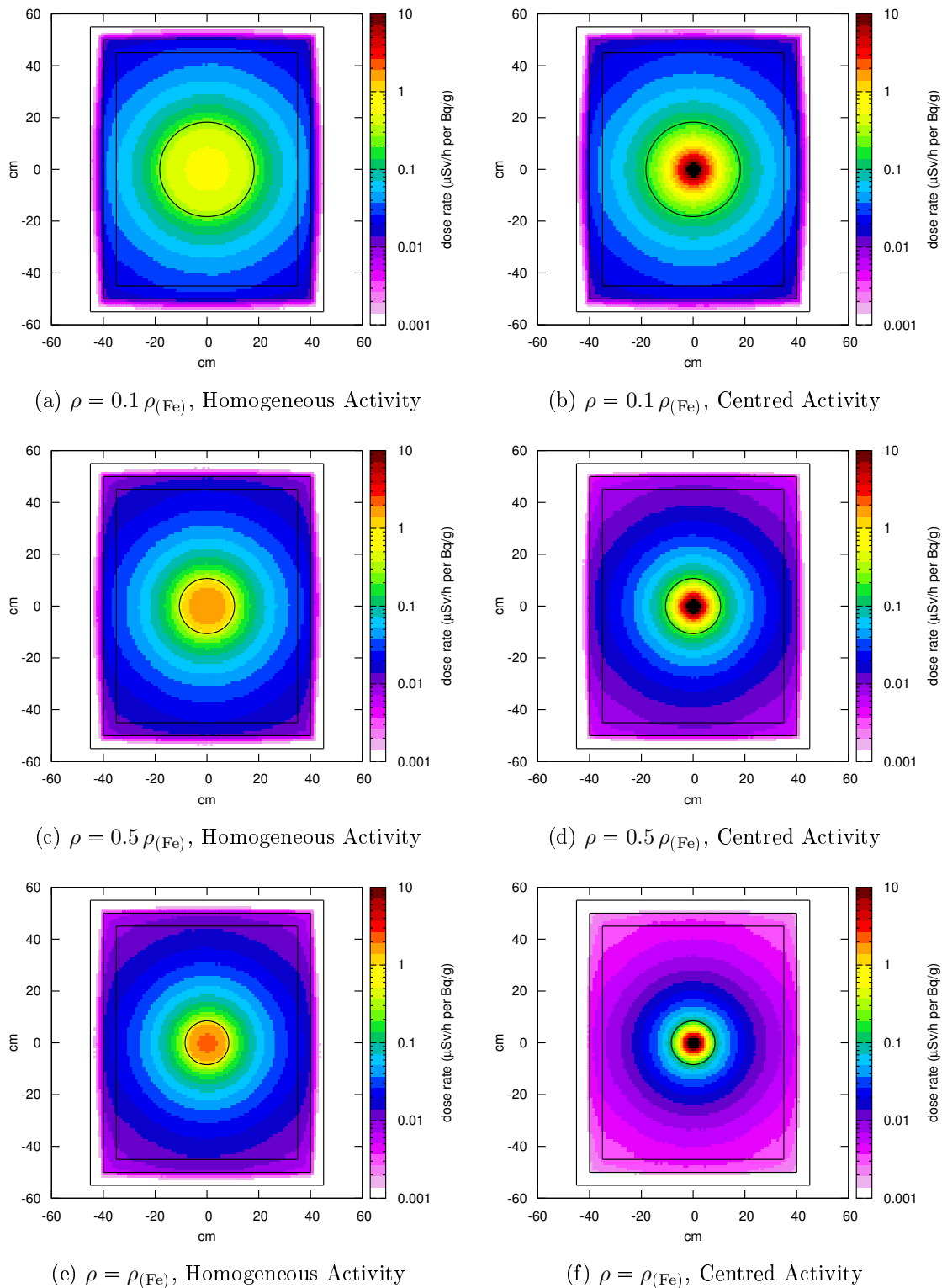
Figure A.5.8: Residual dose rate distribution of an activated iron sphere placed in the center of the RADOS RTM 661. The dose rate is calculated per $\mathrm{Bq\,g^{-1}}$ of $^{60}\mathrm{Co}$ for different material densities of a 20 kg sphere as well as for different activity distributions.

Residual Dose Rate, Copper Sphere of 10 kg
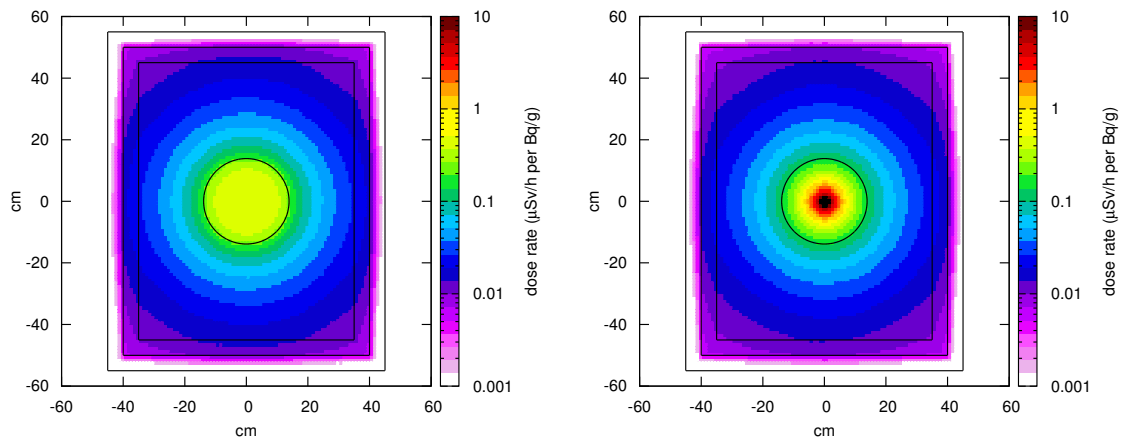
(a) $\rho = 0.1\,\rho_{(\mathrm{Cu})}$, Homogeneous Activity
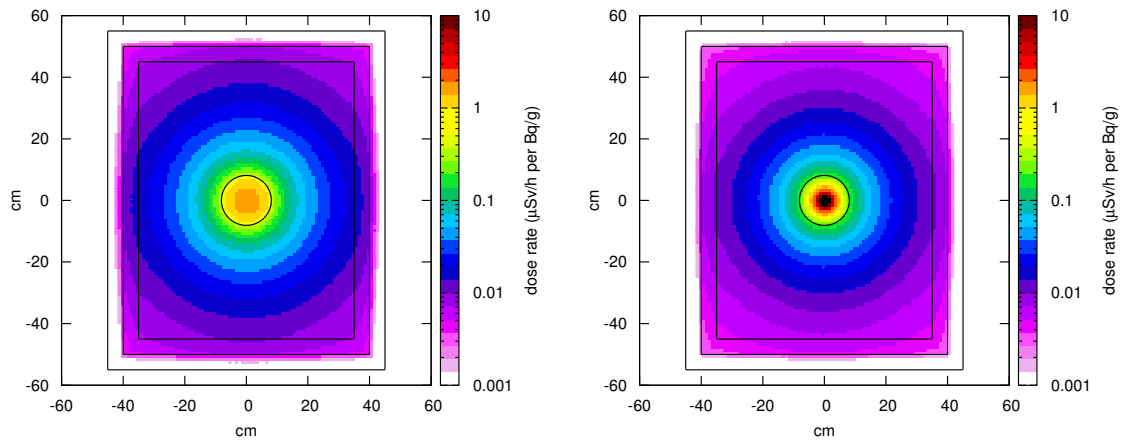
(b) $\rho = 0.1\,\rho_{(\mathrm{Cu})}$, Centred Activity

(c) $\rho = 0.5\,\rho_{(\mathrm{Cu})}$, Homogeneous Activity

(d) $\rho = 0.5\,\rho_{(\mathrm{Cu})}$, Centred Activity
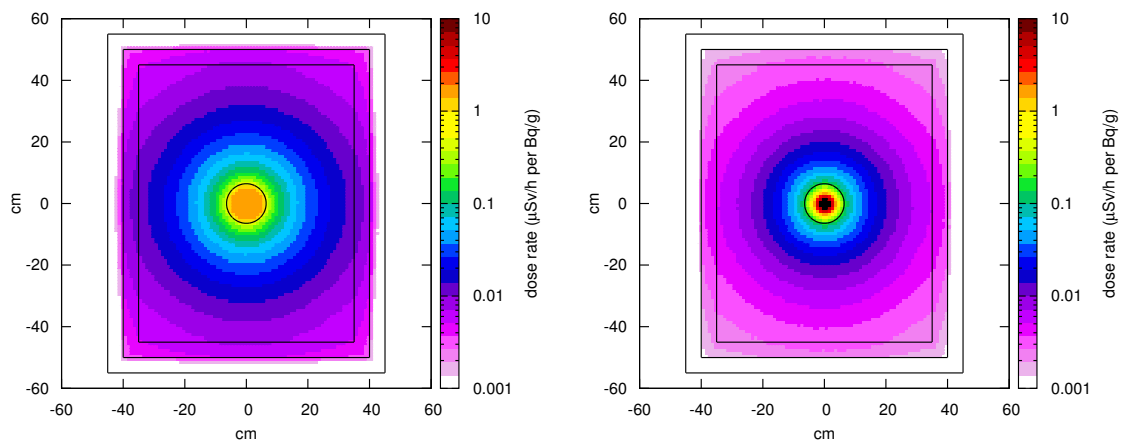
(e) $\rho = \rho_{(\mathrm{Cu})}$, Homogeneous Activity

(f) $\rho = \rho_{(\mathrm{Cu})}$, Centred Activity

Figure A.5.9: Residual dose rate distribution of an activated copper sphere placed in the center of the RADOS RTM 661. The dose rate is calculated per $\mathrm{Bq\,g^{-1}}$ of ^{60}Co for different material densities of a 10 kg sphere as well as for different activity distributions.

Residual Dose Rate, Copper Sphere of 20 kg
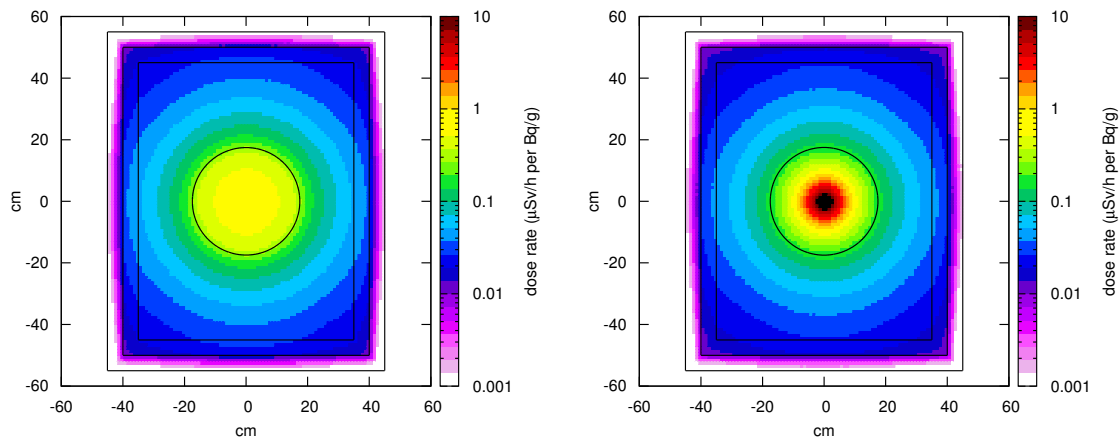
(a) $\rho = 0.1\,\rho_{(Cu)}$, Homogeneous Activity
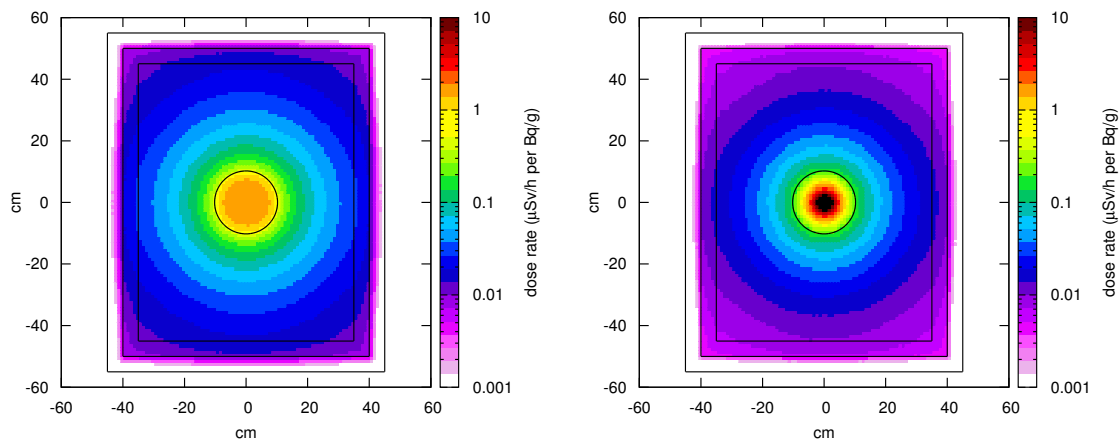
(b) $\rho = 0.1\,\rho_{(Cu)}$, Centred Activity

(c) $\rho = 0.5\,\rho_{(Cu)}$, Homogeneous Activity

(d) $\rho = 0.5\,\rho_{(Cu)}$, Centred Activity
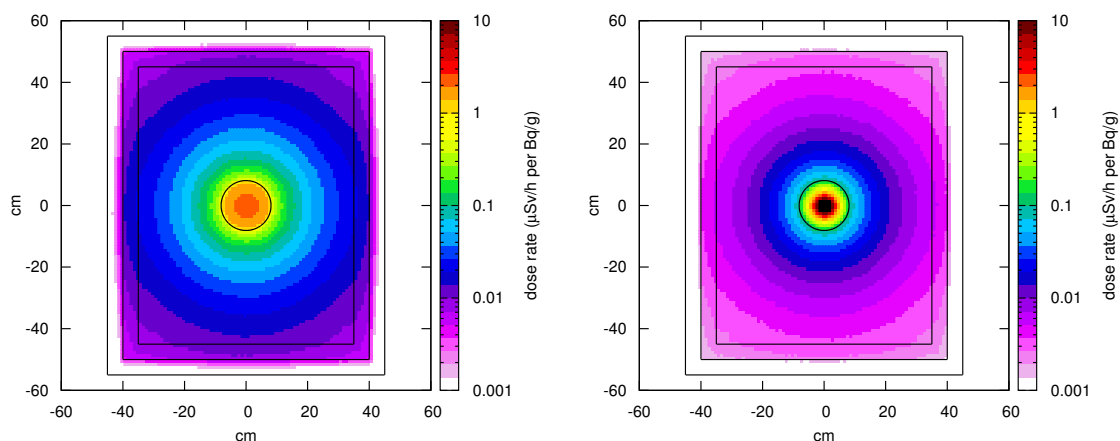
(e) $\rho = \rho_{(Cu)}$, Homogeneous Activity

(f) $\rho = \rho_{(Cu)}$, Centred Activity

Figure A.5.10: Residual dose rate distribution of an activated copper sphere placed in the center of the RADOS RTM 661. The dose rate is calculated per $Bq\,g^{-1}$ of ^{60}Co for different material densities of a 20 kg sphere as well as for different activity distributions.

Residual Dose Rate, Aluminium Sphere of 10 kg

(a) $\rho = 0.1\,\rho_{(\mathrm{Al})}$, Homogeneous Activity

(b) $\rho = 0.1\,\rho_{(\mathrm{Al})}$, Centred Activity

(c) $\rho = 0.5\,\rho_{(\mathrm{Al})}$, Homogeneous Activity

(d) $\rho = 0.5\,\rho_{(\mathrm{Al})}$, Centred Activity

(e) $\rho = \rho_{(\mathrm{Al})}$, Homogeneous Activity

(f) $\rho = \rho_{(\mathrm{Al})}$, Centred Activity
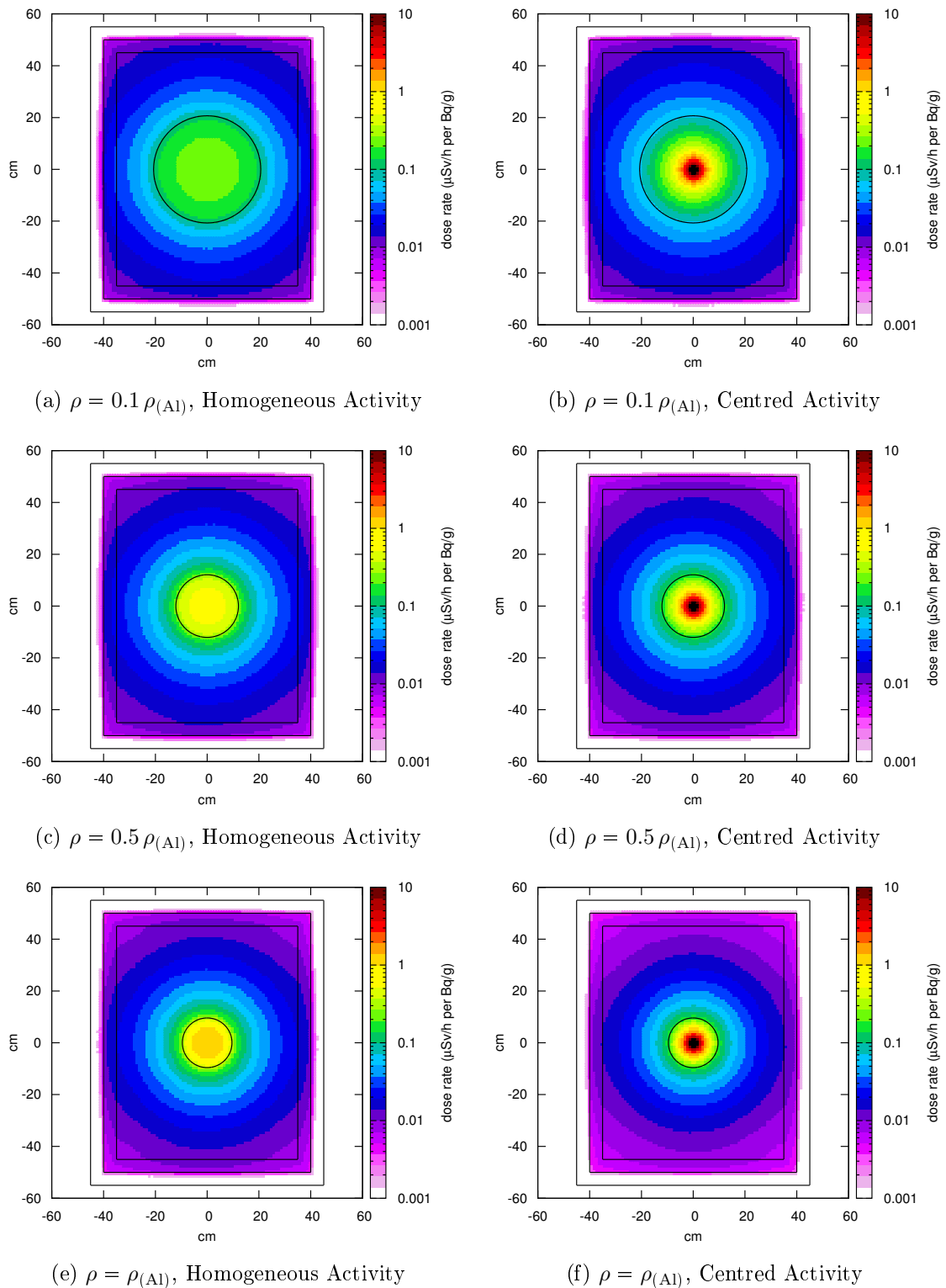
Figure A.5.11: Residual dose rate distribution of an activated aluminium sphere placed in the center of the RADOS RTM 661. The dose rate is calculated per $\mathrm{Bq\,g^{-1}}$ of ^{22}Na for different material densities of a 10 kg sphere as well as for different activity distributions.

Residual Dose Rate, Aluminium Sphere of 20 kg

(a) $\rho = 0.1\,\rho_{(\mathrm{Al})}$, Homogeneous Activity

(b) $\rho = 0.1\,\rho_{(\mathrm{Al})}$, Centred Activity

(c) $\rho = 0.5\,\rho_{(\mathrm{Al})}$, Homogeneous Activity

(d) $\rho = 0.5\,\rho_{(\mathrm{Al})}$, Centred Activity

(e) $\rho = \rho_{(\mathrm{Al})}$, Homogeneous Activity

(f) $\rho = \rho_{(\mathrm{Al})}$, Centred Activity
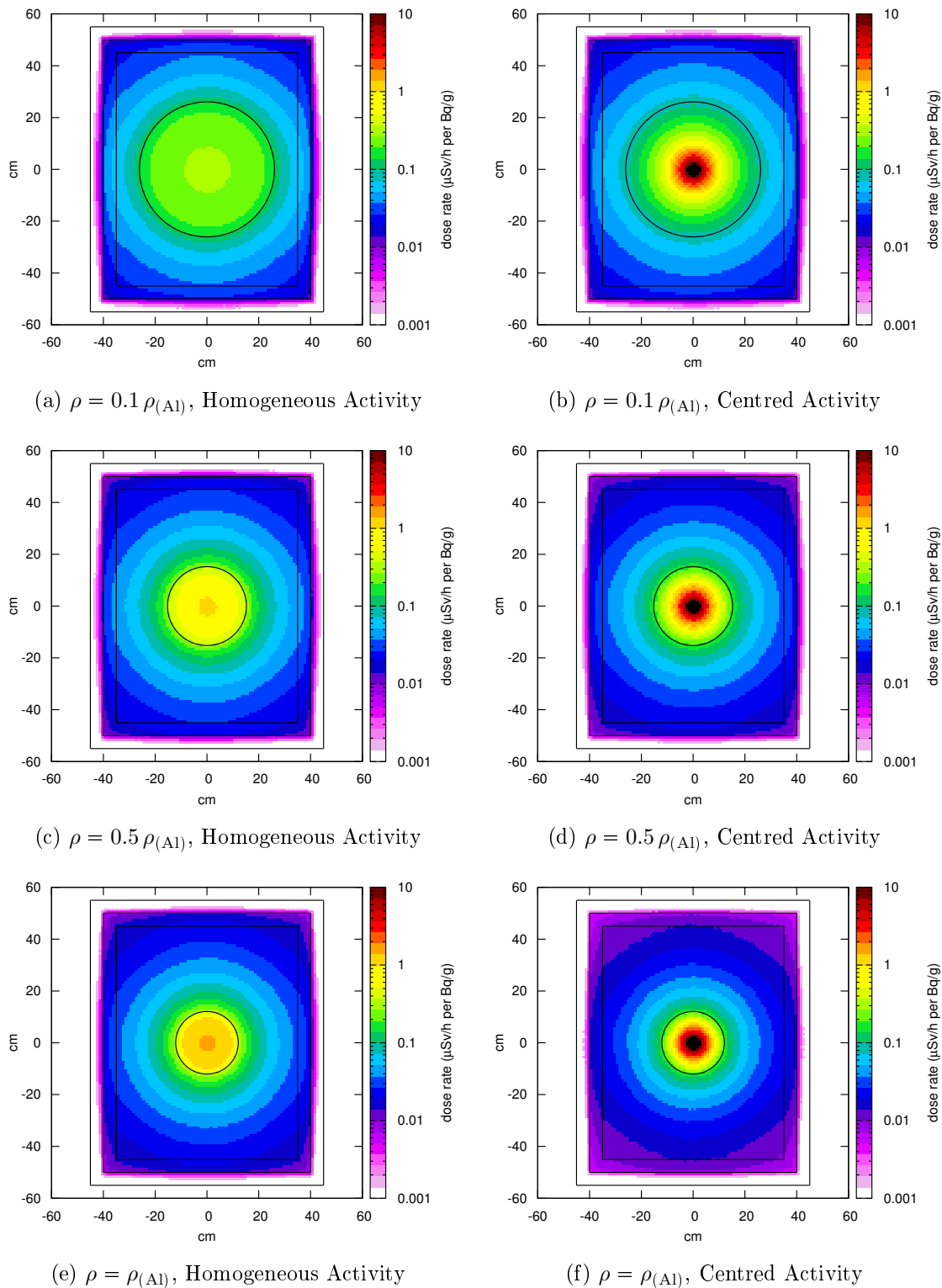
Figure A.5.12: Residual dose rate distribution of an activated aluminium sphere placed in the center of the RADOS RTM 661. The dose rate is calculated per Bq g^{-1} of ^{22}Na for different material densities of a 20 kg sphere as well as for different activity distributions.

A.6 Common Radionuclides

A.6.i Swiss Exemption Limits of Common Radionuclides

Table A.6.1: Swiss exemption limits for mass specific activity and surface contamination of common radionuclides. The data is taken from the ORaP [36].

Radionuclide	Half-life	LE_i $[\mathrm{Bq\,g^{-1}}]$	CS_i $[\mathrm{Bq\,cm^{-2}}]$
$^{3}\mathrm{H}^{\#}$	12.35 a	200	1000
$^{7}\mathrm{Be}$	53.3 d	400	1000
$^{14}\mathrm{C}^{\#}$	5730 a	20	30
$^{22}\mathrm{Na}$	2.6 a	3	3
$^{24}\mathrm{Na}$	15 h	20	3
$^{36}\mathrm{Cl}^{\#}$	301000 a	10	3
$^{44}\mathrm{Sc}$	3.927 h	30	3
$^{44}\mathrm{Ti}$	47.3✠ a	2	30
$^{49}\mathrm{V}$	330 d	600	100
$^{51}\mathrm{Cr}$	27.704 d	300	100
$^{54}\mathrm{Mn}$	312.5 d	10	100
$^{55}\mathrm{Fe}^{\#}$	2.7 a	30	300
$^{56}\mathrm{Co}$	78.76 d	4	10
$^{57}\mathrm{Co}$	270.9 d	50	100
$^{58}\mathrm{Co}$	70.80 d	10	30
$^{60}\mathrm{Co}$	5.271 a	1	3
$^{63}\mathrm{Ni}^{\#}$	96 a	70	1000
$^{64}\mathrm{Cu}$	12.701 h	80	10
$^{65}\mathrm{Zn}$	243.9 d	3	30
$^{110m}\mathrm{Ag}$	249.9 d	4	10
$^{137}\mathrm{Cs}$	30.0 a	0.8	3
$^{152}\mathrm{Eu}$	13.33 a	7	10

✠ for further calculation this value has been replaced by $\mathrm{T}_{1/2} = 60\,\mathrm{a}$ [52]

difficult-to-measure radionuclide according to ISO 21238 [17]

(for further information see footnote[1] on page 8)

A.6.ii   Decay Schemes and Emission Spectra of Common *Key Radionuclides*

Figure A.6.1: The figure shows on the following pages, in various sub-figures, the decay schemes and the emission spectra of common *key radionuclides* as defined in Tab. A.6.1. The decay schemes are extracted from the 'Recommended Data - Table de Radionucléides' provided by the 'Decay Data Evaluation Project', an international collaboration, which includes members of the BNM-CEA/LNHB (France), PTB (Germany), INEEL (USA), KRI (Russia), LBNL (USA), NPL (United Kingdom), CIEMAT (Spain), with the objective of providing carefully produced recommended data. Updates of the recommended data pages are realized by the 'Laboratoire National Henri Becquerel' in Paris, France. The radiation emission spectra are created with the web-based tool 'Nucleide Datasheets++' from NUCLEONICA [62]. The plots are based on data of the JEFF-3.1.1 nuclear data library [52].

Decay Scheme and Emission Spectrum of ^{7}Be
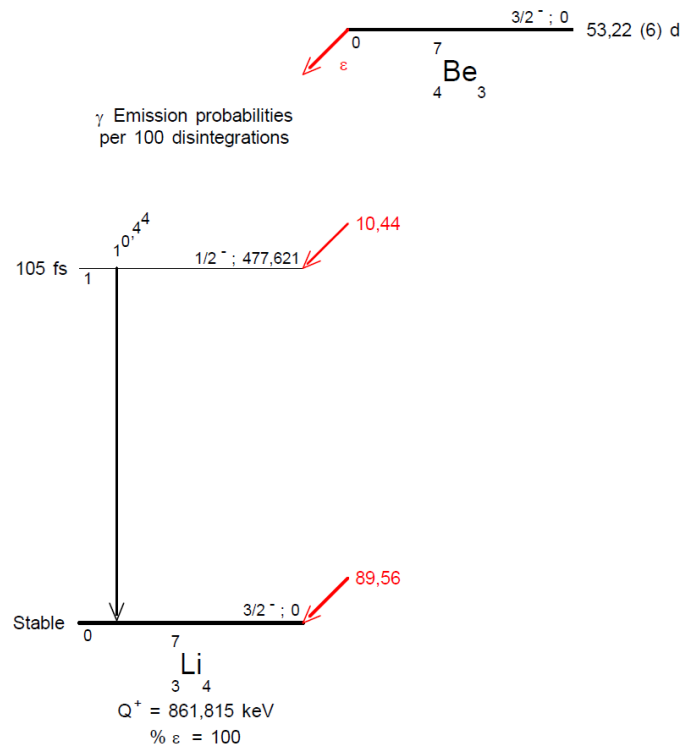
(A.6.2−1) ^{7}Be decay scheme, $T_{1/2}$ = 53.22 d
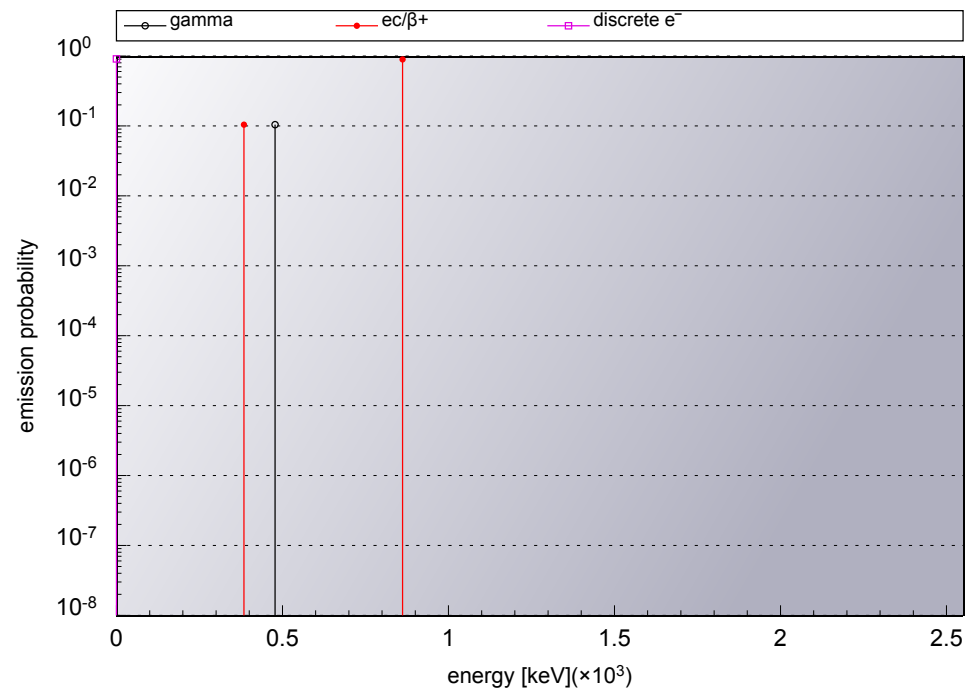
(A.6.2−2) ^{7}Be emission spectrum

Decay Scheme and Emission Spectrum of ^{22}Na
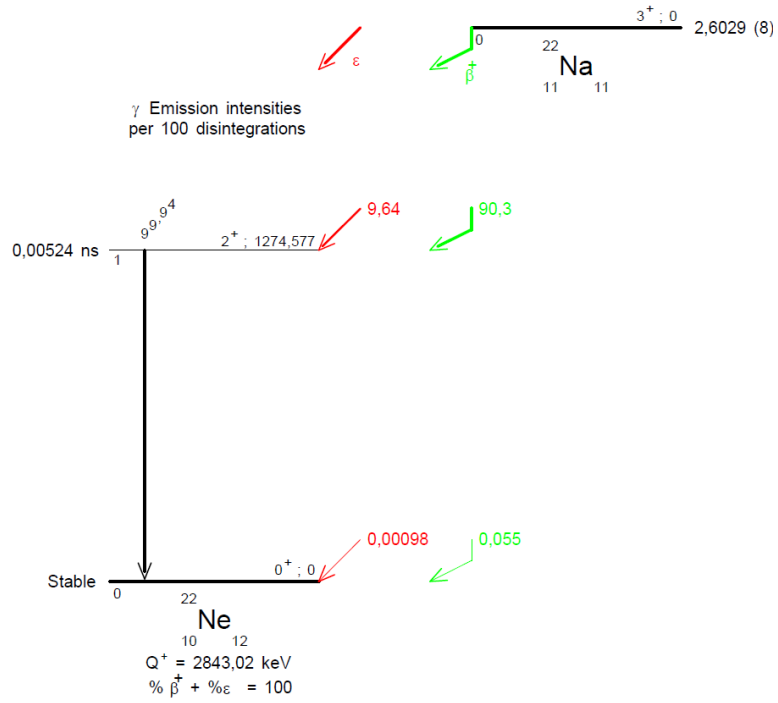
(A.6.3−1) ^{22}Na decay scheme, T$_{1/2}$ = 2.60 a
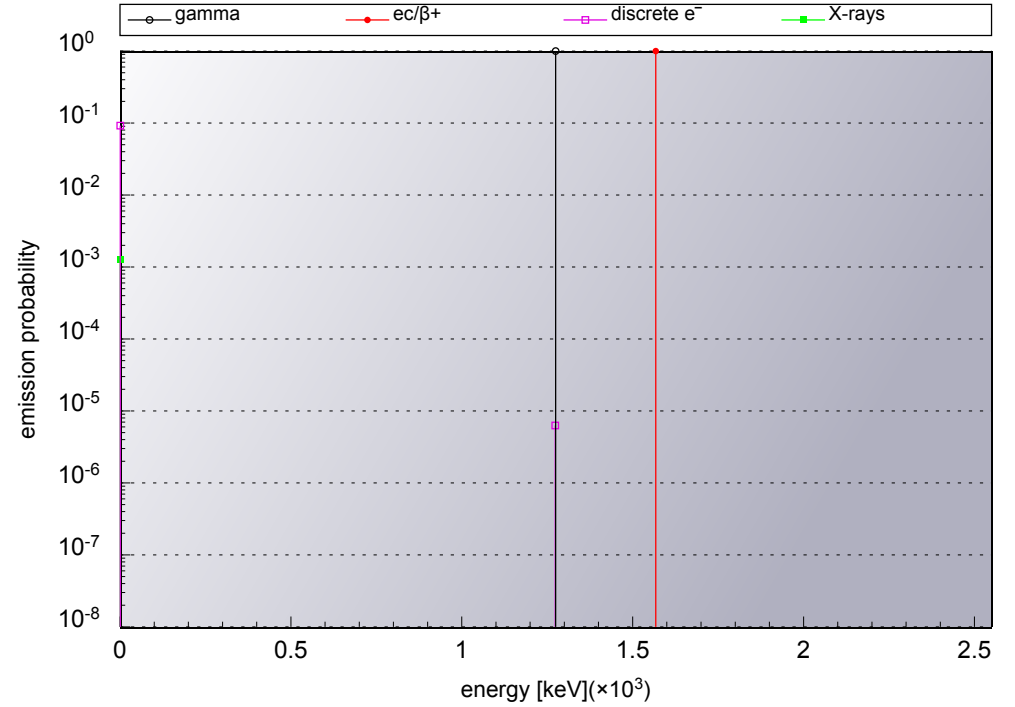
(A.6.3−2) ^{22}Na emission spectrum

Decay Scheme and Emission Spectrum of ^{24}Na

(A.6.4−1) ^{24}Na decay scheme, $T_{1/2} = 15$ h

(A.6.4−2) ^{24}Na emission spectrum

Decay Schemes and Emission Spectra of ^{44}Sc/^{44}Ti
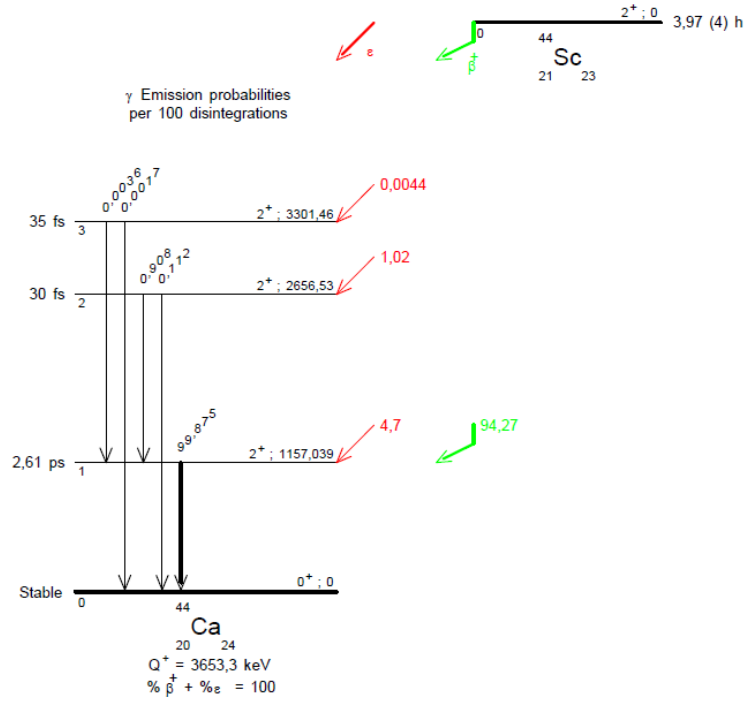
(A.6.5−1) ^{44}Sc decay scheme, T$_{1/2}$ = 3.97 h
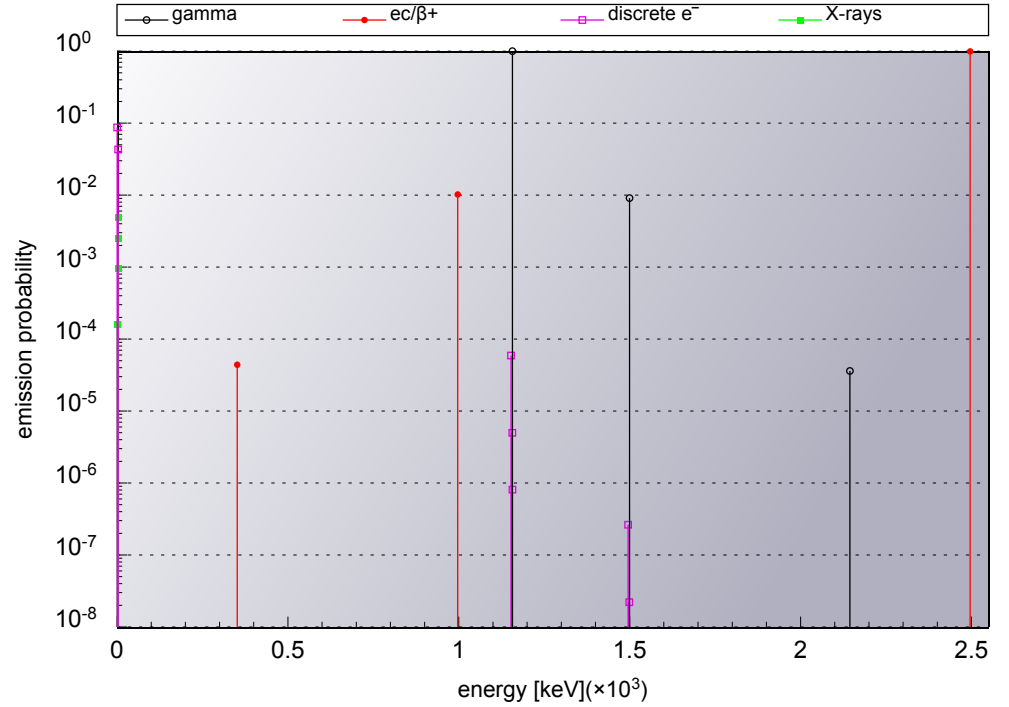
(A.6.5−2) ^{44}Sc emission spectrum

APPENDIX A.6

Decay Schemes and Emission Spectra of ^{44}Sc/^{44}Ti, cont'd
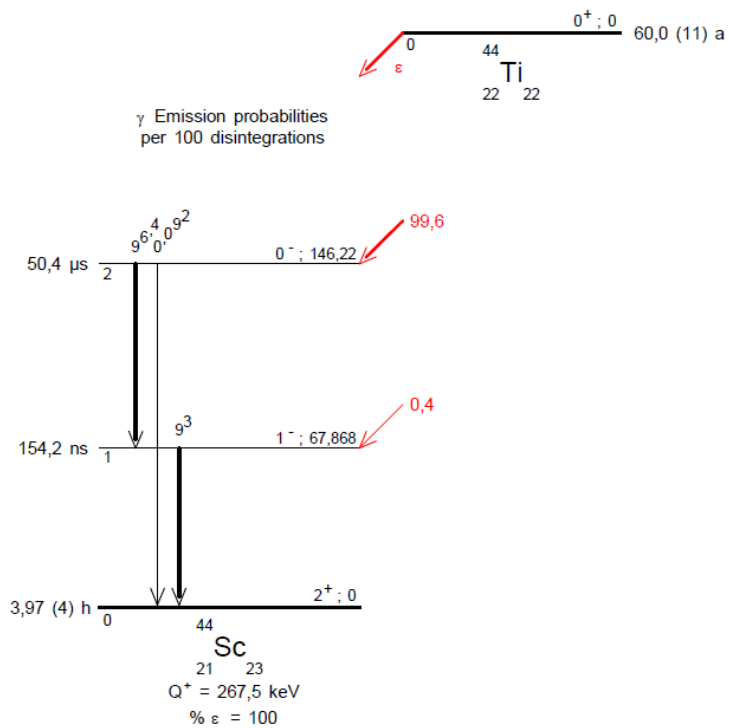
(A.6.6−1) ^{44}Ti decay scheme, T$_{1/2}$ = 60.0 a
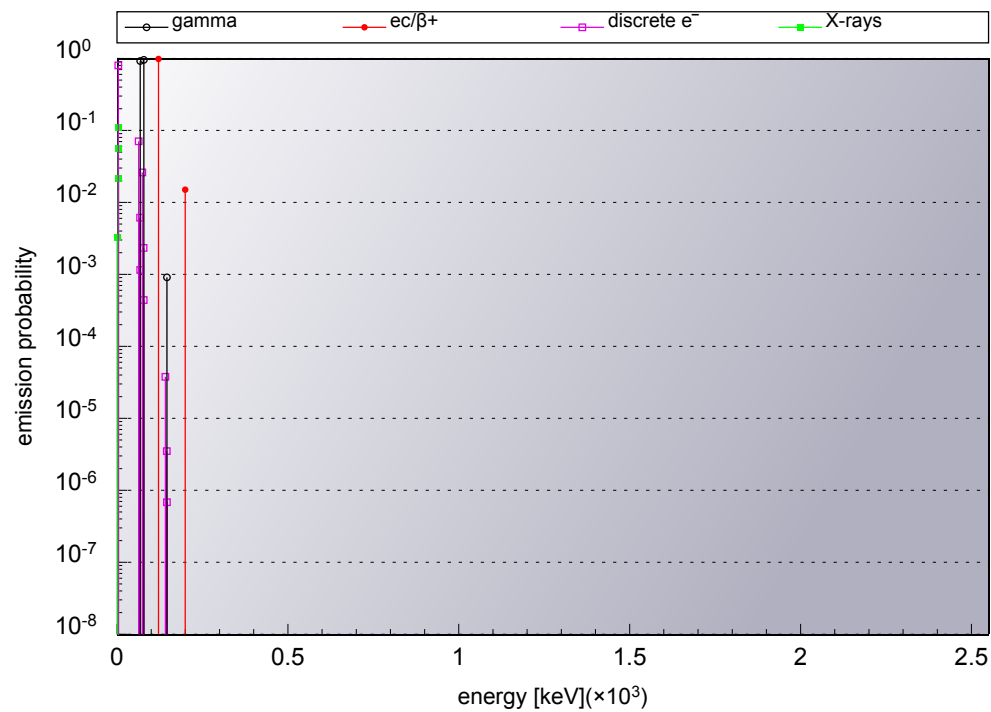
(A.6.6−2) ^{44}Ti emission spectrum

Decay Scheme and Emission Spectrum of ^{51}Cr

7/2$^-$; 0   27,703 (3) d

0
ε

$^{51}_{24}$Cr$_{27}$

γ Emission probabilities
per 100 disintegrations

9,89

$^{9'}_{8}{}^{7}$
0,184 ns   5/2$^-$; 320,0835
1

90,11

Stable   7/2$^-$; 0
0

$^{51}_{23}$V$_{28}$

Q$^+$ = 752,73 keV
% ε = 100
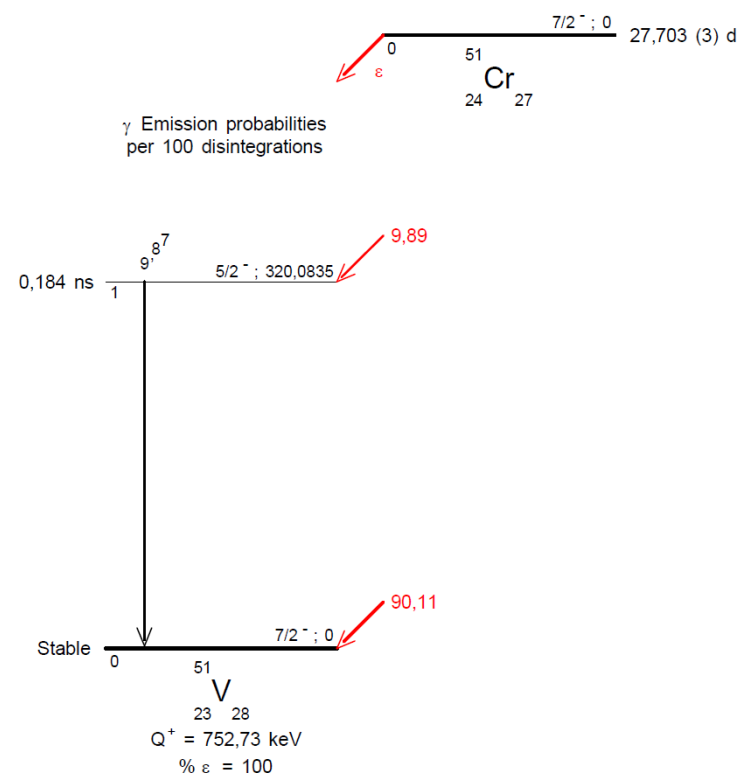
(A.6.7−1) ^{51}Cr decay scheme, T$_{1/2}$ = 27.70 d
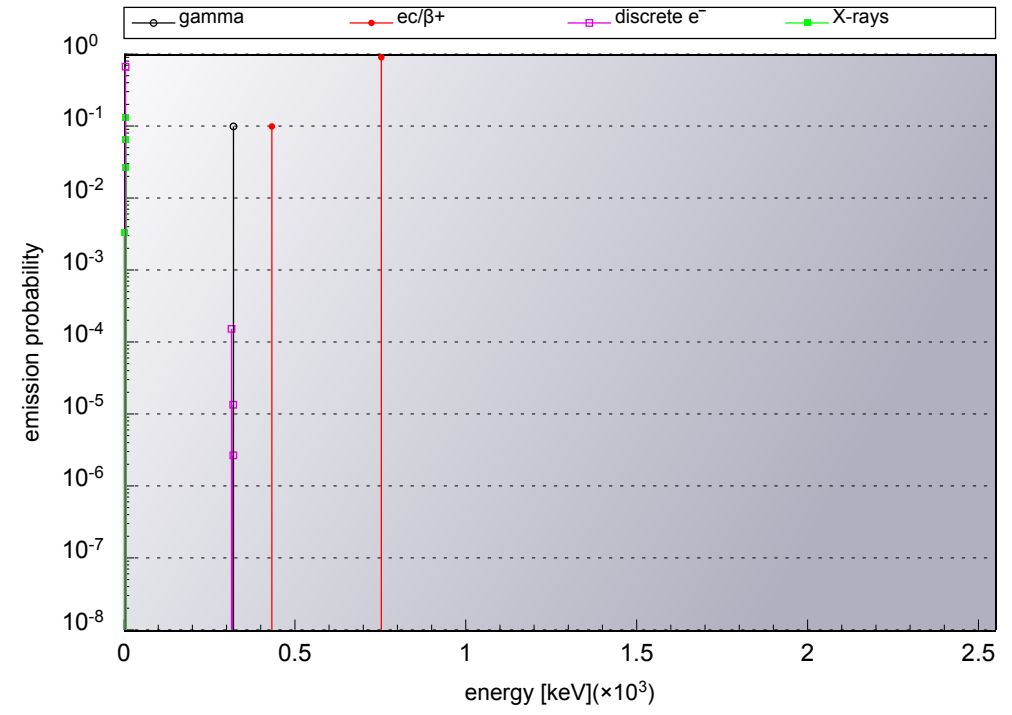
(A.6.7−2) ^{51}Cr emission spectrum

Decay Scheme and Emission Spectrum of ^{54}Mn
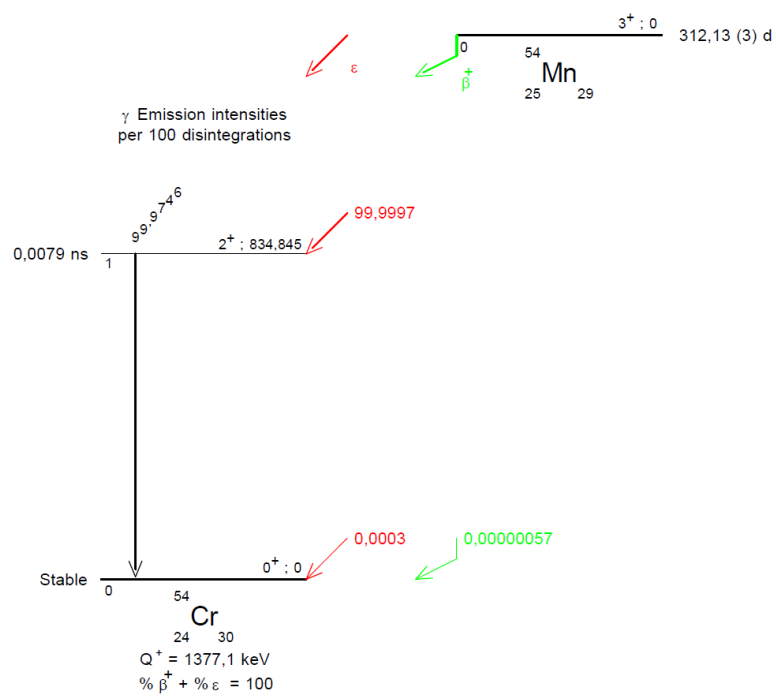
(A.6.8−1) ^{54}Mn decay scheme, $T_{1/2} = 312.13$ d
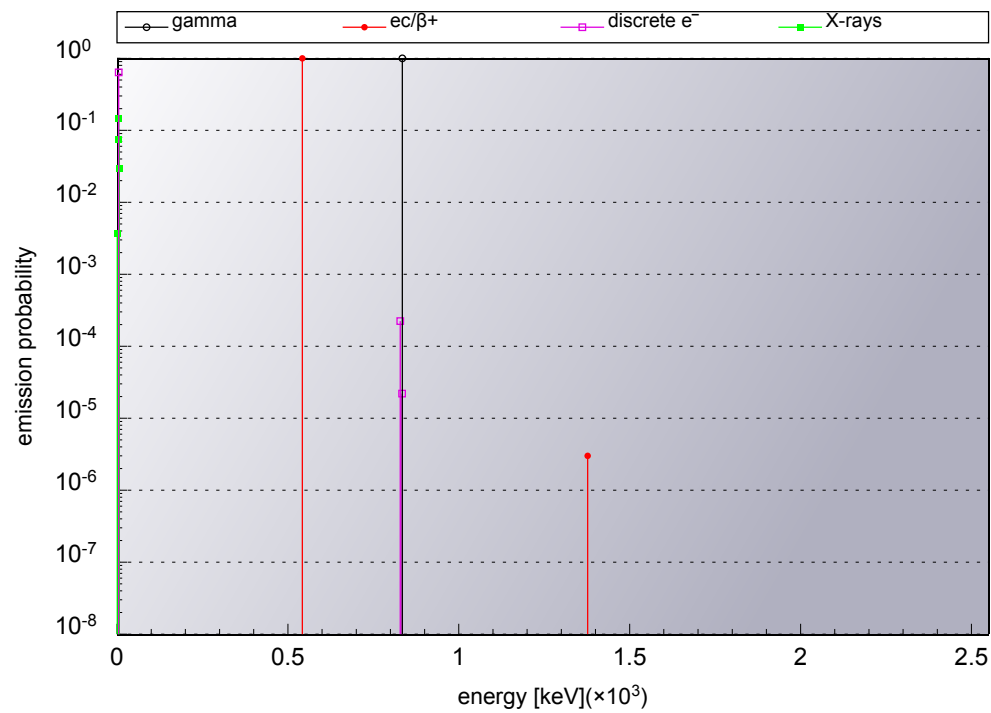
(A.6.8−2) ^{54}Mn emission spectrum

Decay Scheme and Emission Spectrum of ^{56}Co
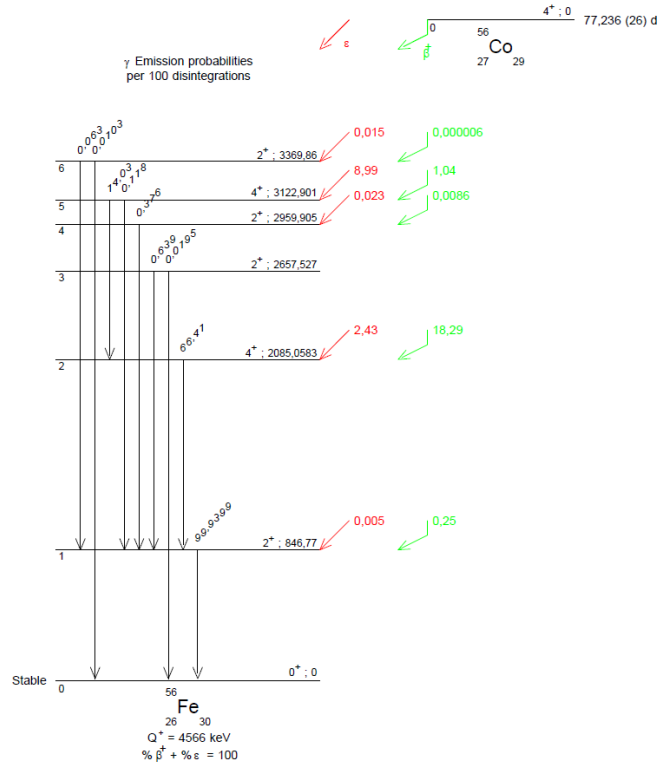
(A.6.9−1) ^{56}Co decay scheme (partial), T$_{1/2}$ = 77.24 d
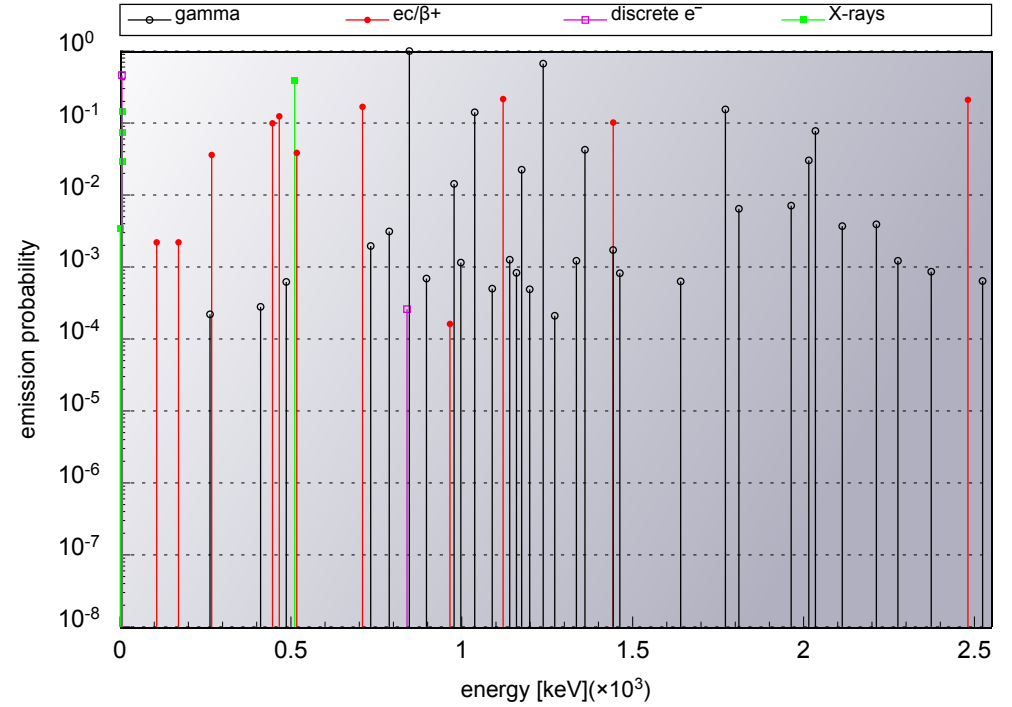
(A.6.9−2) ^{56}Co emission spectrum

Decay Scheme and Emission Spectrum of ^{57}Co
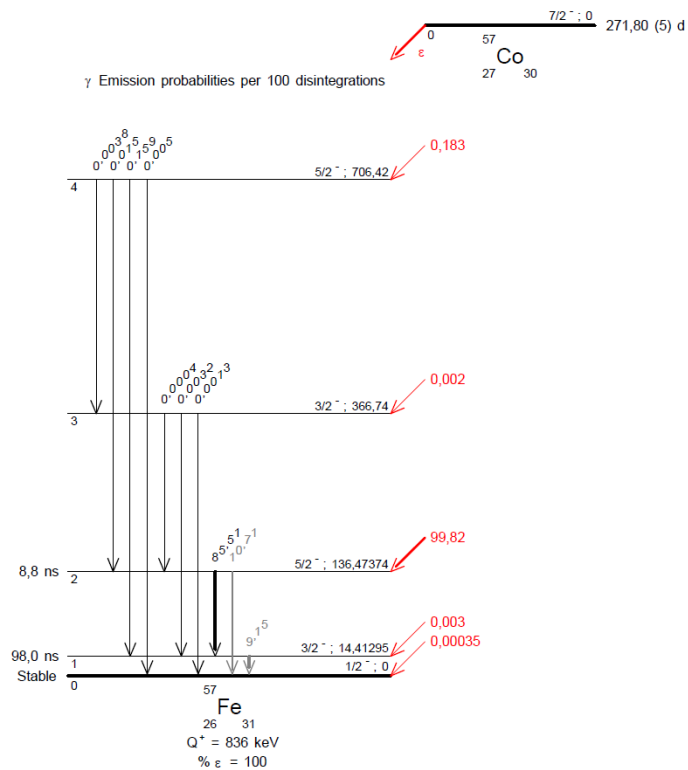
(A.6.10−1) ^{57}Co decay scheme, $T_{1/2} = 271.80$ d
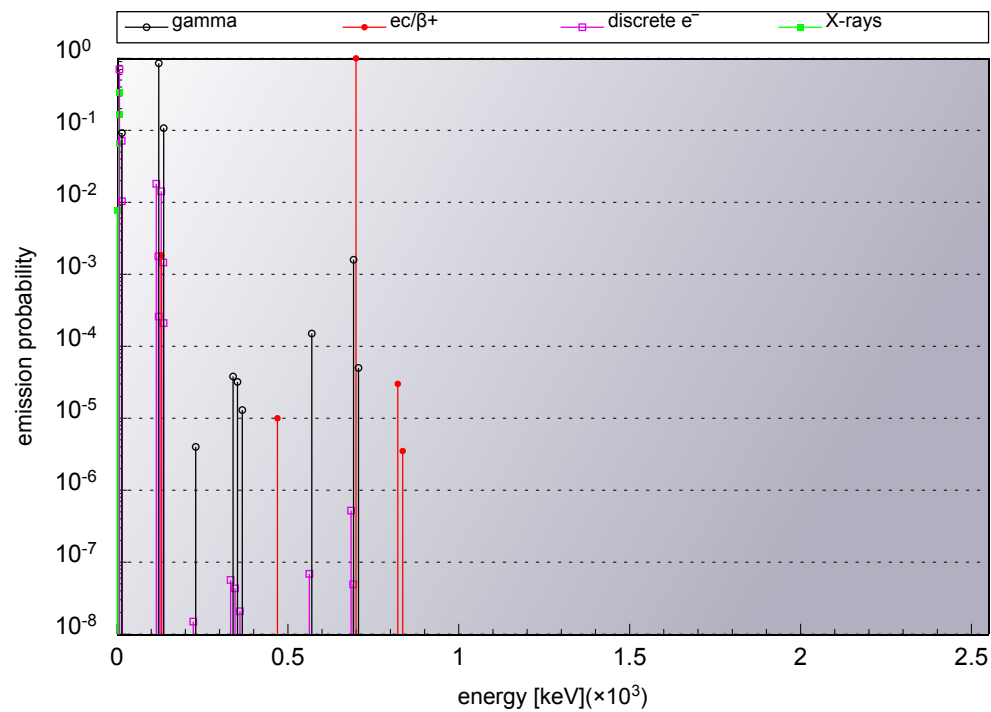
(A.6.10−2) ^{57}Co emission spectrum

Decay Scheme and Emission Spectrum of ^{58}Co
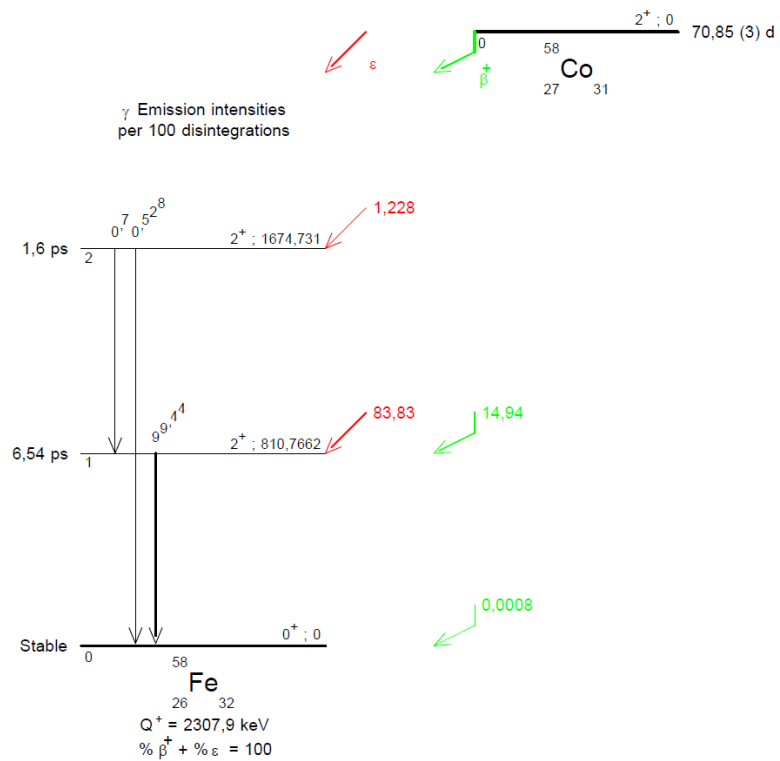
(A.6.11−1) ^{58}Co decay scheme, T$_{1/2}$ = 70.85 d
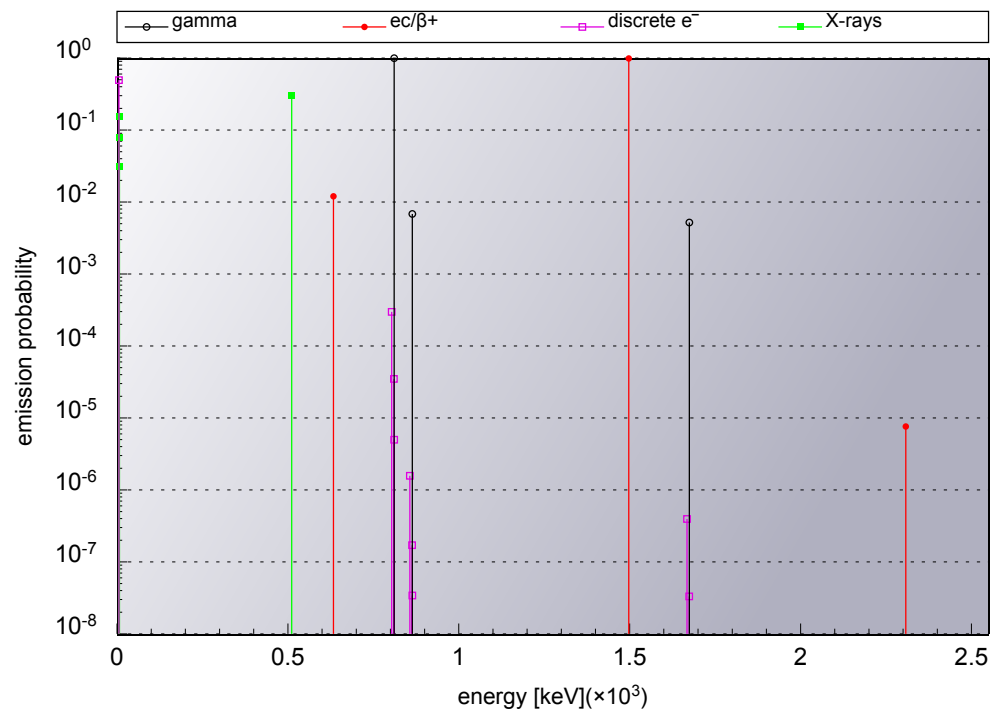
(A.6.11−2) ^{58}Co emission spectrum

Decay Scheme and Emission Spectrum of ^{60}Co
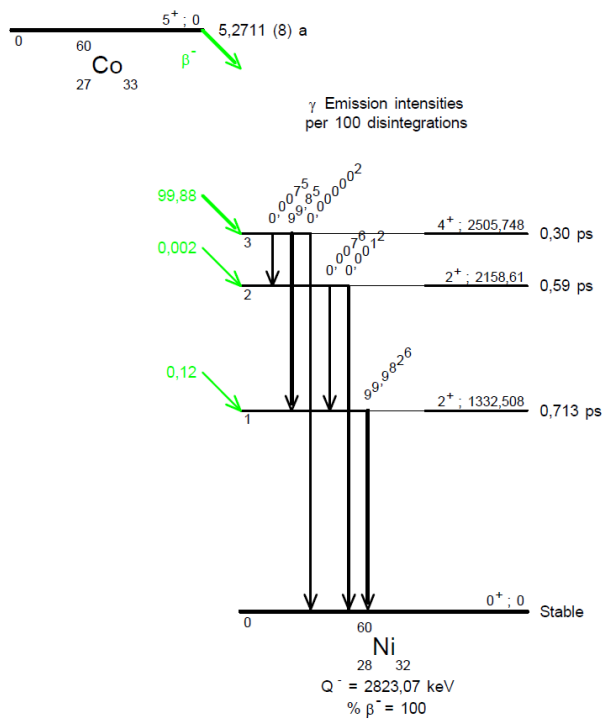
(A.6.12−1) ^{60}Co decay scheme, T$_{1/2}$ = 5.27 a
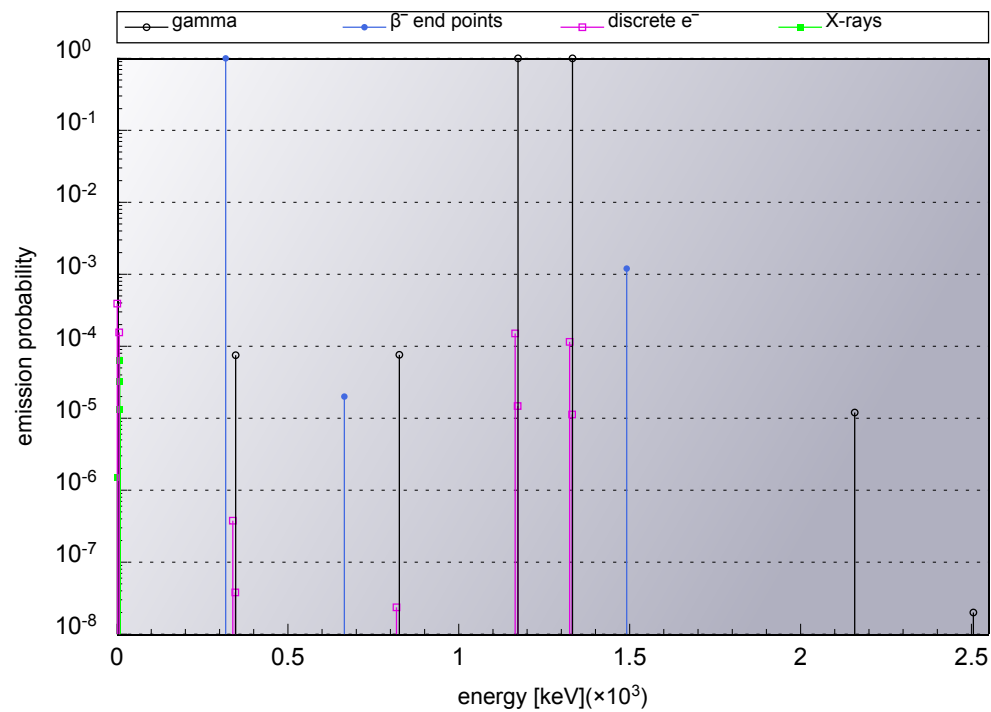
(A.6.12−2) ^{60}Co emission spectrum

Decay Scheme and Emission Spectrum of ^{64}Cu
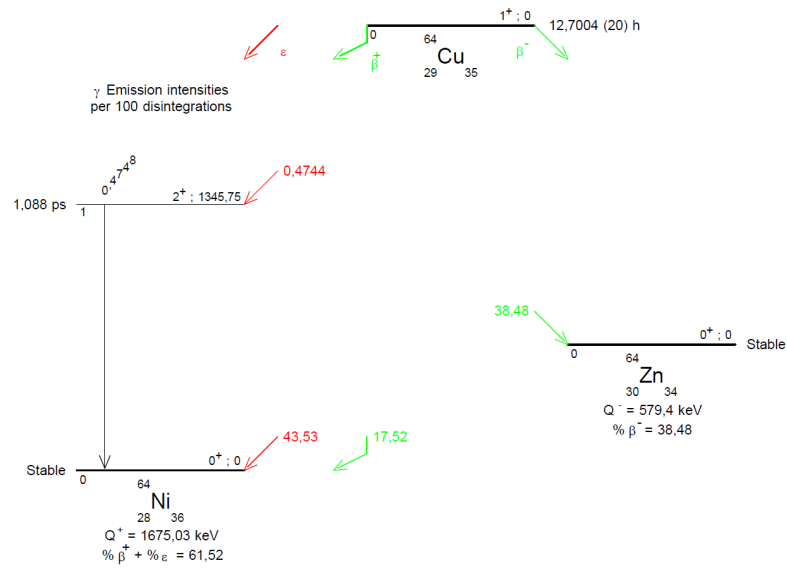
(A.6.13−1) ^{64}Cu decay scheme, T$_{1/2}$ = 12.70 h
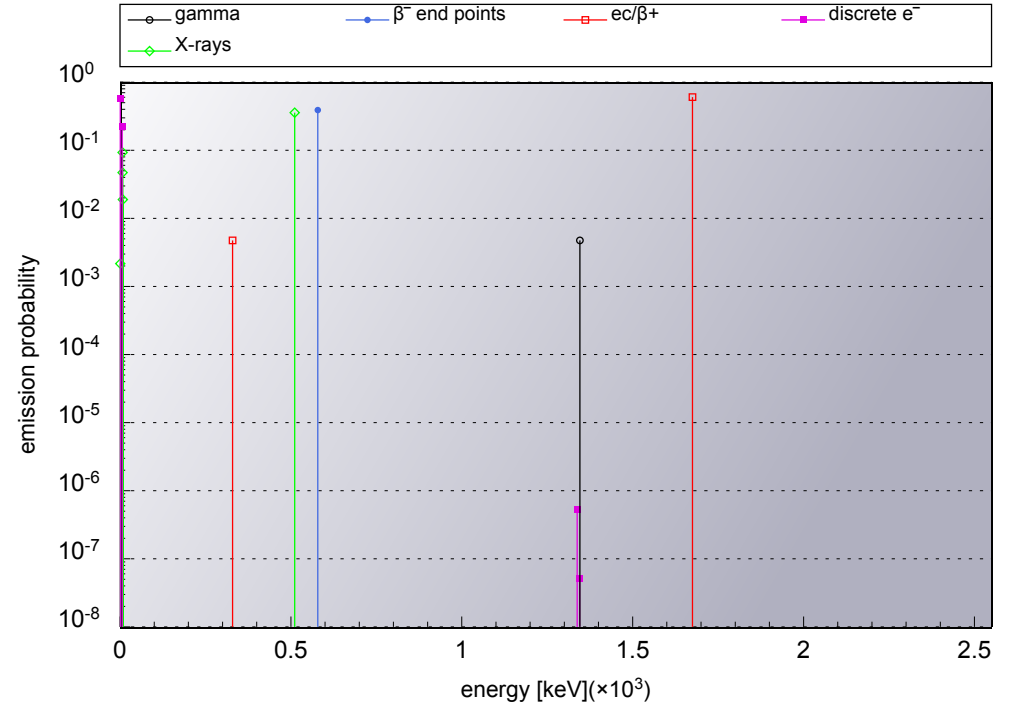
(A.6.13−2) ^{64}Cu emission spectrum

Decay Scheme and Emission Spectrum of ^{65}Zn
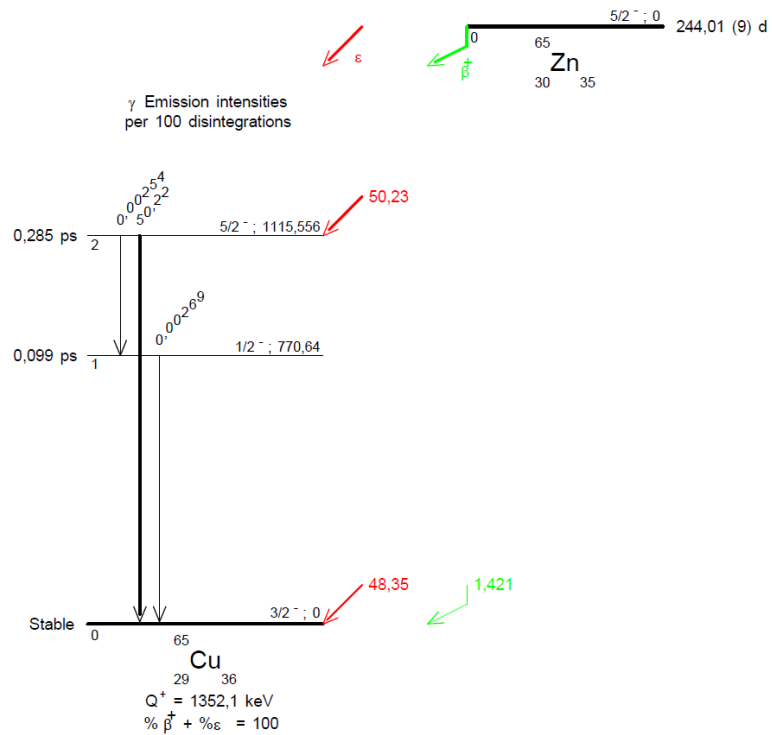
(A.6.14−1) ^{65}Zn decay scheme, $T_{1/2} = 244.01$ d
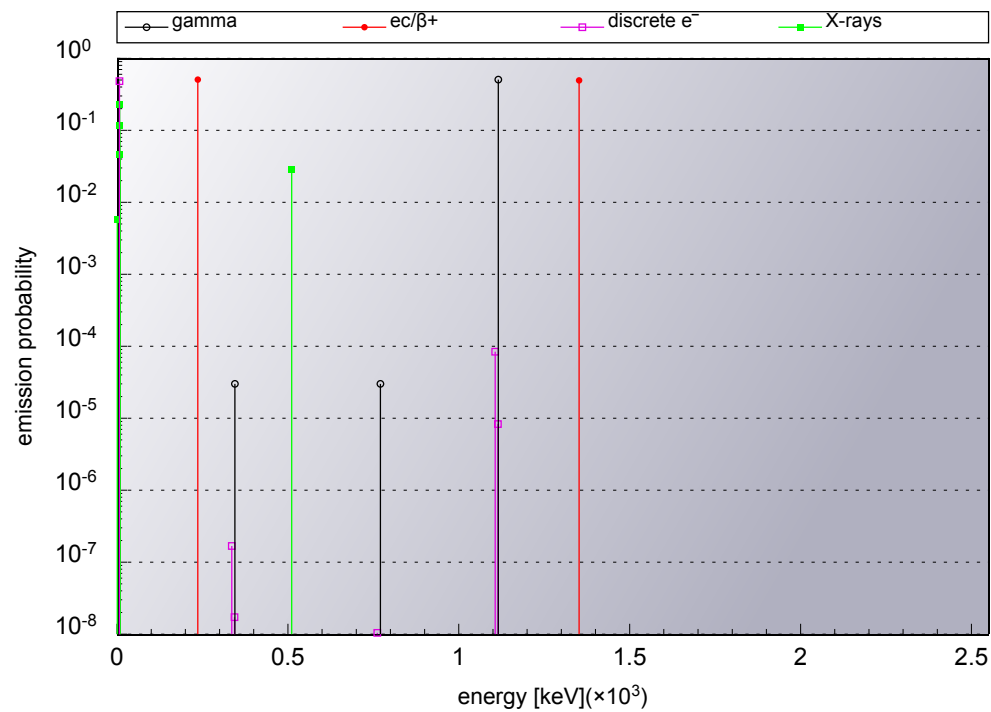
(A.6.14−2) ^{65}Zn emission spectrum
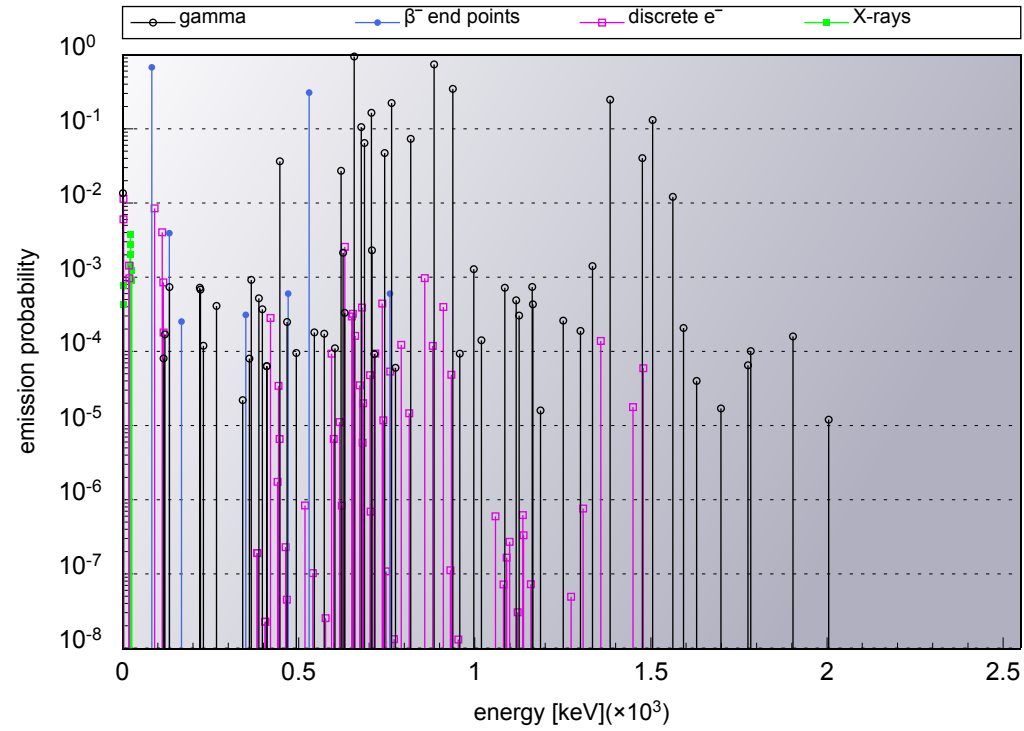
$(\text{A.6.15}-1)\ ^{110\text{m}}$Ag emission spectrum, $T_{1/2} = 249.9\ d$

Decay Schemes and Emission Spectra of ^{137}Cs/^{137m}Ba
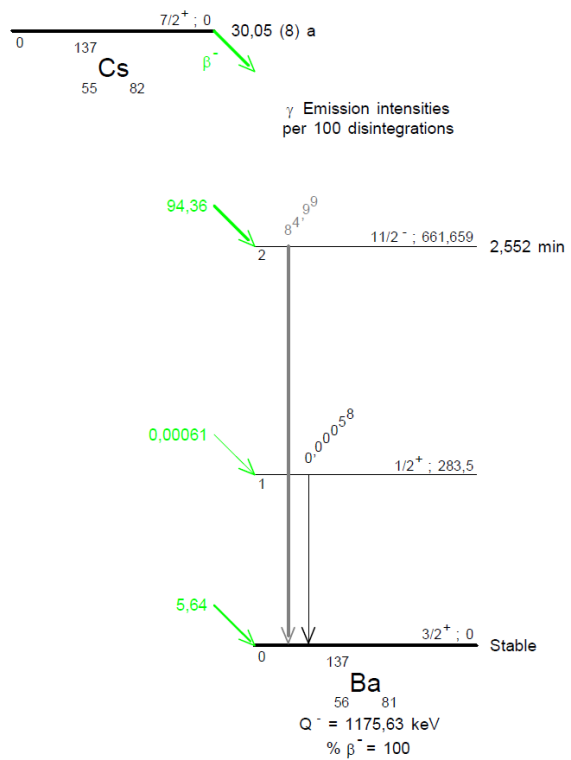
(A.6.16−1) ^{137}Cs decay scheme, T$_{1/2}$ = 30.05 a
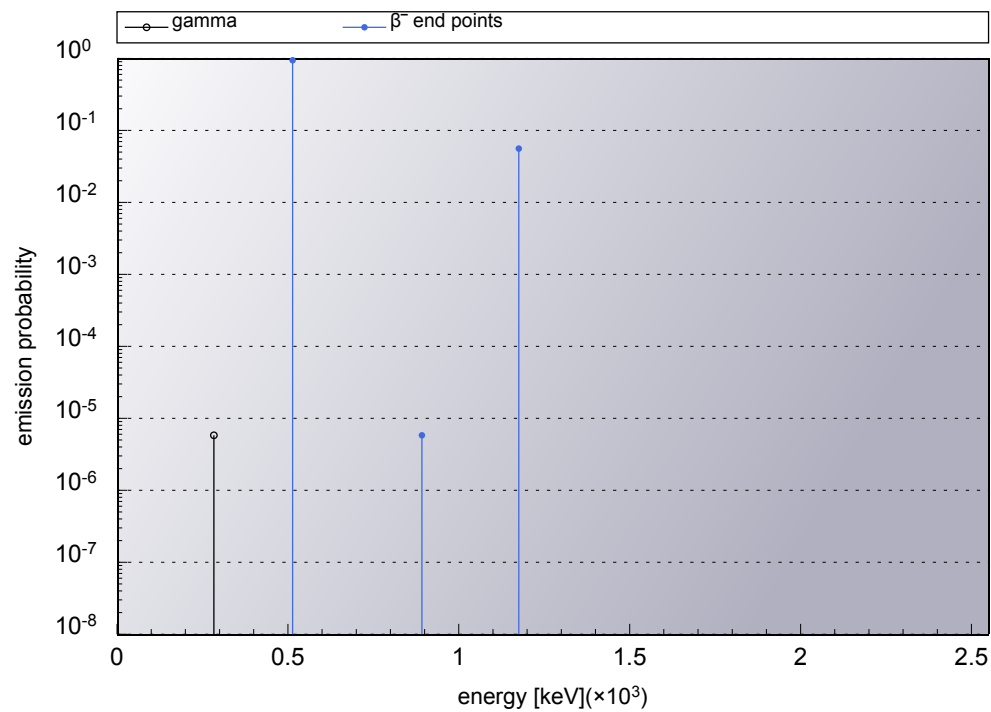
(A.6.16−2) ^{137}Cs emission spectrum

Decay Schemes and Emission Spectra of ^{137}Cs/^{137m}Ba, cont'd

γ Emission probabilities
per 100 disintegrations

90,07

11/2$^-$; 661,659   2,552 min

1

3/2$^+$; 0   Stable

0   137

Ba

56   81

Q^{IT} = 661,659 keV

% IT = 100

(A.6.17−1) ^{137m}Ba decay scheme, T$_{1/2}$ = 2.55 m
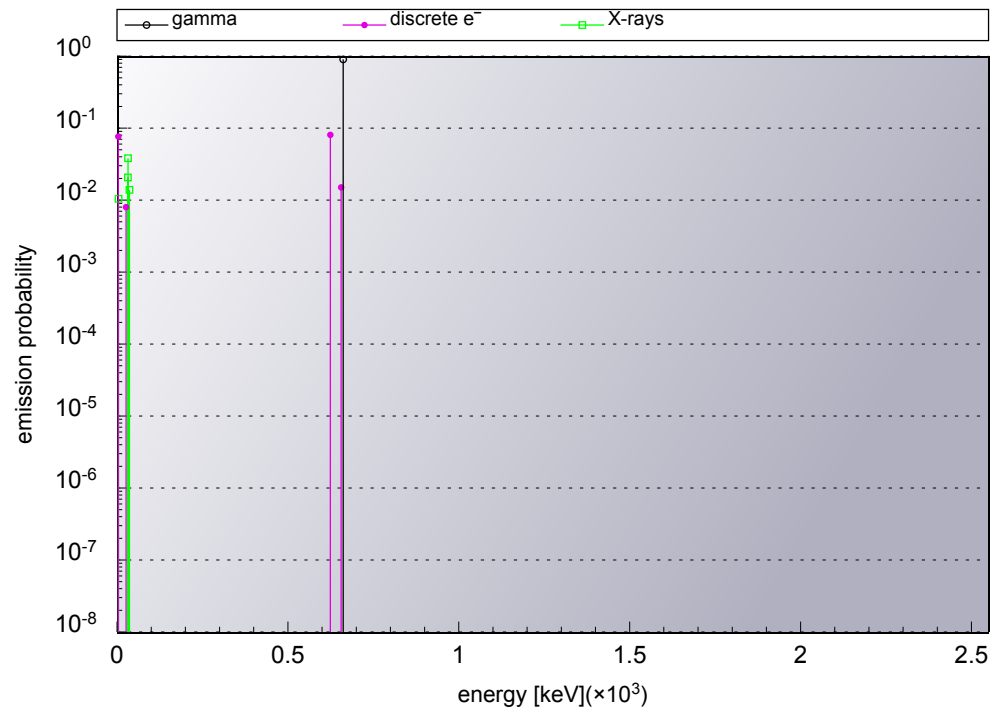
(A.6.17−2) ^{137m}Ba emission spectrum

energy [keV](×10^3)

emission probability

gamma   discrete e$^-$ X-rays

A.6.iii   Decay Schemes and Emission Spectra of Common *Difficult-to-measure Radionuclides*

Figure A.6.18: The figure shows on the following pages, in various sub-figures, the decay schemes and the emission spectra of common *difficult-to-measure radionuclides* as defined in Tab. A.6.1. The decay schemes are extracted from the 'Recommended Data - Table de Radionucléides' provided by the 'Decay Data Evaluation Project', an international collaboration, which includes members of the BNM-CEA/LNHB (France), PTB (Germany), INEEL (USA), KRI (Russia), LBNL (USA), NPL (United Kingdom), CIEMAT (Spain), with the objective of providing carefully produced recommended data. Updates of the recommended data pages are realized by the 'Laboratoire National Henri Becquerel' in Paris, France. The radiation emission spectra are created with the web-based tool 'Nucleide Datasheets++' from NUCLEONICA [62]. The plots are based on data of the JEFF-3.1.1 nuclear data library [52].

(A.6.19−1) ^{3}H decay scheme, $T_{1/2} = 12.31$ a

(A.6.19−2) ^{3}H emission spectrum

Decay Scheme and Emission Spectrum of ^{14}C
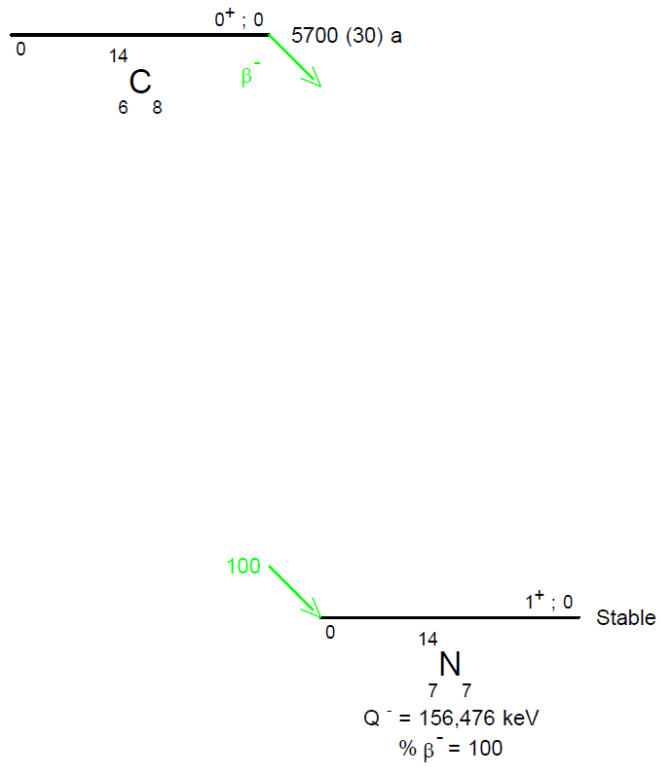
(A.6.20−1) ^{14}C decay scheme, T$_{1/2}$ = 5700 a
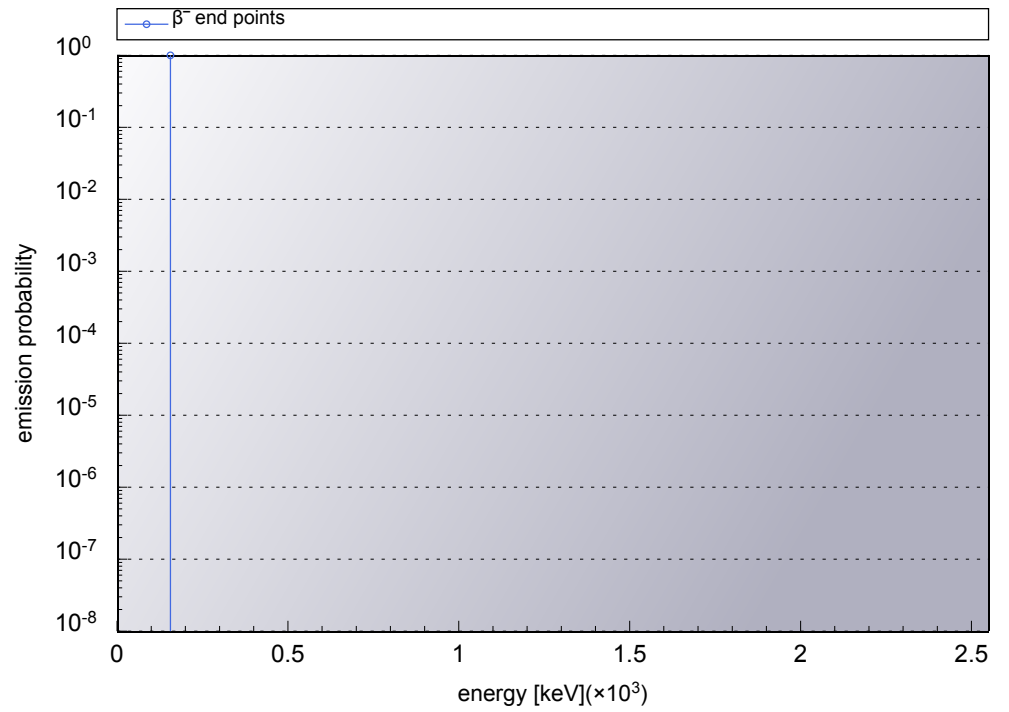
(A.6.20−2) ^{14}C emission spectrum

Decay Scheme and Emission Spectrum of ^{36}Cl

2^+ ; 0
302 (4) x10^3 a

ε

$^{36}_{17}$Cl$_{19}$

β^+

β^-

98,1

0^+ ; 0   Stable

1,9

0,00157

0    $^{36}_{18}$Ar$_{18}$

Q$^-$ = 709,55 keV
% β^- = 98,1

Stable 0^+ ; 0

0    $^{36}_{16}$S$_{20}$

Q$^+$ = 1142,14 keV
% β^+ + %$_\varepsilon$ = 1,9
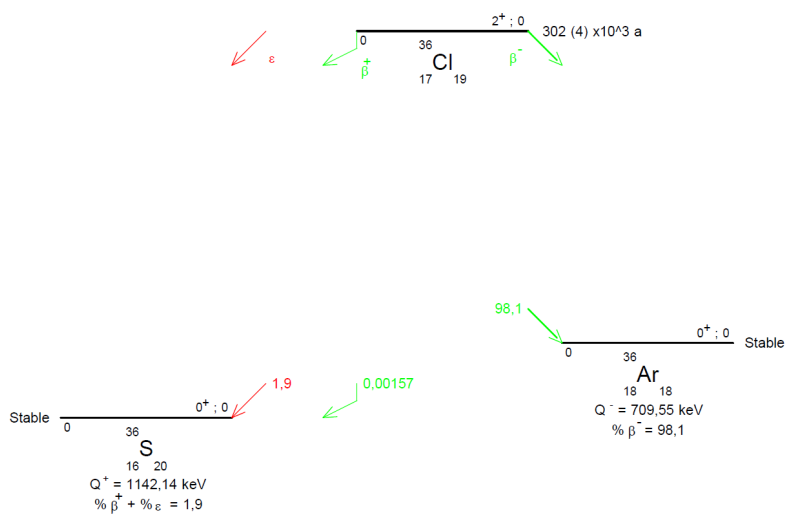
(A.6.21−1) ^{36}Cl decay scheme, T$_{1/2}$ = 3.02 E05 a
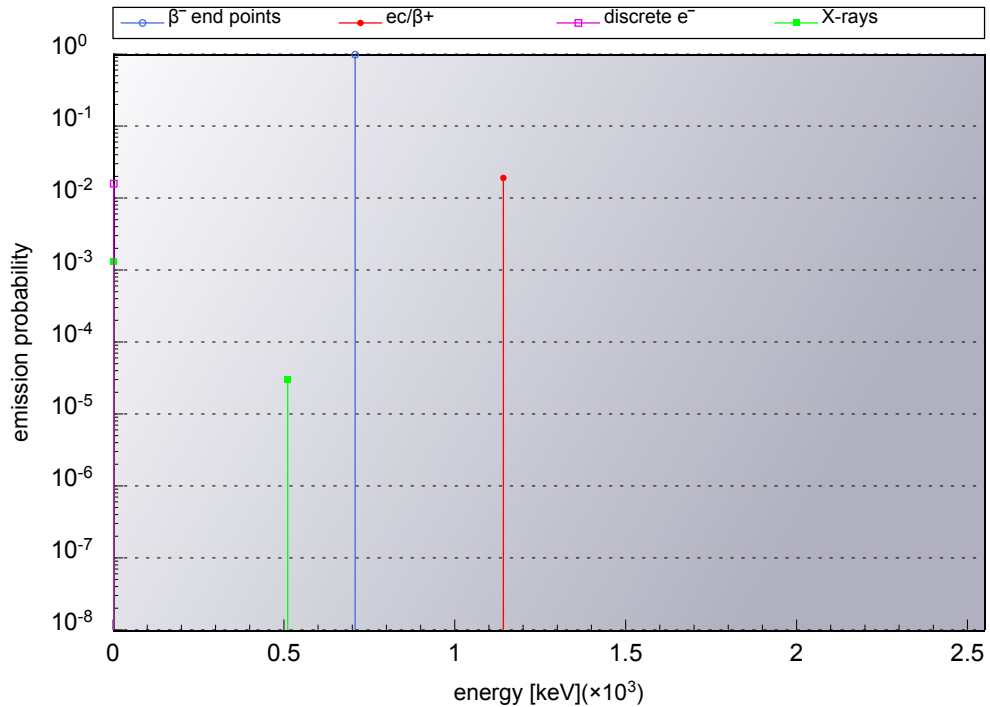
(A.6.21−2) ^{36}Cl emission spectrum

Decay Scheme and Emission Spectrum of ^{55}Fe
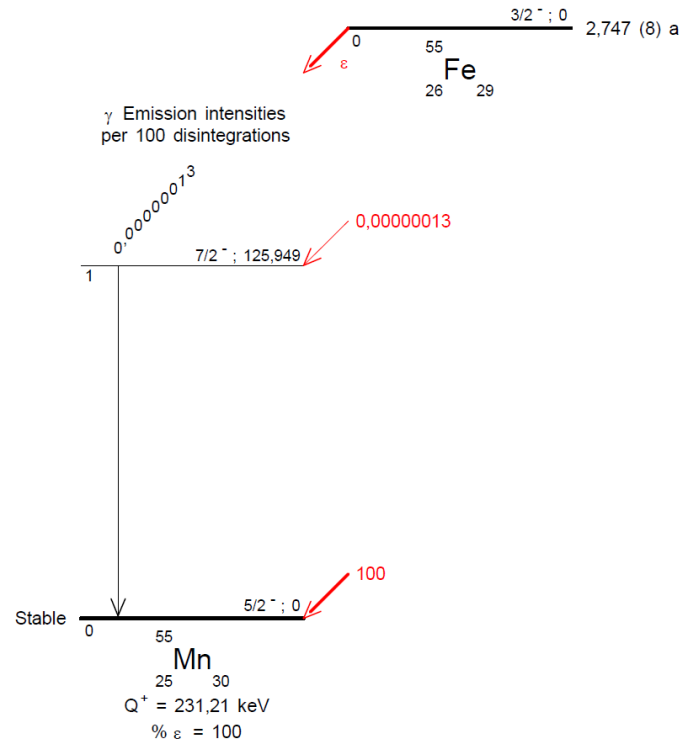
(A.6.22−1) ^{55}Fe decay scheme, $T_{1/2} = 2.75$ a
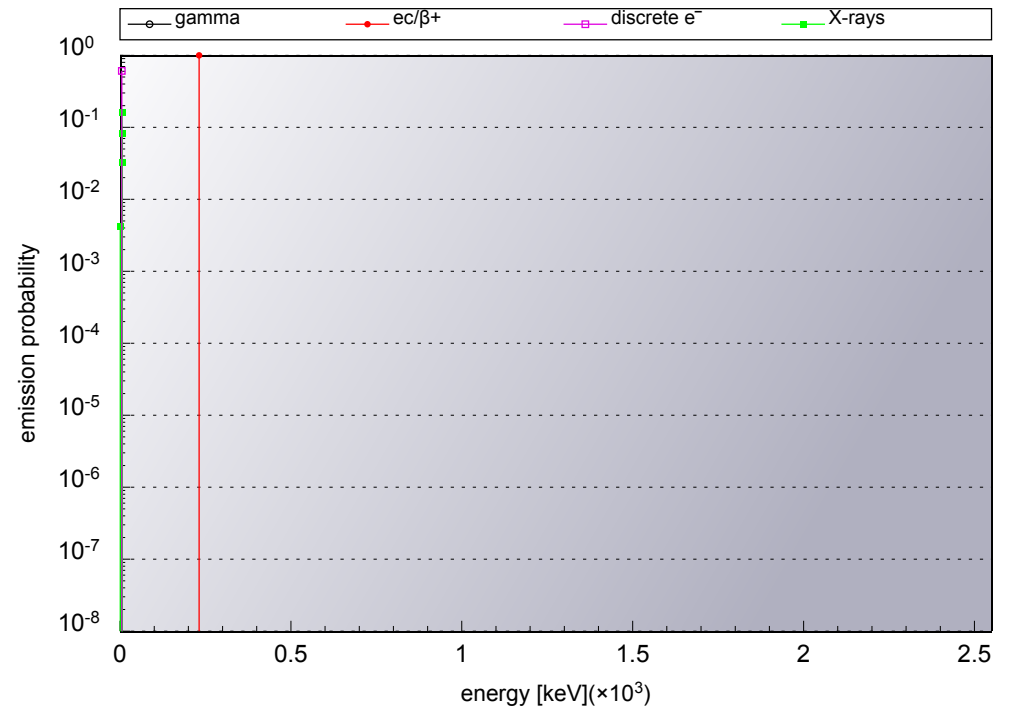
(A.6.22−2) ^{55}Fe emission spectrum

Decay Scheme and Emission Spectrum of ^{63}Ni
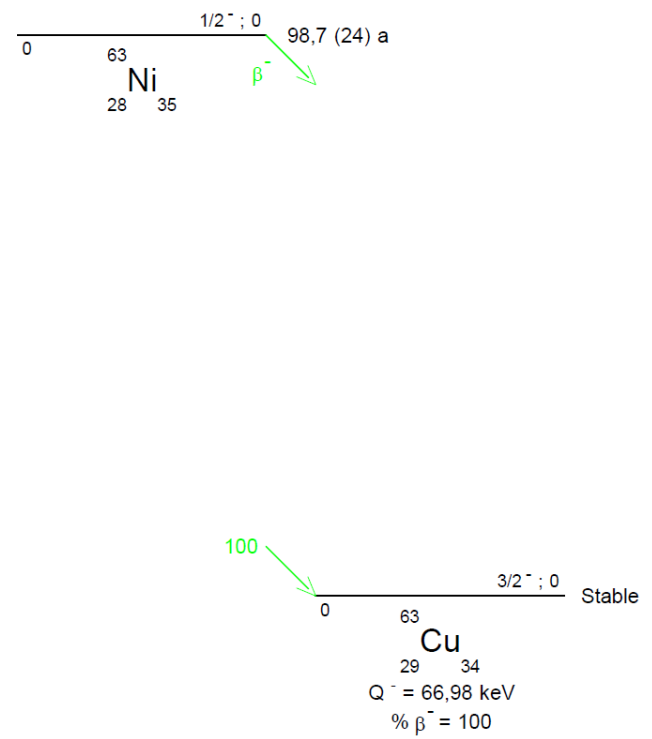
(A.6.23−1) ^{63}Ni decay scheme, T$_{1/2}$ = 98.7 a
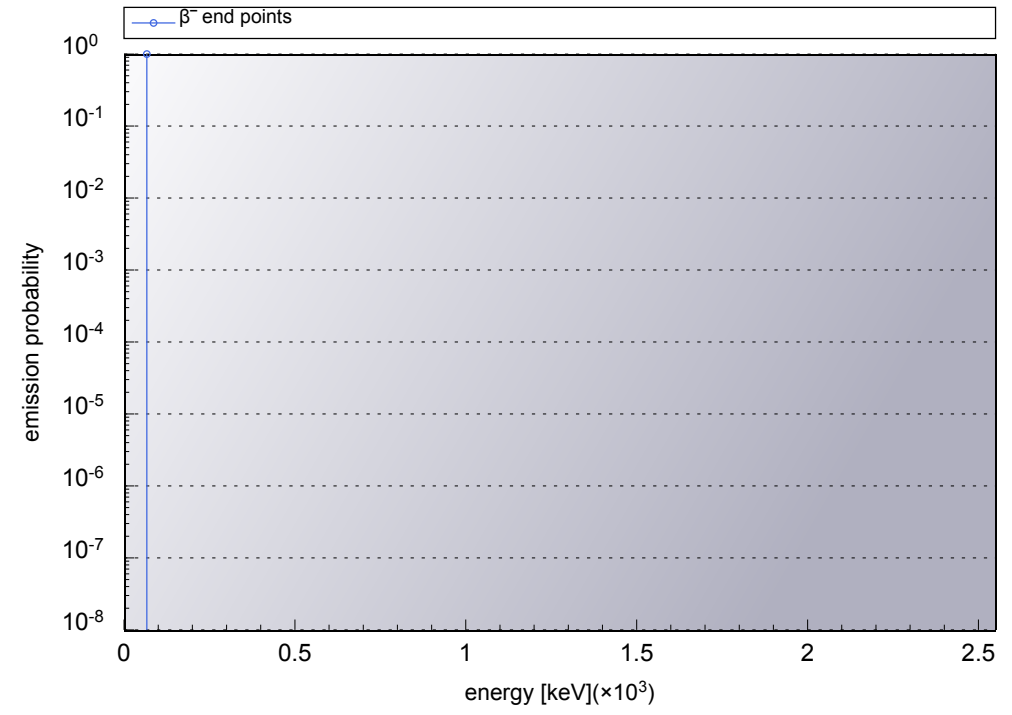
(A.6.23−2) ^{63}Ni emission spectrum

References

[1] CERN, "CERN Internet Presence," Jan. 2014. [Online]. Available: www.CERN.ch

[2] L. Evans and P. Bryant (editors), "LHC Machine," *Journal of Instrumentation*, vol. 3(08):S080001, 2008.

[3] ATLAS Collaboration, G. Aad et al., "The ATLAS Experiment at the CERN Large Hadron Collider," *Journal of Instrumentation*, vol. 3(08):S080003, 2008.

[4] ALICE Collaboration, K. Aamodt et al., "The ALICE experiment at the CERN LHC," *Journal of Instrumentation*, vol. 3(08):S080002, 2008.

[5] CMS Collaboration, S. Chatrchyan et al., "The CMS experiment at the CERN LHC," *Journal of Instrumentation*, vol. 3(08):S080004, 2008.

[6] LHCb Collaboration, A. Augusto Alves et al., "The LHCb Detector at the LHC," *Journal of Instrumentation*, vol. 3(08):S080005, 2008.

[7] K. Nakamura et al (Particle Data Group) 2010 J. Phys. G: Nucl. Part. Phys. 37 075021.

[8] C. Grupen, *Introduction to Radiation Protection: Practical Knowledge for Handling Radioactive Sources.* Berlin: Springer, 2010.

[9] K. S. Krane, *Introductory Nuclear Physics.* New York, NY: Wiley, 1988.

[10] G. F. Knoll, *Radiation Detection and Measurement*, 4th ed. Hoboken: Wiley, 2010.

[11] N. Tsoulfanidis and S. Landsberger, *Measurement and detection of radiation*, 3rd ed. Boca Raton, FL: CRC Press, 2011.

[12] G. Gilmore, *Practical Gamma-ray Spectroscopy*, 2nd ed. Chichester: Wiley, 2008.

[13] W. R. Leo, *Techniques for nuclear and particle physics experiments: a how-to approach*, 2nd ed. Berlin: Springer, 1994.

[14] J. E. Martin, *Physics for Radiation Protection*, 3rd ed. Weinheim: Wiley, 2013.

[15] The International Commission on Radiation Units and Measurements, "Fundamental Quantities and Units for Ionizing Radiation, I.C.R.U. Report No.85," Tech. Rep., 2011.

[16] International Organization for Standardization (ISO), "ISO 80000-1:2009(E), Quantities and units - Part 1: General," Geneva, Tech. Rep., 2009.

[17] ——, "ISO 21238:2007, Nuclear energy - Nuclear fuel technology - Scaling factor method to determine the radioactivity of low- and intermediate-level radioactive waste packages generated at nuclear power plants," Geneva, Tech. Rep., 2007.

[18] J. P. De Carvalho Saraiva, "Radiological Characterization of TFA metallic tubes from CERN Accelerator Complex," Master's thesis, University of Coimbra, Portugal, 2012.

[19] A. Beiser, "Nuclear Emulsion Technique," *Reviews of Modern Physics*, vol. 24, no. 4, pp. 273–311, 1952.

[20] R. D. Evans, *The Atomic Nucleus*. New York: McGraw-Hill, 1955.

[21] J. K. Shultis and R. E. Faw, *Radiation Shielding*. La Grange Park, IL: American Nuclear Society, 2000.

[22] A. H. Sullivan, *Guide to radiation and radioactivity levels near high energy particle accelerators*. Ashford: Nucl. Techn. Publ., 1992.

[23] M. M. Barbier, *Induced Radioactivity*. Amsterdam: North-Holland, 1969.

[24] J. M. Bernardo and A. Smith, *Bayesian Theory*. Chichester: John Wiley and Sons Ltd., 2000.

[25] International Organization for Standardization (ISO), "ISO 11929:2010, Determination of the characteristic limits (decision threshold, detection limit and limits of the confidence interval) for measurements of ionizing radiation - Fundamentals and application," Geneva, Tech. Rep., 2010.

[26] Personal communication, C. Guenter(MIRION), W. Goedrich(MIRION), R. Froeschl(CERN) and N. Walter, "Meeting on LNC factors, MIRION Techologies Hamburg, 06.02.2014."

[27] N. Walter, "Radionuclide Inventories for Common Materials due to Accelerator Radiation Induced Activation in the CERN Accelerator Complex," CERN, Tech. Rep., 2014, EDMS 1425674.

[28] R. Froeschl and N. Walter, "Validation of LNC (leading nuclide correlation) factors provided by RADOS for the RTM 644/661," CERN, Tech. Rep., 2014, EDMS 1311050.

[29] J. A. Nelder, R. Mead, "A simplex method for function minimization," *The Computer Journal*, vol. 7, pp. 308–313, 1965.

[30] Automation und Messtechnik GmbH, *Scintillator Probe 6150AD-b (/H,/E)*, Ladenburg, Germany, 08 2011.

[31] ——, *6150AD*, Ladenburg, Germany, 01 2011.

[32] International Atomic Energy Agency, "Safety Guides RS-G-1.7, Application of the Concepts of Exclusion, Exemption and Clearance," IAEA, Tech. Rep., 2004.

[33] ——, "Safety Series No.115, International Basic Safety Standards for Protection against Ionizing Radiation and for the Safety of Radiation Sources," IAEA, Tech. Rep., 1996.

[34] European Comission, "Radiation Protection No122, Part I, Practical Use Of The Concepts Of Clearance and Exemptions," EC, Tech. Rep., 2000.

[35] Federal Council of Switzerland, French Government and CERN, "RS/SR 0.814.592.2, Accord entre le Conseil fédéral suisse, le Gouvernement de la République française, et l'Organisation européenne pour la Recherche nucléaire relatif à la Protection contre les rayonnements ionisants et à la Sûreté des Installations de l'Organisation européenne pour la Recherche nucléaire," Tech. Rep., 2011.

[36] Federal Assembly of the Swiss Confederation, "Ordonnance sur la radioprotection (ORaP)," 22 June 1994, (State of 1 January 2014).

[37] International Atomic Energy Agency, "Safety Report Series No44, Derivation of Activity Concentration Values for Exclusion, Exemption and Clearance," IAEA, Tech. Rep., 2005.

[38] ——, "Safety Report Series No67, Monitoring for Compliance with Exemption and Clearance Levels," IAEA, Tech. Rep., 2012.

[39] European Comission, "Radiation Protection No89, Recommended radiological protection criteria for the recycling of metals from the dismantling of nuclear installations," EC, Tech. Rep., 1998.

[40] ——, "Radiation Protection No113, Recommended radiological protection criteria for the clearance of buildings and building rubble from the dismantling of nuclear installations," EC, Tech. Rep., 2000.

[41] ——, "Radiation Protection No157, Comparitive Study of EC and IAEA Guidance on Exemption and Clearance Levels," EC, Tech. Rep., 2010.

[42] Swiss Federal Nuclear Safety Inspectorate(ENSI), "ENSI-B04 - Freimessung von Materialien und Bereichen aus kontrollierten Zonen," Tech. Rep., 2009.

[43] A. Ferrari, P. R. Sala, A. Fassò, J. Ranft, "FLUKA: a multi-particle transport code," CERN 2005-10 (2005), INFN/TC_05/11, SLAC-R-773, Tech. Rep.

[44] G. Battistoni, S. Muraro, P. R. Sala, F. Cerutti, A. Ferrari, S. Roesler, A. Fassò, J. Ranft, Ed., *The FLUKA code: Description and benchmarking*, 2007, Proceedings of the Hadronic Shower Simulation Workshop 2006, Fermilab 6-8 September 2006, M. Albrow, R. Raja eds., AIP Conference Proceeding 896, 31-49.

[45] V. Vlachoudis, Ed., *FLAIR: A Powerful But User Friendly Graphical Interface For FLUKA*. Saratoga Springs, New York: Proc. Int. Conf. on Mathematics, Computational Methods & Reactor Physics (M&C 2009), 2009.

[46] H. Vincke and C. Theis, "ActiWiz - optimizing your nuclide inventory at proton accelerators with a computer code," *Progress in Nuclear Science and Technology*, vol. 4, pp. 228–232, 2014.

[47] R. Froeschl, C. Theis, F. La Torre, H. Vincke, N. Walter, "Radiological Hazard classification of material in CERN's accelerators," CERN, Tech. Rep., 2012, EDMS 1184236.

[48] R. Froeschl, M. Magistris, F. L. Pereira, "JEREMY, a code for the radiological characterization of accelerator components including detailed uncertainty estimation." in *2nd workshop on Accelerator Radiation Induced Activation(ARIA)*, Jerusalem, 2011.

[49] R. Froeschl, M. Magistris, F. L. Pereira, C. Theis, "Computation of radioactivity in particle accelerators and propagation of uncertainties with the JEREMY code," CERN, Tech. Rep., 2014, EDMS 1406467.

[50] S. A. et al. (GEANT4 Collaboration), "Geant4: A simulation toolkit," *Nucl. Instrum. Meth.*, vol. A506, p. 250, 2003.

[51] H. G. Hughes, R. E. Preal, and R. C. Little, "MCNPX - The LAHET/MCNP Code Merger," LANL, Tech. Rep. LA-UR-97-4891, 1997.

[52] A. Santamarina, "The JEFF-3.1.1 Nuclear Data Library." Nuclear Energy Agency(NEA), Paris, JEFF Report 22, 2009.

[53] D. Rochman and A. J. Koning, "TENDL-2010: Reaching completeness and accuracy," OECD/NEA, JEF/DOC-1349, 2010.

[54] H. Bateman, "Solution of a system of differential equations occurring in the theory of radioactive transformations," *Proc. Cambridge Philos. Soc.*, vol. 15, pp. 423–427, 1910.

[55] J. K. Shultis and R. E. Faw, *Fundamentals of nuclear science and engineering.* Abingdon: Dekker, 2002.

[56] R. Froeschl, F. P. La Torre, N. Walter, "The ActiWiz material composition catalogue," CERN, Tech. Rep., 2012, EDMS 1277395.

[57] Personal communication, Prof.Dr.-Ing. W. Bleck (Head of Department of Ferrous Metallurgy, RWTH Aachen) and N. Walter, "Discussion on cobalt content in steel, telephone conference," March 2013.

[58] Personal communication, Dr. G. Brückner (Manager Product Development, ThyssenKrupp Nirosta (Outokumpu)) and N. Walter, "Discussion on cobalt content in steel, telephone conference," March 2013.

[59] M. B. Chadwick et al., "ENDF/B-VII.1 Nuclear Data Library," 2011.

[60] A. J. Koning, D. Rochman et al., "TENDL-2013: TALYS-based Evaluated Nuclear Data Library," 2013.

[61] G. Pfenning et al., "Chart of the Nuclides, 6th edition," 1998.

[62] NUCLEONICA, "Nuclear Science Internet Portal," 2014. [Online]. Available: www.nucleonica.net